Stacey H. Wang (SBN 245195)
Vito Costanzo (SBN 132754)
HOLLAND & KNIGHT LLP
400 South Hope Street 8th Floor
Los Angeles, CA 90071-2040
Telephone: 213-896-2400
Facsimile: 213-896-2450
stacey.wang@hklaw.com
vito.costanzo@hklaw.com

Michael B. Eisenberg (admitted *pro hac vice*)
HOLLAND & KNIGHT LLP
31 West 52nd Street
New York, New York 10019
Telephone: (212) 513-3529
Facsimile: (212) 385-9010
michael.eisenberg@hklaw.com

Jennifer L. Jonak (SBN 191323)
JONAK LAW GROUP, P.C.
2888 Arline Way
Eugene, Oregon 97403
Telephone: (541) 525-9102
Facsimile: (541) 500-0882
jenny@jonak.com

Attorneys for Plaintiff,
SENSOR ELECTRONIC TECHNOLOGY, INC.

UNITED STATES DISTRICT COURT

NORTHERN DISTRICT OF CALIFORNIA

SAN JOSE DIVISION

SENSOR ELECTRONIC TECHNOLOGY, INC., a New York Corporation Plaintiff, vs. BOLB, INC., a Delaware Corporation, QUANTUM EGG, INC., a Delaware Corporation Defendant.	Case No.: 5:18-cv-05194-LHK **SECOND DECLARATION OF MICHAEL B. EISENBERG IN SUPPORT OF REPLY CLAIM CONSTRUCTION BRIEF** Complaint Filed: August 24, 2018

SECOND DECLARATION OF MICHAEL B. EISENBERG

I, Michael B. Eisenberg declare as follows:

I am over the age of 18 and have personal knowledge of the matters stated herein. I could truthfully testify thereto if called upon as a witness.

1. I partner at the law firm of Holland & Knight LLP and am counsel *pro hac vice* for Plaintiff Sensor Electronic Technology, Inc. ("SETi" or "Plaintiff"). I provide this declaration in support of Plaintiffs' Reply Claim Construction brief.

2. Attached hereto as Exhibit 8 is a true and correct copy of U.S. Patent 8,080,833.

3. Attached hereto as Exhibit 9 is a true and correct copy of U.S. Publication 2014/0231745.

I declare under penalty of perjury and under the laws of the United States that the foregoing is true and correct. Executed this 4th day of June, 2019, at New York, New York.

/s/ Michael B. Eisenberg
Michael B. Eisenberg

Holland & Knight LLP
400 South Hope Street, 8th Floor
Los Angeles, CA 90071
Tel: 213.896.2400
Fax: 213.896.2450

EXHIBIT 8

US008080833B2

(12) **United States Patent**
Grandusky et al.

(10) **Patent No.: US 8,080,833 B2**
(45) **Date of Patent: Dec. 20, 2011**

(54) **THICK PSEUDOMORPHIC NITRIDE EPITAXIAL LAYERS**

(75) Inventors: **James R. Grandusky**, Waterford, NY (US); **Leo J. Schowalter**, Latham, NY (US); **Shawn R. Gibb**, Clifton Park, NY (US); **Joseph A. Smart**, Mooresville, NC (US); **Shiwen Liu**, Painted Post, NY (US)

(73) Assignee: **Crystal IS, Inc.**, Green Island, NY (US)

(*) Notice: Subject to any disclaimer, the term of this patent is extended or adjusted under 35 U.S.C. 154(b) by 0 days.

(21) Appl. No.: **12/764,584**

(22) Filed: **Apr. 21, 2010**

(65) **Prior Publication Data**

US 2010/0264460 A1 Oct. 21, 2010

Related U.S. Application Data

(63) Continuation-in-part of application No. 12/020,006, filed on Jan. 25, 2008.

(60) Provisional application No. 60/897,572, filed on Jan. 26, 2007, provisional application No. 61/252,408, filed on Oct. 16, 2009.

(51) **Int. Cl.**
H01L 33/00 (2010.01)

(52) **U.S. Cl.** **257/190**; 257/13; 257/94; 257/103; 257/E33.028; 257/E33.067; 438/47

(58) **Field of Classification Search** 257/190, 257/94

See application file for complete search history.

(56) **References Cited**

U.S. PATENT DOCUMENTS

3,531,245	A	9/1970	Dietz
3,600,701	A	8/1971	Gouldthorpe
3,603,414	A	9/1971	Stebley
3,607,014	A	9/1971	Huml et al.
3,634,149	A	1/1972	Knippenberg et al.
3,768,983	A	10/1973	Elkins et al.
3,903,357	A	9/1975	Woolfson et al.
3,933,573	A	1/1976	Dugger
4,008,851	A	2/1977	Hirsch
4,088,515	A	5/1978	Blakeslee et al.
4,234,554	A	11/1980	Rabenau et al.
4,547,471	A	10/1985	Huseby et al.
5,070,393	A	12/1991	Nakagawa et al.
5,087,949	A	2/1992	Haitz
5,292,487	A	3/1994	Tatsumi et al.
5,312,698	A	5/1994	Sato et al.

(Continued)

FOREIGN PATENT DOCUMENTS

DE	102 48 964	4/2004

(Continued)

OTHER PUBLICATIONS

Gaska et al, Applied Physics Letters vol. 81, No. 24 Dec. 9, 2002 "Deep-ultraviolet . . . AlN" pp. 4658-4660.*

(Continued)

Primary Examiner — Jerome Jackson, Jr.
(74) *Attorney, Agent, or Firm* — Bingham McCutchen LLP

(57) **ABSTRACT**

In various embodiments, a semiconductor device includes an aluminum nitride single-crystal substrate, a pseudomorphic strained layer disposed thereover that comprises at least one of AlN, GaN, InN, or an alloy thereof, and, disposed over the strained layer, a semiconductor layer that is lattice-mismatched to the substrate and substantially relaxed.

20 Claims, 8 Drawing Sheets

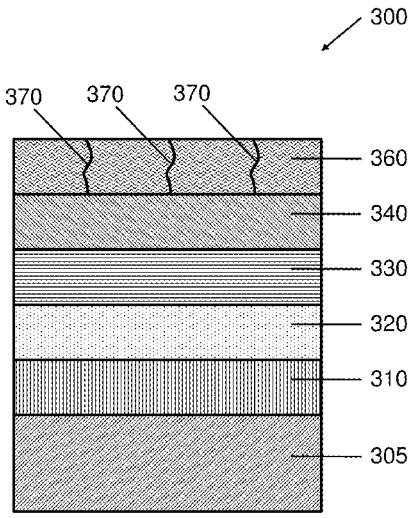

U.S. PATENT DOCUMENTS

5,494,861	A		2/1996	Yamaga et al.
5,520,785	A		5/1996	Evans et al.
5,525,320	A		6/1996	Pratsinis et al.
5,571,603	A		11/1996	Utumi et al.
5,670,798	A	*	9/1997	Schetzina 257/96
5,703,397	A		12/1997	Endo et al.
5,728,635	A		3/1998	Kobayashi et al.
5,858,085	A		1/1999	Arai et al.
5,858,086	A		1/1999	Hunter
5,868,837	A		2/1999	DiSalvo et al.
5,909,036	A		6/1999	Tanaka et al.
5,924,874	A		7/1999	Gotoh et al.
5,954,874	A		9/1999	Hunter
5,972,109	A		10/1999	Hunter
5,981,980	A		11/1999	Miyajima et al.
6,000,174	A		12/1999	Yamazaki et al.
6,001,748	A		12/1999	Tanaka et al.
6,006,620	A		12/1999	Lawrie et al.
6,045,612	A		4/2000	Hunter
6,048,813	A		4/2000	Hunter
6,063,185	A		5/2000	Hunter
6,066,205	A		5/2000	Hunter
6,086,672	A		7/2000	Hunter
6,091,085	A		7/2000	Lester
6,187,089	B1		2/2001	Phillips et al.
6,211,089	B1		4/2001	Kim et al.
6,270,569	B1		8/2001	Shibata et al.
6,296,956	B1		10/2001	Hunter
6,398,867	B1		6/2002	D'Evelyn et al.
6,404,125	B1		6/2002	Garbuzov et al.
6,447,604	B1		9/2002	Flynn et al.
6,468,347	B1		10/2002	Motoki et al.
6,515,308	B1		2/2003	Kneissl et al.
6,548,405	B2		4/2003	Kraus et al.
6,592,663	B1		7/2003	Sarayama et al.
6,596,079	B1		7/2003	Vaudo et al.
6,719,843	B2		4/2004	Schowalter et al.
6,770,135	B2		8/2004	Schowalter et al.
6,777,717	B1		8/2004	Karlicek
6,791,119	B2		9/2004	Slater, Jr. et al.
6,831,302	B2		12/2004	Erchak
6,840,431	B1		1/2005	Kim
6,861,729	B2		3/2005	Kozaki et al.
6,936,357	B2		8/2005	Melnik et al.
6,995,402	B2		2/2006	Ludowise et al.
7,026,659	B2		4/2006	Slater, Jr. et al.
7,037,738	B2	*	5/2006	Sugiyama et al. 438/29
7,037,838	B2		5/2006	Schowalter et al.
7,056,383	B2		6/2006	Helava et al.
7,063,741	B2		6/2006	D'Evelyn et al.
7,087,112	B1		8/2006	Rojo et al.
7,125,734	B2		10/2006	Sackrison
7,186,580	B2		3/2007	Tran et al.
7,211,146	B2		5/2007	Schowalter et al.
7,211,831	B2		5/2007	Erchak et al.
7,244,520	B2		7/2007	Kumakura et al.
7,250,637	B2		7/2007	Shimizu
7,274,043	B2		9/2007	Erchak et al.
7,276,779	B2		10/2007	Shibata
7,288,152	B2		10/2007	Kitaoka et al.
7,420,218	B2		9/2008	Nagai
7,420,222	B2		9/2008	Slater, Jr. et al.
7,439,552	B2		10/2008	Takigawa et al.
7,476,910	B2	*	1/2009	Fujimoto et al. 257/95
7,518,158	B2		4/2009	Keller et al.
7,524,376	B2		4/2009	Wang
7,554,128	B2		6/2009	Okamoto et al.
7,631,986	B2		12/2009	Harrah
7,638,346	B2		12/2009	Schowalter et al.
7,641,735	B2		1/2010	Slack et al.
7,674,699	B2		3/2010	Shibata
7,678,195	B2		3/2010	Schlesser et al.
7,713,844	B2		5/2010	Nishiura et al.
7,755,103	B2		7/2010	Ueno
7,776,153	B2		8/2010	Schowalter
7,803,733	B2		9/2010	Teratani et al.
2001/0000209	A1		4/2001	Krames et al.
2001/0024871	A1		9/2001	Yagi
2001/0051433	A1		12/2001	Francis et al.
2002/0170490	A1		11/2002	Vodakov et al.
2003/0047816	A1		3/2003	Dutta
2003/0160254	A1		8/2003	Henrichs
2003/0168003	A1		9/2003	Schowalter et al.
2003/0213964	A1		11/2003	Flynn
2003/0216011	A1		11/2003	Nakamura et al.
2004/0130002	A1		7/2004	Weeks et al.
2004/0187766	A1		9/2004	Letertre
2004/0206978	A1		10/2004	Saxler
2004/0213309	A9		10/2004	Amano et al.
2004/0224484	A1		11/2004	Fareed et al.
2004/0226917	A1		11/2004	Laconto et al.
2004/0245535	A1		12/2004	D'Evelyn et al.
2005/0062392	A1		3/2005	Sakai et al.
2005/0072986	A1		4/2005	Sasaoka
2005/0103257	A1		5/2005	Xu et al.
2005/0142391	A1		6/2005	Dmitriev et al.
2005/0161697	A1		7/2005	Nakahata et al.
2005/0214992	A1		9/2005	Chakraborty et al.
2005/0269577	A1		12/2005	Ueda et al.
2005/0277214	A1		12/2005	Uematsu et al.
2005/0285141	A1		12/2005	Piner et al.
2006/0005763	A1		1/2006	Schowalter et al.
2006/0029832	A1		2/2006	Xu et al.
2006/0054075	A1		3/2006	Dwilinski et al.
2006/0244011	A1		11/2006	Saxler
2006/0255341	A1		11/2006	Pinnington et al.
2006/0281205	A1		12/2006	Park
2006/0288929	A1		12/2006	Slack et al.
2007/0018184	A1		1/2007	Beeson et al.
2007/0101932	A1		5/2007	Schowalter et al.
2007/0102721	A1		5/2007	Denbaars et al.
2007/0131160	A1		6/2007	Slack et al.
2007/0134827	A1		6/2007	Bondokov et al.
2007/0243653	A1		10/2007	Morgan et al.
2007/0257333	A1		11/2007	Schlesser et al.
2008/0012034	A1		1/2008	Thielen et al.
2008/0036038	A1		2/2008	Hersee et al.
2008/0054280	A1		3/2008	Reginelli et al.
2008/0121910	A1		5/2008	Bergmann et al.
2008/0135861	A1		6/2008	Pokrovskiy et al.
2008/0142817	A1		6/2008	Ibbetson et al.
2008/0144688	A1		6/2008	Chua et al.
2008/0149945	A1		6/2008	Nagai
2008/0149960	A1		6/2008	Amo et al.
2008/0157111	A1		7/2008	Erchak et al.
2008/0173887	A1		7/2008	Baba et al.
2008/0182092	A1		7/2008	Bondokov et al.
2008/0187016	A1		8/2008	Schowalter et al.
2008/0191225	A1		8/2008	Medendorp
2008/0251808	A1		10/2008	Kususe et al.
2008/0258165	A1		10/2008	Zimmerman et al.
2009/0008654	A1		1/2009	Nagai
2009/0014742	A1		1/2009	Erchak
2009/0039373	A1		2/2009	Saito et al.
2009/0050050	A1		2/2009	Slack et al.
2009/0065791	A1		3/2009	Yen et al.
2009/0078957	A1		3/2009	Hoshina
2009/0121246	A1		5/2009	Denbaars et al.
2009/0121250	A1		5/2009	Denbaars et al.
2009/0140279	A1		6/2009	Zimmerman et al.
2009/0141502	A1		6/2009	Sonoda et al.
2009/0155989	A1		6/2009	Uematsu et al.
2009/0159910	A1		6/2009	Lin et al.
2009/0166657	A1		7/2009	Yamada et al.
2009/0173958	A1		7/2009	Chakraborty et al.
2009/0233394	A1		9/2009	Batres et al.
2009/0239357	A1		9/2009	Amano et al.
2009/0256163	A1		10/2009	Chakraborty
2009/0261372	A1		10/2009	Ueda
2009/0267098	A1		10/2009	Choi
2009/0278148	A1		11/2009	Nabekura et al.
2009/0315054	A1		12/2009	Kim et al.
2009/0321758	A1		12/2009	Liu et al.
2009/0321771	A1		12/2009	Hattori et al.
2010/0006870	A1		1/2010	Lee et al.
2010/0012956	A1		1/2010	Yoo et al.
2010/0025717	A1		2/2010	Fujii et al.

2010/0025719	A1	2/2010	Li
2010/0135349	A1	6/2010	Schowalter et al.
2010/0187541	A1	7/2010	Slack et al.
2010/0264460	A1	10/2010	Grandusky et al.
2010/0314551	A1	12/2010	Bettles et al.
2011/0008621	A1	1/2011	Morgan et al.
2011/0011332	A1	1/2011	Rojo et al.

FOREIGN PATENT DOCUMENTS

EP	0 609 799	8/1994
EP	0 811 708	12/1997
EP	0 979 883	2/2000
EP	1 211 715	6/2002
EP	1 732 145	12/2006
EP	1 754 810	2/2007
EP	2 099 068	9/2009
JP	61/236686	10/1986
JP	02/018379	1/1990
JP	03/285075	12/1991
JP	4355920	12/1992
JP	00/154090	6/2000
JP	01/192647	7/2001
JP	06/169173	6/2006
WO	WO-99/34037	7/1999
WO	WO-00/22203	4/2000
WO	WO-01/11116	2/2001
WO	WO-03/007383	1/2003
WO	WO-03/081730	10/2003
WO	WO-2005/012602	2/2005
WO	WO-2006/110512	10/2006
WO	WO-2007/062250	5/2007
WO	WO-2008/042020	4/2008

OTHER PUBLICATIONS

Arulkumaran et al., "Improved dc characteristics of AlGaN/GaN high-electron-mobility transistors on Aln/sapphire templates," (2002) *Applied Physics Letters*, vol. 81, No. 6, pp. 1131-1133.

Balkas et al., "Sublimation Growth and Characterizations of Bulk Aluminum Nitride Single Crystals," *J. Crystal Growth*, (1997) 179, p. 363.

Barin, *Thermochemical Data of Pure Substances, 2nd Ed.*, (1993) pp. 42, 1334-1335, 1337, 1381-1382, 1636-1639.

Bickermann et al., "Characterization of bulk AlN with low oxygen content," *Jrl. of Crys. Growth*, vol. 269, Nos. 2-4, pp. 432-442.

Bockowski et al., "Combustion Synthesis of Aluminum Nitride Under High Pressure of Nitrogen and Nitrogen-Argon Mixtures," *5 J. Mat. Synthesis & Processing 6*, (1997) pp. 449-458.

Bolgar et al., "Vaporization of the Nitirides of B, Al, and Ga," in *Khim Fiz. Nitrodov*, pp. 151-156 (1968) [Chem Abstr. 71, 34003j (1969)].

Chase et al., *J. Phys. Chem. Ref.* Data 14, Supplement No. 1 (1985).

Chase, *J. Phys. Chem.*, Ref. Data, Monograph No. 9, NIST-JANAF Thermochemical Tables, 4th Ed. (1998).

Chitnis et al., "Milliwatt Power AlGaN Quantum Well Deep Ultraviolet Light Emitting Diodes," *Phys. Sat. Sol.* (*a*), (2003) vol. 200, No. 1, pp. 99-101.

Constantin et al., "Mixing rocksalt and wurtzite structure binary nitrides to form novel ternary alloys: ScGaN and MnGaN," *Mat. Res. Soc. Symp. Proc.*, 799 (2004) Z9.5.1.

Cox et al., "On the Preparation, Optical Properties and Electrical Behaviour of Aluminum Nitride," *J. Phys. Chem. Solids*, (1967) vol. 28, pp. 543-548.

Dalmau et al., Mat. Res. Soc. Proc., (2004) vol. 798, p. Y2.9.1.

DeVries et al., "Phase equilibria pertinent to the growth of cubic boron nitride," J. Cryst. Growth, 13/14 (1972) 88.

Dryburgh, "The Estimation of Maximum Growth Rate for Aluminum Nitride Crystals by Direct Sublimation," J. Crystal Growth, (1992) 125, pp. 65-68.

Dugger, "The single crystal synthesis and some properties of Aluminum Nitride", Air Force Cambridge Research Laboratories, Physical Science Research Papers, No. 656 (Aug. 1, 1975).

Dugger, The synthesis of Aluminum Nitride single crystals:, *Mat. Res. Bulletin*, 9 (1974) 331.

Epelbaum et al., "Sublimation growth of bulk AlN crystals: materials compatibility and crystal quality," *Mat. Sci. Forum*, (2002) 389-393, 1445.

Gorbatov et al., "Electrical Conductivity of Materials from Mixed Aluminum and Silicon Nitrides," *Sov. Powd. Met. Met. Ceram.*, (1970) vol. 9, pp. 917-920.

Hacke et al., "Photoluminescence Intensity and Spectral Distribution of GaN Films on SiC," (1999) *Phys. Stat. Sol.* (*b*), 216, 639.

Hermann et al., "Highly Si-doped AlN Grown by Plasma-Assisted Molecular-Beam Epitaxy," *Applied Phys. Letters*, (2005) vol. 86, pp. 192108-1-192108-3.

Honig, "Vapor Pressure Data for the Solid and Liquid Elements", *RCA Review*, vol. 23 (1962).

International Search Report and Written Opinion for PCT/US2006/022329, mailed Dec. 12, 2006.

International Preliminary Report on Patentability and Written Opinion for PCT/US2006/045540, mailed Jun. 12, 2008.

International Preliminary Report on Patentability and Written Opinion for PCT/US2006/046300, mailed Jun. 12, 2006.

International Search Report and Written Opinion for PCT/US2007/011075, mailed Jul. 11, 2008.

International Search Report and Written Opinion for PCT/US2007/07980, mailed Oct. 12, 2007.

International Search Report and Written Opinion for PCT/US2008/000597, mailed May 20, 2008.

International Search Report and Written Opinion for PCT/US2008/001003, mailed Aug. 5, 2008.

International Search Report for PCT/US2006/045540, mailed Jul. 6, 2007.

International Search Report for PCT/US2006/046300, mailed May 30, 2007.

Jahnen et al., "Pinholes, Dislocations and Strain Relaxation in InGaN," *MRS Internet J. Nitride Semicond. Res.*, (1998) 3:39.

Kanechika et al., "n-type AlN Layer by Si Ion Implantation," *Applied Phys. Letters*, (2006) vol. 88, p. 202106.

Karel et al., "The luminescence properties of AlN with Manganese and rare earth activators under ultraviolet and cathode-ray excitation", *Czech. J. Phys.*, B20 (1970) 46.

Karpinski et al., "Equilibrium pressure of N_2 over GaN and high pressure solution growth of GaN", *J. Cryst. Growth*, 66 (1984) 1.

Karpov et al., "Sublimation Growth of AlN in Vacuum and in a Gas Atmosphere," *Phys. Stat. Sol.* (*a*), (1999) 176, p. 435.

Kasu et al., "Formation of Solid Solution of Al1-xSixN (0<x?12%) Ternary Alloy," *Jap. J. Appl. Phys.*, (2001) vol. 40, Part 2, No. 10A, pp. L1048-L1050.

Kawabe et al., "Electrical and Optical Properties of AlN-a Thermostable Semiconductor," *Elec. Engin. In Japan*, (1967) vol. 87, pp. 62-70.

Kordis, "The BeO-MgO system", *J. Nuc. Mater.*, 14 (1964) 322.

Lawson et al., "Preparation of Single Crystals", Academic Press, New York (1958) pp. 18-20.

Liu et al., "A Global Growth Rate Model for Aluminum Nitride Sublimation," *J. Electrochemical Soc.*, (2002) 149, p. G12.

Liu et al., "Characterization of AlN Crystals Grown by Sublimation," *Phys. Stat. Sol.* (a), (2001) 18, p. 769.

Liu et al., "Misfit Dislocation Generation in InGaN Epilayers on Free-Standing GaN," *Jap. J. Appl. Physics*, (2006) 46:22, pp. L549-L551.

Ludwig et al., "Dimers [Al_2N_4]", *Zeitsch. f. Naturforsch.*, B54 (1999) pp. 461-465.

Matthews et al., "Defects in Epitaxial Multilayers," *J. Crystal Growth*, (1974) 27, p. 118.

Mokhov et al., "Sublimation growth of AlN bulk crystals in Ta crucibles," *Jrl. of Crys. Growth*, (Jul. 15, 2005) vol. 281, No. 1, pp. 93-100.

Naidu et al., Eds. "Phase Diagrams of Binary Tungsten Alloys," Indian Institute of Metals, Calcutta, pp. 7-13 (1991).

Nakanishi et al., "Effects of Al Composition on luminescence properties of europim implanted $Al_xGa_{1-x}N$ (0∠×∠1)", *Phys. Stat. Sol.* (c), 0 (2003) 2623.

Nassau et al., "The Physics and Chemistry of Color," Wiley-Interscience Publication (New York 1983).

Niewa et al., "$Li_3[ScN_2]$: The first nitridoscandate (III)—Tetrahedral Sc Coordination and unusual MX_2 framework", *Chem. Eur. J.* 9 (2003) 4255.

Niewa et al., "Recent developments in nitride chemistry", *Chem. Mater.*, 10 (1998) 2733.
Noveski et al., "Growth of AlN Crystals on AlN/SiC Seeds by AlN Powder Sublimation in Nitrogen Atmosphere," *MRS Internet J. Nitride Semicond. Res.*, (2004) 9, 2.
Noveski et al., "Mass Transfer in AlN Crystal Growth at High Temperatures," *J. Crystal Growth*, (2004) 264, pp. 369-378.
Office Action in Japanese Patent Application No. 2003-579324, May 27, 2008 (English Translation).
Sun et al., "Phase relationships in the system Y-Al-O-N", *Mater. Letters*, 3-4 (1991) 76.
Parker et al., "Determination of the critical layer thickness in the InGaN/GaN heterostructures," *Applied Phys. Letters.*, (1999) vol. 75, No. 18, pp. 2776-2778.
Proc. of NATO Advanced Study Inst. on Nitrogen Ceramics, University of Kent, Canterbury, U.K. (1976).
Raghothamachar et al., "Synchrotron White Beam Topography Characterization of Physical Vapor Transport Grown AlN and Ammonothermal GaN," *J. Crystal Growth*, (2002) 246, pp. 271-280.
Rojo et al., "Growth and Characterization of Epitaxial Layers on Aluminum Nitride Substrates Prepared from Bulk, Single Crystals," *J. Crystal Growth*, (2002) 240, p. 508.
Rojo et al., "Progress in the Preparation of Aluminum Nitride Substrates from Bulk Cystals," *Mat.Res. Soc. Symp. Pro.*, (2002) vol. 722, pp. 5-13.
Rojo et al., "Report on the Growth of Bulk Aluminum Nitride and Subsequent Substrate Preparation," *J. Crystal Growth*, (2001) 231, p. 317.
Schlesser et al., "Growth of AlN Bulk Crystals from the Vapor Phase," *Mat. Res. Soc. Symp. Proc.*, (2002) 693, p. I9.4.1.
Schlesser et al., "Seeded Growth of AlN Bulk Single Srystals by Sublimation," *J. Crystal Growth*, 241, pp. 416-420.
Schowalter et al., "Fabrication of Native, Single-Crystal AlN Substrates," *Phys. Stat. Sol.* (*c*), (2003) 1-4.
Segal et al., "On Mechanisms of Sublimination Growth of AlN bulk Crystals," *J. Crystal Gowth*, (2000) 211, pp. 68-72.
Shih et al, "High-quality and crack-free $A1_xGa_{1-x}N$ (x-0.2) grown on sapphire by a two-step growth method," *Jrl. of Crys. Growth*, (Apr. 15, 2005) vol. 277, No. 1-4, pp. 44-50.
Silveira et al., "Excitonic Structure of Bulk AlN from Optical Reflectivity and Cathodoluminescense Measurements," *Phys. Review* B71, 041201® (2006).
Singh et al., "Physical Vapor Transport Growth of Large AlN Crystals," *J. Cryst. Growth*, (2003) 250, p. 107.
Slack et al., "AlN Single Crystals," *J. Crystal Growth*, (1977) 42, pp. 560-563.
Slack et al., "Growth of High Purity AlN Crystals," *Journal of Crystal Growth*, (1976) vol. 34, pp. 263-279.
Slack et al., "Properties of Crucible Materials for Bulk Growth of AlN," *Mat. Res. Soc. Proc.*, (2004) vol. 798, pp. Y10.74.1-Y10.74.4.
Slack et al., "Some Effects of Oxygen Impurities on AlN and GaN," *J. Crystal Growth*, (2002) 246, pp. 287-298.
Smart et al., "AlGaN/GaN Heterostructures on Insulating AlGaN Nucleation Layers," *Appl. Phys. Letters*, (1999) 75, p. 388.
Solid State Lighting Report (Dept. of Energy, 2007).
Song, "Strain relaxation due to V-pit formation in InxGa1-xN/GaN epilayers grown on sapphire," *J. Applied Phys.*, (2005) 98: 084906.
Takeuchi et al., "Optical Properties of Strained AlGaN and GaInN on GaN," *Jap. J. Appl. Phys.*, (1997) vol. 36, pp. L177-L179.
Takeya et al., "Degradation in AlGaInN Lasers," *Phys. Stat. Sol.* (*c*), (2003) 0, No. 7, pp. 2292-2295.
Taniyasu et al., "An aluminum nitride light-emitting diode with a wavelength of 210 nanometres", *Nature*, 441 (2006) 325.
Taniyasu et al., "Intentional control of n-type conduction for Si-doped AlN and $Al_xGa_{1-x}N$ (0.42∠×∠1)", *Applied Physics Letters*, 81 (2002) 1255.
Tomiya et al., "Dislocations in GaN-Based Laser Diodes on Epitaxial Lateral Overgrown GaN Layers," *Phys. Stat. Sol.* (*a*), (2001) vol. 188, No. 1, pp. 69-72.
Van de Walle et al., "Doping of AlGaN Alloys," *MRS Internet J. Nitride Semicond. Res.*, (1999) 4S1, G10.4, pp. 1-12.
Van de Walle et al., "DX-center Formation in Wurtzite and Zinc-blende AlxGa1-xN," *Phys. Rev.*, (1998) B57, R2033.
Vendl et al., "The melting points of some rare-earth metal nitrides as function of the nitrogen pressure", High Temperatures—High Pressures, 9 (1977) 313.
Venugopal et al., "Comparison of Various Buffer Schemes to Grow GaN on Large-Area Si(111) Substrates Using Metal-Organic Chemical-Vapor Deposition," *32 J. Electronic Mat.*, vol. 32, No. 5 (2003) pp. 371-374.
Vinogradov et al., "Determination of the Melting Parameters of Aluminum Nitride," *High Temperatures—High Pressures*, (1991) 23:685.
Wentorf Jr., "Synthesis of the cubic form of boron nitride", *J. Chem. Phys.*, 34 (1961) 809.
Yamane et al., "Preparation of GaN single crystals using a Na flux", *Chem. Mater.*, 9 (1997) 413.
Yano et al., "Growth of nitride crystals, BN. AlN and GaN by using a Na flux", *Diamond and Related Materials*, 9 (2000) 512.
Zeisel et al., "DX-behavior of Si in AlN," *Phys. Rev.*, (2000) B61, R16283.
Zhuang et al., "Seeded growth of AlN single crystals by physical vapor transport," *Jrl. of Crys. Growth*, (Jan. 25, 2006), vol. 287, No. 2, pp. 372-375.
Atobe—JJAP, 29, 150, 1990—F-Type Centers in Neutron-Irradiated AlN.
Berzina—RadEFF 157, 1089, 2002—Luminescence mechanisms of O-related defects in AlN.
Bickermann et al., "Point Defect Content and Optical Transitions in Bulk Aluminum Nitride Crystals," Phys. Stat. Sol. B 246, No. 6, pp. 1181-1183 (2009).
Bickerman pssc 0, 1993-1996, 2003—PVT growth of bulk AlN.
Bickerman—APL,103,073522, 2008—Polarization dependent below BG optical absorption of AlN bulk crystals.
Bradley—JVacSciTechB 21, 2558, 2003—Deep level defects and doping in high Al mole fraction AlGaN.
Summons to Attend Oral Proceedings in European Patent Application No. 03808366.3, Dec. 17, 2007, 5 pages.
Tavernier et al., "Chemical Mechanical Polishing of Gallium Nitride," Electrochemical and Solid State Latters, v. 5(8), pp. G61-G64 (2002).
Brunner—JAppPhys 82, 5090, 1997—Optical constants of epitaxial AlGaN films and their temperature dependence.
Collins—PRB 158, 833, 1967—Lattice vibration spectra of AlN.
Edgar—JCrGrwth 310, 4002, 2008-Native oxide and hydroxides and their implications for bulk AlN crystal growth.
Evans—APL 88, 06112, 2006—EPR of a donor in AlN crystals.
Freitas—pssb 240, 330, 2003—Shallow donors in GaN.
Freitas—APL 83, 2584,2003—Properties of bulk AlN grown by thermodecomposition of AlCl3-NH3.
Freitas—JCrGrwth 281, 168, 2005—Optical studies of bulk and homoepitaxial films of III-V nitride semiconductors.
Gutierrez—Phil.Mag.Let. 79, 147, 1999—The formation of nanopipes caused by donor impurities in GaN; a theoretical study for the case of oxygen.
Honda—JJAP 29, L652, 1990—Electron paramagnetic center in neutron-irradiated AlN.
Hossain—SPIE 2877, 42, 1996—Study of CL spectroscopy of AlN.
Jones—JMR 14, 4344, 1999—Optical properties of Aln from VUS and ellipsometry.
Kazan—Diamond15, 1525, 2006—Phonon dynamics in AlN lattice contaminated by O.
Kazan—JAP, 98, 103529,2005—Oxygen behavior in AlN.
Klemens—PhysB, 316-317,413, 2002—Effect of point defects on the decay of the longitudinal optical mode.
Kovalenkov—JCrGrwth 28187, 2005—Thick AlN layers grown by HVPE.
Mason—PRB 59, 1937, 1999—Optically detected EPR of AlN single crystals.
McCluskey—PRL 80 4008 1998—Metastability of oxygen donors in AlGaN.
Meyer—Mat.Scie.EngB71,69,2000—Defects and defect identication in group III-nitrides.
Morita—JJAP 21, 1102, 1982—Optical absorption and CL of epitaxial AlN films.

Nakahata—JAmCerSoc 80, 1612, 1997—Electron spin resonance analysis of lattice defects in poly AlN.
Nakarmi—APL 94, 091903, 2009—PL studies of impurity transitions Mg-doped AlGaN alloys.
Nam—APL 86, 222108, 2005—Deep Impurity transitions involving cation vacancies and complexes in AlGaN alloys.
Nepal—APL 84, 1091, 2004—Optical properties of the nitrogen vacancyin AlN epilayers.
Nepal—APL 89, 092107, 2006—Photoluminescene studies of impurity transitions in AlGaN alloys.
Wongchotigul et al., "Low Resistivity Aluminum Nitride:Carbon (AlN:C) Films Grown by Metal Organic Chemical Vapor Deposition," 26 Materials Letters, pp. 223-226 (Mar. 1996).
Pantha—APL 91, 121117, 2007—Correlation between biaxial stress and free exciton transition in AlN.
Perry and Rutz—APL 33, p319, 1978—The optical absorption edge of single-crystal AlN prepared by a closed-spaced vapor process.
Salzman—pssc 0, 2541, 2003—Reduction of oxygen contamination in AlN.
Sarua—MRS 798, Y17.1, 2004—Effect of impurities on Raman and PL spectra of AlN bulk crystals.
Schlesser—JCrGrwth 281, 75, 2005—Crucible materials for growth of aluminum nitride crystals.
Schweizer—ppsb 219, 171, 2000—Investigation of oxygen-related luminescence centres in AlN ceramic.
Sedhain—APL 93, 014905, 2008—Photoluminescence properties of AlN homeopilayers with different orientations.
Shi—APL89, 163127, 2006—Luminescence properties of AlN nanotips.
Stampfl—PRB 65, 155212, 2002—Theoretical investigation of native defects, impurities and complexes in aluminum nitride.
Strassburg—JAP 96, 5870,2004—Growth and optical properties of large high quality AlN single crystals.
Thomas—J.Eur.Cer.Soc. 1991—Determination of the concentration of oxygen dissolved in the AlN lattice.
Trinkler—JphysCondMatt 13, 8931, 2001—Radiation induced recombination processes in AlN ceramics.
Trinkler—RadiationMeasurements 33, 731, 2001—Stimulated luminescence of AlN ceramics induced by UV radiation.
Trinkler—SPIE 2967, 85, 1997—Spectral properties of AlN ceramics.
Tuomisto—JCrGrwth 2008—Characterization of bulk AlN crystals with position annihilation spectroscopy.
Vail—JPhysCondMat18,21225, 2006—The nitrogen vacancy in AlN.
Van de Walle—AppPhysRev 95,3852 2004—First principles calculations for defects and impurities—Application s to iii-nitrides.
Watanabe—JMR13,2956,1998—Changes in optical transmittance and surface morphology of AlN thin films exposed to atmosphere.
Katayama-Yoshida et al., "Codoping method for the Fabrication of Low-Resistivity Wide Band-Gap Semiconductors in p-type GaN, p-type AlN and n-type Diamond: Prediction versus Experiment," 13 J. of Physics: Condensed Matter, pp. 8901-8914 (2001).
Office Action in Australian Patent Application No. 2003303485, Oct. 9, 2008, 2 pages.
Office Action in Canadian Patent Application No. 2,467,806, Aug. 13, 2009, 4 pages.
Office Action in Canadian Patent Application No. 2,467,806, Feb. 23, 2010, 2 pages.
Office Action in European Patent Application No. 02803675.4, May 2, 2007, 4 pages.
Office Action in European Patent Application No. 02806723.9, Aug. 8, 2008, 3 pages.
Office Action in European Patent Application No. 02806723.9, dated Feb. 16, 2010 (2 pages).
Office Action in European Patent Application No. 02806723.9, Feb. 7, 2007, 4 pages.
Office Action in European Patent Application No. 02806723.9, Jan. 17, 2008, 4 pages.
Office Action in European Patent Application No. 03808366.3, dated Sep. 28, 2006, 4 pages.
Office Action in European Patent Application No. 06844804.2, Mar. 4, 2009, 3 pages.
Office Action in Japanese Patent Application No. 2003-545445, mailed Nov. 10, 2009, 3 pages (translation).
Office Action in Japanese Patent Application No. 2003-545445, mailed Sep. 30, 2008, 3 pages (translation).
Office Action in Japanese Patent Application No. 2003-579324, Sep. 8, 2009, 1 page (translation).
Office Action in Japanese Patent Application No. 2004-564648, Feb. 3, 2010, 2 pages (translation).
Office Action in Japanese Patent Application No. 2004-564648, Jun. 24, 2009, 2 pages (translation).
Office Action in Taiwan Patent Application No. 91137050, Apr. 6, 2004, 1 page (translation).
Partial International Search Report for International Application No. PCT/US07/11075, dated May 7, 2008 (2 pages).
Raghothamachar et al., "X-ray Characterization of Bulk AlN Single Crystals Grown by the Sublimation Technique," J. Crystal Growth 250(1-2), pp. 244-250 (2003).

* cited by examiner

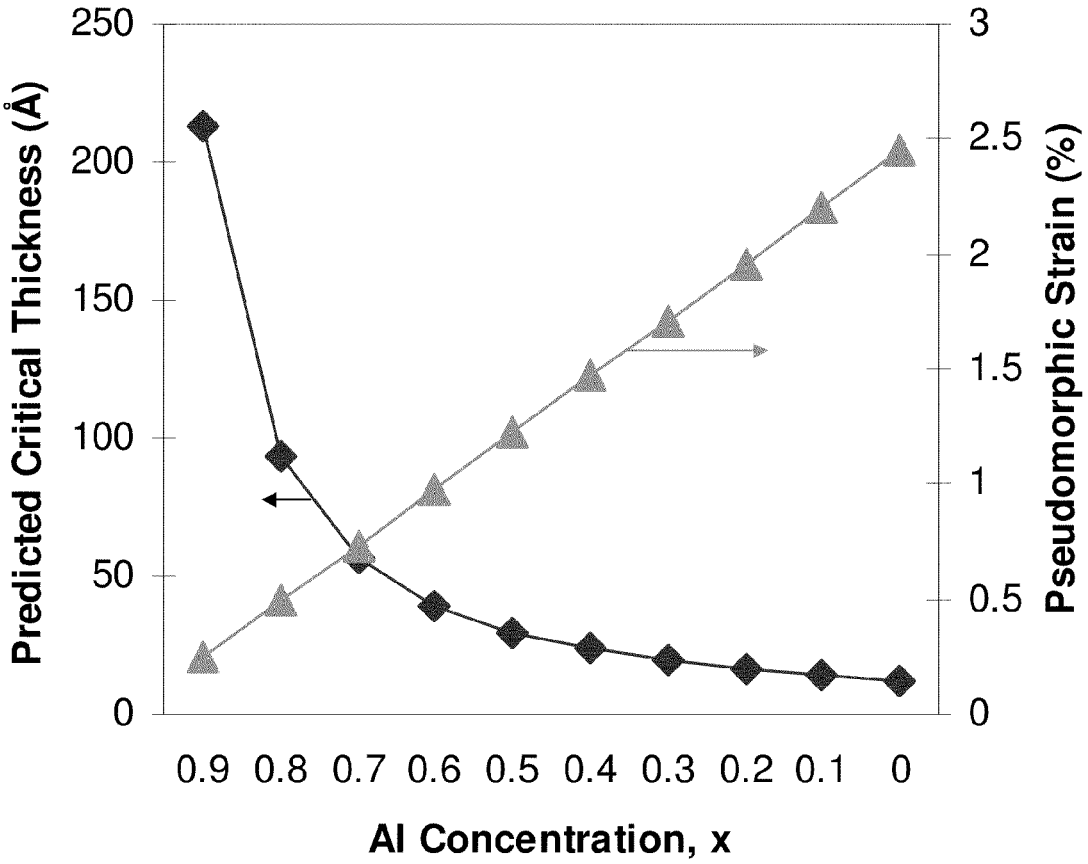
Predicted Critical Thickness (Å)
250
200
150
100
50
0
3
2.5
2
1.5
1
0.5
0
Pseudomorphic Strain (%)
0.9 0.8 0.7 0.6 0.5 0.4 0.3 0.2 0.1 0
Al Concentration, x

FIG. 1

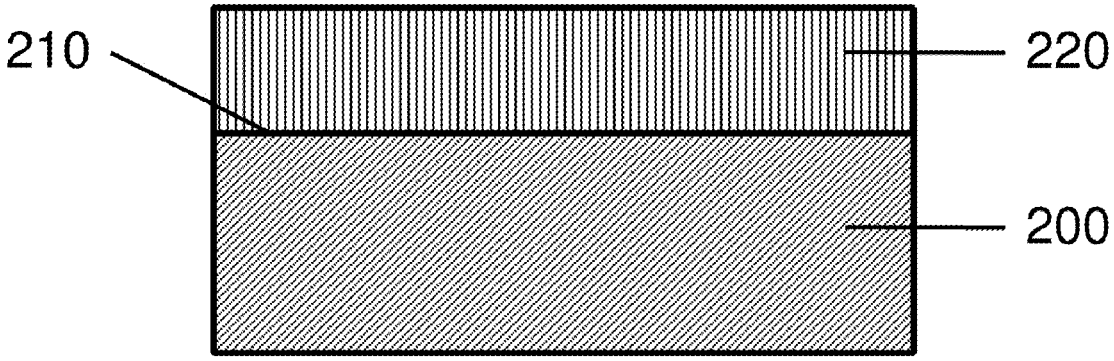

FIG. 2

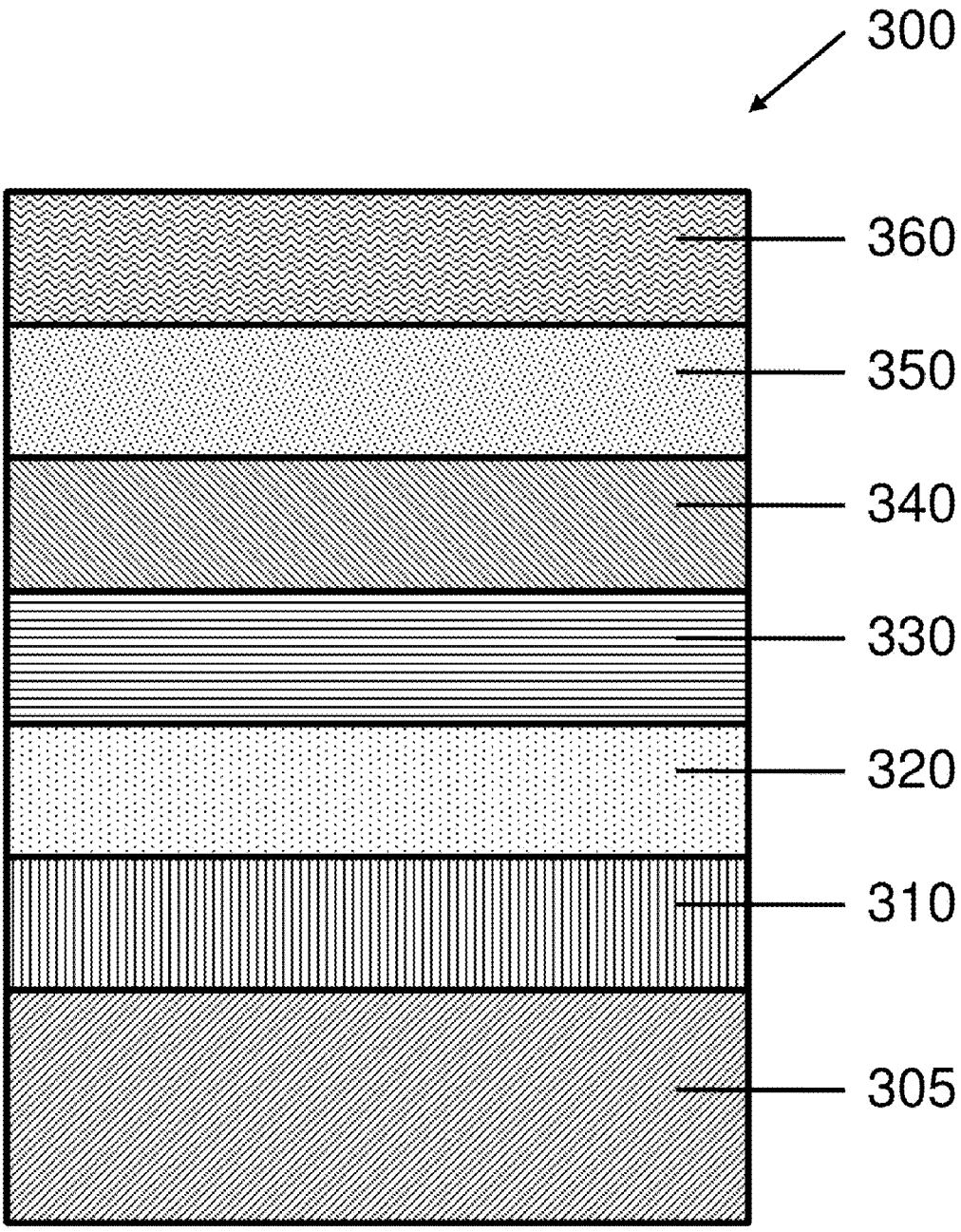

FIG. 3A

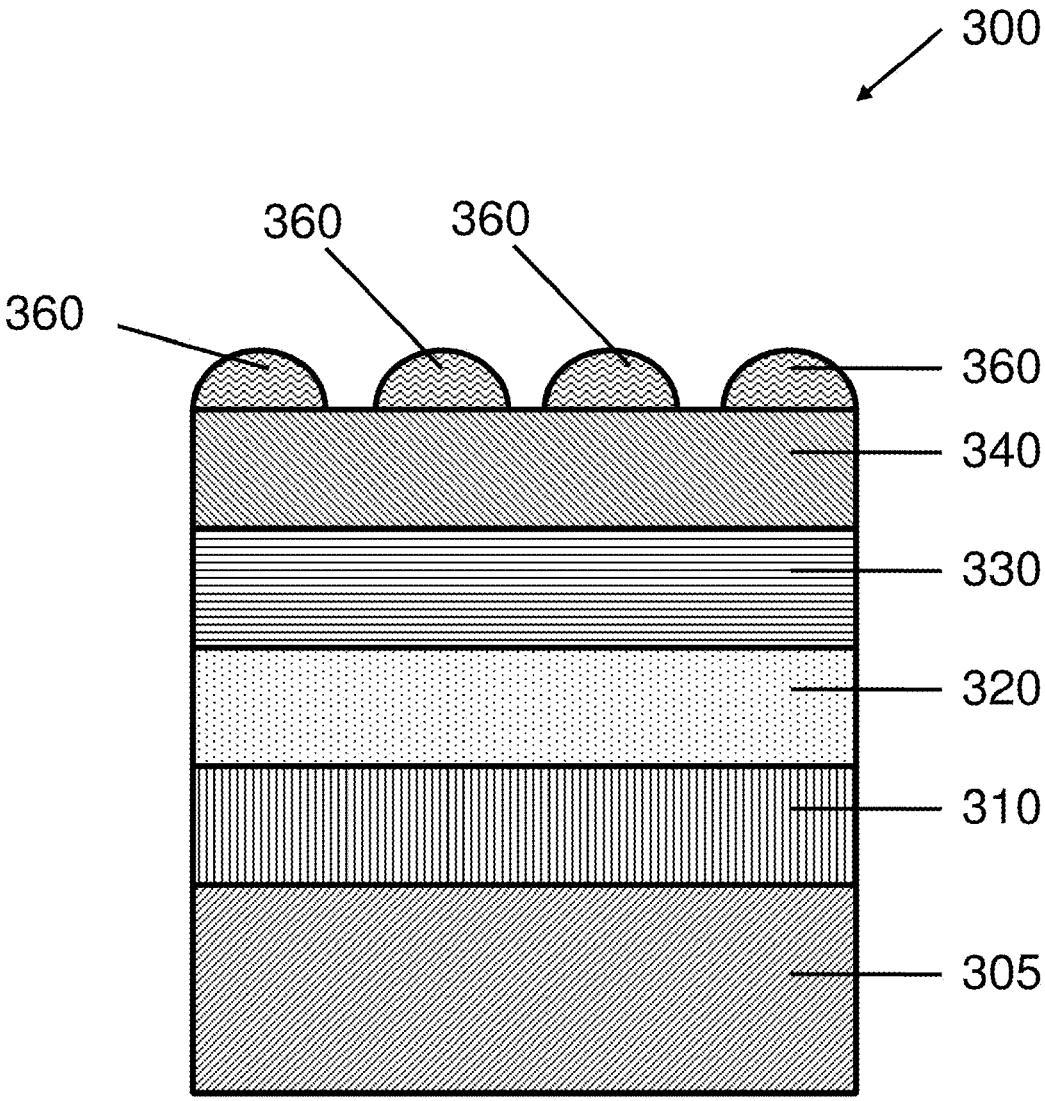

FIG. 3B

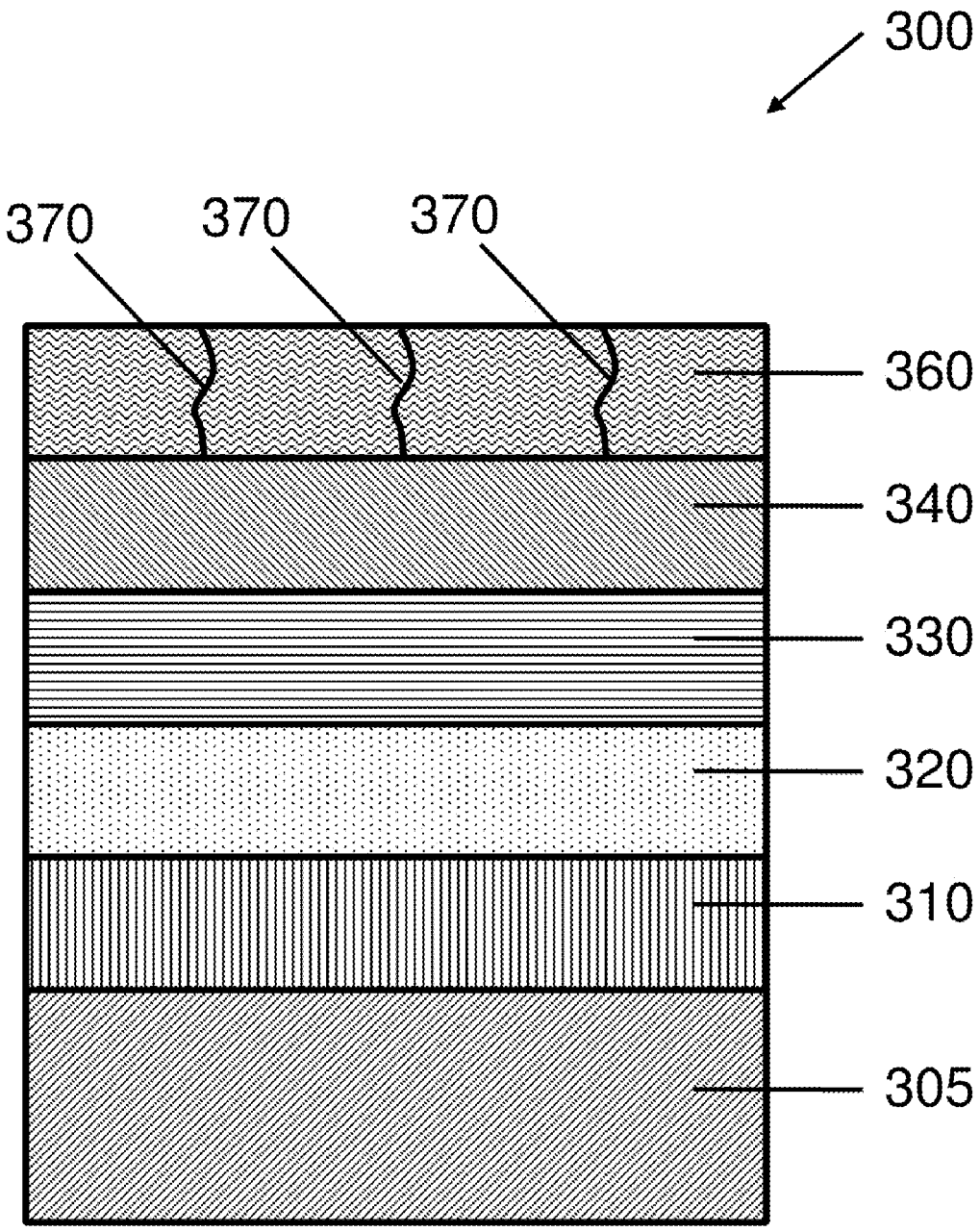

FIG. 3C

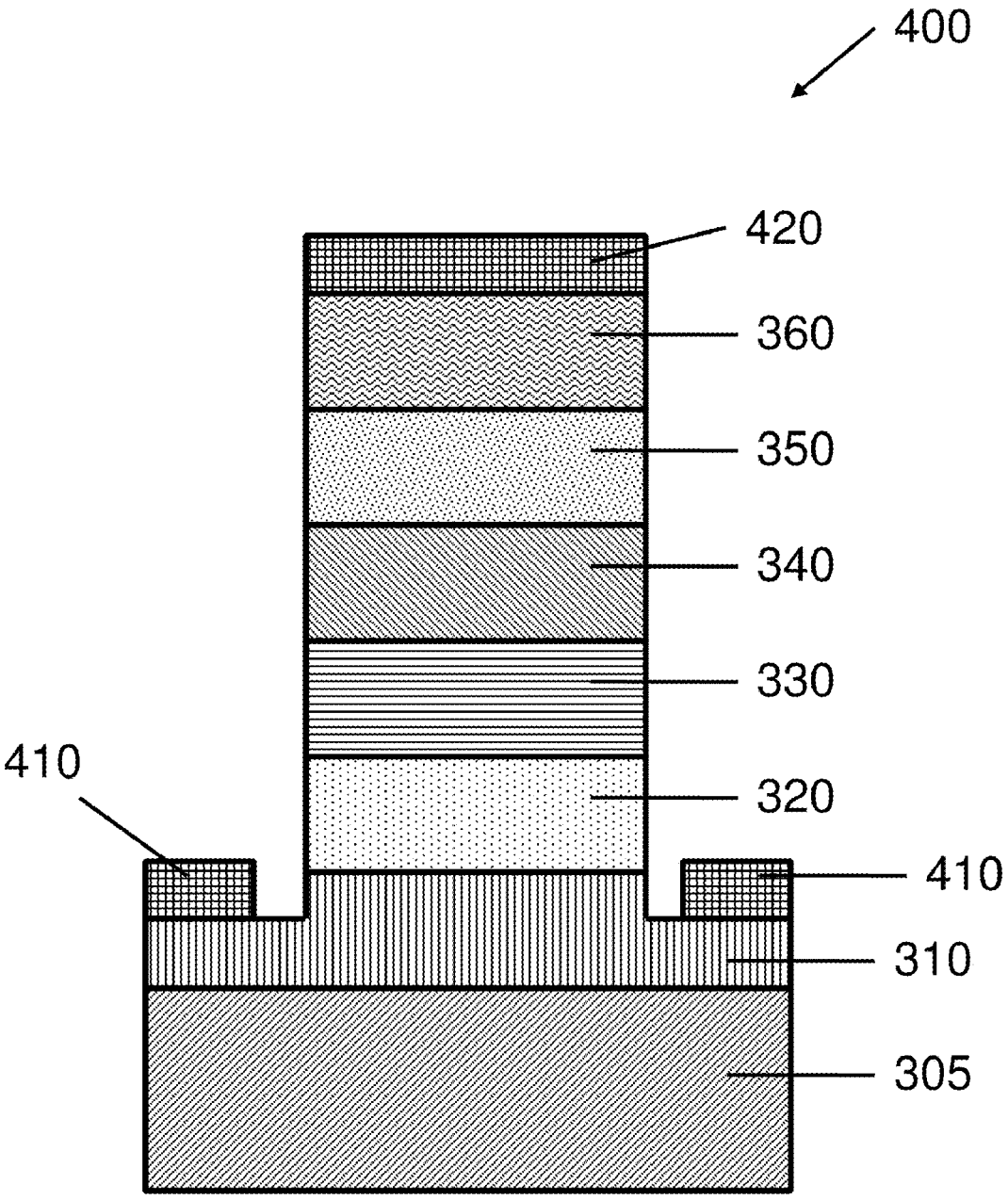

FIG. 4A

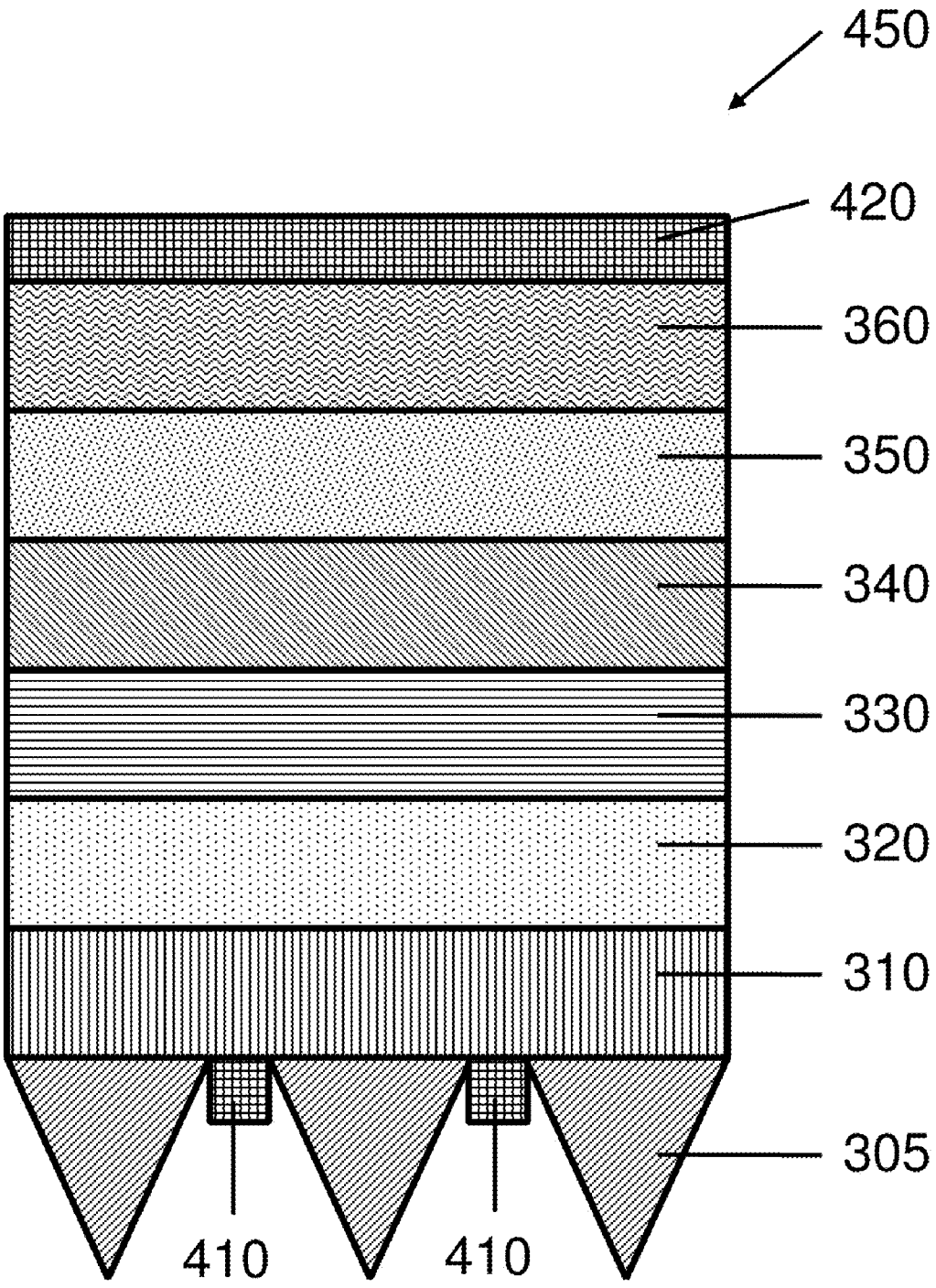

FIG. 4B

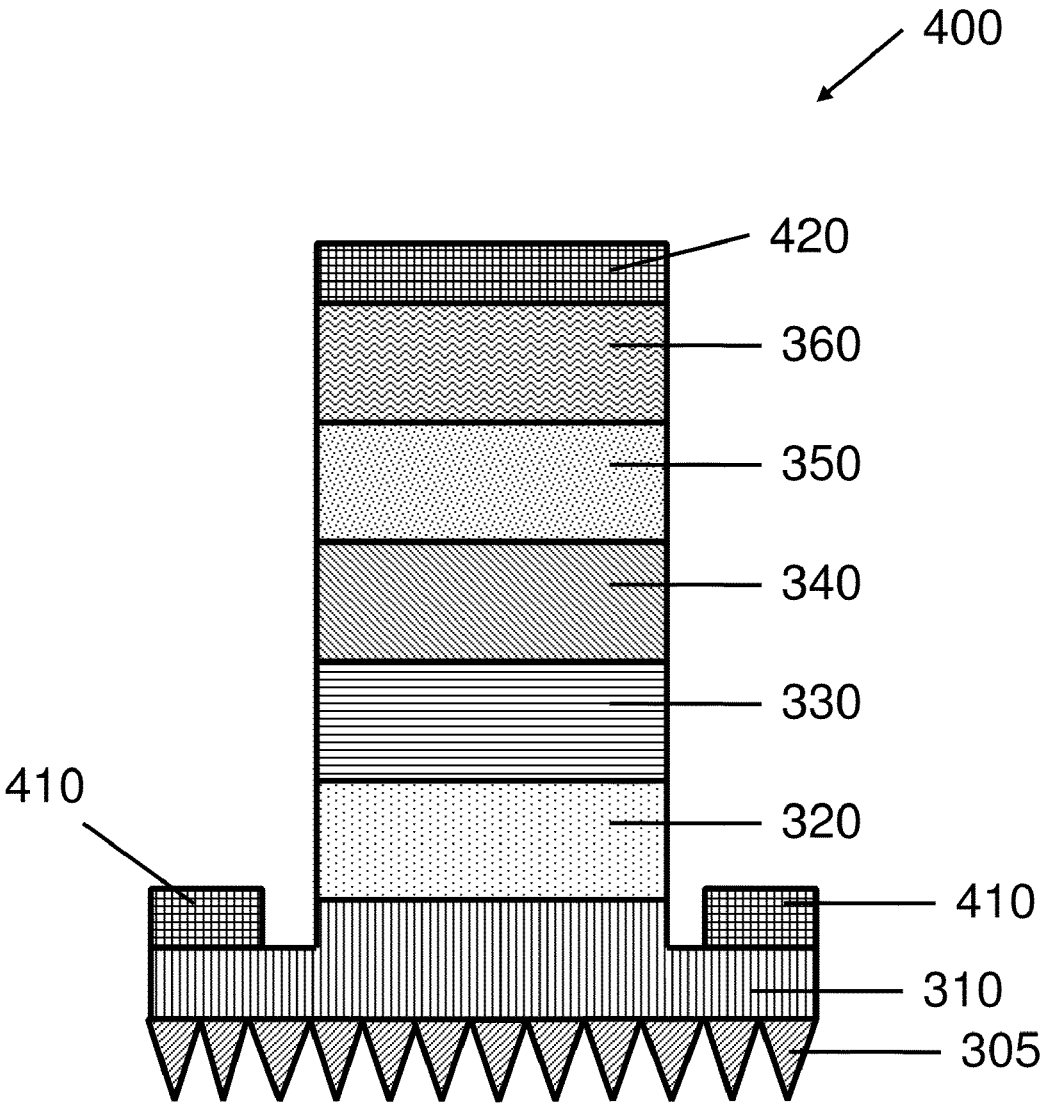

FIG. 4C

THICK PSEUDOMORPHIC NITRIDE EPITAXIAL LAYERS

RELATED APPLICATIONS

This application is a continuation-in-part of U.S. patent application Ser. No. 12/020,006, filed Jan. 25, 2008, which claims the benefit of and priority to U.S. Provisional Application Ser. No. 60/897,572, filed Jan. 26, 2007. This application also claims the benefit of and priority to U.S. Provisional Application Ser. No. 61/252,408, filed Oct. 16, 2009. The entire disclosure of each of these applications is hereby incorporated by reference.

GOVERNMENT SUPPORT

This invention was made with United States Government support under 70NANB7H7020 awarded by the National Institute of Standards and Technology (NIST). The United States Government has certain rights in the invention.

FIELD OF THE INVENTION

The technology disclosed herein relates generally to lattice-mismatched semiconductor heterostructures, in particular pseudomorphic layers having a thickness greater than the critical thickness predicted therefor.

BACKGROUND

Achieving low defect densities throughout a semiconductor active device layer is important for the fabrication of a commercially practical nitride-based semiconductor device. As described in U.S. patent application Ser. No. 11/503,660 ("the '660 application"), the entire disclosure of which is hereby incorporated by reference, it is possible to form large-diameter, low-defect-density AlN substrates. However, many desirable device applications preferably incorporate device layers based on alloys of AlN, GaN, and InN to be grown on the AlN substrate. As the concentration of GaN and InN is increased, the lattice mismatch with respect to the AlN substrate also increases. For instance, the lattice parameter in the c-plane of GaN is approximately 2.4% larger than that of AlN. When a lattice-mismatched layer is epitaxially grown on a substrate, the initial layer typically grows pseudomorphically—that is, the epitaxial layer will be compressed (experience compressive strain) in the plane of the substrate surface if the intrinsic lattice parameter of the substrate is smaller than that of the epitaxial layer. The epitaxial layer will be stretched or put under tensile strain when the intrinsic lattice parameter of the epitaxial layer is smaller than that of the substrate. However, as the thickness of the epitaxial layer is increased, the strain energy in the epitaxial layer will grow and, typically, the layer will find some way to reduce the strain energy. This may occur by plastic flow through the motion of dislocations, through the creation of surface morphological features which allow strain relaxation, or, particularly when the strain is tensile, through cracking of the film.

Pseudomorphic layers are attractive for at least two reasons. The first is that when an epitaxial layer is grown on a low-dislocation substrate, the pseudomorphic epitaxial layer may also be grown with very low dislocation densities, often with the same dislocation density as the substrate. The second advantage accrues from the ability to tailor the band structure through the large resulting biaxial strains. For example, the strain can be used to break the degeneracy between heavy and light carrier bands and, as a result, obtain higher carrier mobilities.

However, even thick pseudomorphic layers may be insufficient for the fabrication of high-output-power light-emitting devices such as light-emitting diodes (LEDs) and lasers. Such devices are generally sensitive to strain-relieving defects, placing constraints on not only the light-emitting active layer(s) (which are generally one or more strained quantum wells), but also adjoining layers, as defects in adjoining layers may propagate through the active layer(s) even if the active layer(s) remain pseudomorphically strained. Because adjoining layers generally require particular thicknesses and/or compositions to enable, e.g., adequate electrical contact to the device, if these layers are maintained in a pseudomorphic state, the allowable thickness for the active layer(s) (in order to maintain the entire "stack" of layers in a pseudomorphic state) may be diminished, thus decreasing the potential output power of the finished device. Moreover, such layers may require high doping levels to enable low-resistance contacts to the device, and compositions closely lattice-matched with device active layers and/or the underlying substrate may be difficult to dope at high levels. Thus, there is a need for devices having pseudomorphic active layer(s) the thickness of which is not constrained by the strain state of adjoining layers but that remain substantially defect-free (e.g., having a density of defects such as threading dislocations that is approximately equal to the defect level of the underlying substrate), and that are capable of being doped at high levels.

SUMMARY

A technique is provided for growing very thick pseudomorphic films of alloys of AlN, GaN, and InN on high-quality AlN substrates. A pseudomorphic film is one where the strain parallel to the interface is approximately that needed to distort the lattice in the film to match that of the substrate. Thus, the parallel strain in a pseudomorphic film will be nearly or approximately equal to the difference in lattice parameters between an unstrained substrate parallel to the interface and an unstrained epitaxial layer parallel to the interface. As used herein, "very thick" refers to a thickness of the epitaxial layer that substantially exceeds (by a factor of at least 5 for substantially In-free layers or by a factor of at least 10 for layers including In) the expected critical thickness for the epitaxial film based on standard calculations of the thickness where strain relaxation should start to occur through the nucleation and/or motion of threading dislocations (or energy equilibrium calculations). The expected critical thickness may be calculated as described in, e.g., Matthews and Blakeslee, *J. Crystal Growth* 27, 118 (1974), and/or U.S. Pat. No. 4,088,515, the entire disclosure of each being hereby incorporated by reference.

The pseudomorphic layers are utilized as active layers of light-emitting devices such as LEDs and lasers, thus enabling fabrication of such devices having high output power. The electrical properties of the devices are optimized, via maximization of the thickness of the pseudomorphic active layers, by intentional relaxation of other layers in the device. The intentional relaxation, performed by, e.g., deposition of at least a portion of the layer in a substantially islanded growth mode, is performed only in layers contributing to majority carrier transport (i.e., not minority carrier transport, which is vastly more sensitive to defects) and in regions where resulting strain-relieving defects do not intersect the active layer(s). Thus, the thickness of the pseudomorphic active layers and other layers (e.g., contact layers) may be maximized, increas-

ing output power and efficiency while decreasing contact resistance. The intentional relaxation also enables the use of contact or capping layers not closely lattice-matched to the active layers or the underlying substrate and/or that are more easily doped to high dopant concentrations. In one aspect, embodiments of the invention feature a semiconductor device including or consisting essentially of an aluminum nitride single-crystal substrate, at least one pseudomorphic strained layer disposed thereover, and, disposed over the strained layer(s), a semiconductor layer that is lattice-mismatched to the substrate and substantially relaxed. The at least one strained layer may include or consist essentially of AlN, GaN, InN, and/or an alloy thereof. An array of misfit dislocations may be disposed at the interface between the strained layer and the semiconductor layer.

Embodiments of the invention may include one or more of the following in any of a variety of combinations. The relaxed semiconductor layer may include a plurality of defects that do not propagate into the at least one strained layer. A metal contact layer may be disposed over the relaxed semiconductor layer. The relaxed semiconductor layer may include or consist essentially of gallium nitride, e.g., p-type-doped gallium nitride. The relaxed semiconductor layer may be p-type doped to a hole concentration at room temperature ranging between approximately $1\times10^{17}/cm^3$ and approximately $1\times10^{20}/cm^3$. The at least one strained layer may have a thickness exceeding the predicted critical thickness associated therewith by at least a factor of 5, the predicted critical thickness being calculated with the Matthews-Blakeslee theory. The thickness of the at least one strained layer may exceed the predicted critical thickness by at least a factor of 10. A pattern including or consisting essentially of a plurality of cones may be disposed on the bottom surface of the substrate. Each of the plurality of cones may have an apex angle of approximately 26°. The defect density of the relaxed semiconductor layer may be at least two orders of magnitude, or even at least five orders of magnitude, larger than the defect density of the substrate.

In another aspect, embodiments of the invention feature a method of forming a semiconductor device. At least one pseudomorphic strained layer is formed over a single-crystal substrate, the strained layer(s) including or consisting essentially of AlN, GaN, InN, and/or an alloy thereof. A semiconductor layer that is lattice-mismatched to the substrate and substantially relaxed is formed over the at least one strained layer without (i) relaxing the at least one strained layer, and (ii) propagation of defects from the semiconductor layer into the at least one strained layer. An array of misfit dislocations may be formed at the interface between the relaxed semiconductor layer and the at least one strained layer.

Embodiments of the invention may include one or more of the following in any of a variety of combinations. The at least one strained layer may have a thickness exceeding the predicted critical thickness associated therewith by at least a factor of 5, the predicted critical thickness being calculated with the Matthews-Blakeslee theory. The thickness of the at least one strained layer may exceed the predicted critical thickness by at least a factor of 10. A metal contact layer may be formed over the relaxed semiconductor layer. The substrate may include or consist essentially of aluminum nitride, and the relaxed semiconductor layer may include or consist essentially of gallium nitride. Forming the semiconductor layer may include or consist essentially of forming at least a portion of the relaxed semiconductor layer as a series of islands. The thickness of the semiconductor layer may be increased such that the series of islands coalesces into a unified layer. The at least one strained layer and the relaxed semiconductor layer may both be formed by epitaxial deposition. A pattern of cones may be formed, e.g., by etching, on the back surface of the substrate. At least a portion of the substrate may be removed, e.g., by grinding or polishing.

These and other objects, along with advantages and features of the invention, will become more apparent through reference to the following description, the accompanying drawings, and the claims. Furthermore, it is to be understood that the features of the various embodiments described herein are not mutually exclusive and can exist in various combinations and permutations. As used herein, the term "substantially" means±10%, and in some embodiments, ±5%.

BRIEF DESCRIPTION OF THE DRAWINGS

In the drawings, like reference characters generally refer to the same parts throughout the different views. Also, the drawings are not necessarily to scale, emphasis instead generally being placed upon illustrating the principles of the invention. In the following description, various embodiments of the present invention are described with reference to the following drawings, in which:

FIG. **1** is a graph of predicted critical thickness and pseudomorphic strain for $Al_xGa_{1-x}N$ layers of various Al contents x formed on AlN substrates;

FIG. **2** is a schematic depicting a pseudomorphic strained layer formed on a substrate;

FIGS. **3**A, **3**B, and **3**C are schematics of pseudomorphic strained layer-based device structures; and

FIGS. **4**A, **4**B and **4**C are schematics of processed devices utilizing the layer structure of FIG. **3**A or **3**C.

DETAILED DESCRIPTION

Fabrication Techniques

The predicted critical thickness, calculated in accordance with the Matthews-Blakeslee theory as a function of Al concentration in $Al_xGa_{1-x}N$ layer growth on a c-face AlN substrate, is shown in FIG. **1**. Also shown is the pseudomorphic strain of the $Al_xGa_{1-x}N$ layers attained in the absence of relaxation. Unexpectedly, we have found that it is possible to grow pseudomorphic layers with thicknesses much greater than the predicted critical thickness. For example, the critical thickness of an $Al_xGa_{1-x}N$ layer with x=0.6 is about 40 nanometers (nm), as shown in FIG. **1**. We have been able to grow layers with this Al concentration to a thickness exceeding 1 micrometer (μm) and still obtain a pseudomorphically strained layer that is of very high quality and mirror smooth. As used herein, the term "high quality" refers to epitaxial layers having a threading dislocation density of approximately 10^6 cm^{-2} or less. In certain embodiments, 10^4 cm^{-2} or less, or even approximately 10^2 cm^{-2} or less. The term "pseudomorphic" is utilized herein to refer to epitaxial layers strained to at least approximately 80% of a lattice parameter of an underlying substrate (i.e., less than approximately 20% relaxed to its innate lattice parameter). In some embodiments, a pseudomorphic layer may be approximately fully strained to the lattice parameter of the underlying substrate. The term "mirror smooth" refers to layer root-mean-squared ("RMS") surface roughnesses less than approximately 5 nm in a 5 μm×5 μm area (as measured by an atomic-force microscope). In preferred embodiments the RMS surface roughness is less than approximately 1 nm in a 5 μm×5 μm area.

A thick pseudomorphic semiconductor layer fabricated in accordance herewith is shown in FIG. **2**. A semiconductor substrate **200** is provided. In an embodiment, semiconductor substrate **200** includes or consists essentially of AlN. The top

surface **210** of semiconductor substrate **200** may be prepared for epitaxial growth by at least one of planarization (e.g., by chemical-mechanical polishing) or cleaning prior to deposition of one or more epitaxial layers thereon. A strained epitaxial layer **220** is then deposited on semiconductor substrate **200**, e.g., by organometallic vapor-phase epitaxy, to a thickness exceeding its predicted critical thickness. As can be seen in FIG. **1**, the predicted critical thickness of an exemplary epitaxial layer **220** consisting of $Al_xGa_{1-x}N$ grown on a semiconductor substrate **200** consisting of AlN depends on the Al content x. In an embodiment, the thickness of epitaxial layer **220** exceeds its predicted critical thickness by at least a factor of 5, or even by at least a factor of 10, and epitaxial layer **220** remains pseudomorphic. The thickness of epitaxial layer **220** may even exceed its predicted critical thickness by a factor of 20 or more.

In certain embodiments, epitaxial layer **220** may actually consist of a plurality of discrete layers, each one pseudomorphically strained to the lattice parameter of semiconductor substrate **200**. The plurality of layers may include layers with graded composition, e.g., layers including AlN, InN, and/or GaN in which the concentration of one or more of the group III atoms changes with thickness. Such layers may be graded in discrete steps or linearly in composition.

Strained epitaxial layer **220** may also be deposited on an optional relaxed semiconductor layer (not shown) formed over semiconductor substrate **200**. In this case, the strain in epitaxial layer **220** and the predicted critical thickness therefor will be a function of the lattice parameter of the relaxed semiconductor layer rather than that of semiconductor substrate **200**. Epitaxial layer **220** remains pseudomorphic, and the thickness of epitaxial layer **220** exceeds this predicted critical thickness by at least a factor of 5. In certain embodiments, the thickness of epitaxial layer **220** exceeds this predicted critical thickness by at least a factor of 10 or even at least a factor of 20. Thus, either semiconductor substrate **200** or the optional relaxed semiconductor layer can act as a relaxed "platform" to which epitaxial layer **220** is strained.

The ability to grow highly strained alloys of III-nitride on substrates with low threading dislocation density ("TDD"), e.g., certain AlN substrates, has been found to be dependent on: (i) substrate crystal quality, (ii) surface preparation, (iii) crystal orientation of the substrate surface, (iv) alloy concentration, (v) growth conditions including substrate temperature and V-III ratio during growth, and/or (vi) rate of grading of the alloy concentration. Relaxation of epitaxial layer **220** may be minimized or eliminated by maintenance of low surface roughness during epitaxial growth. Roughening of the layer surface or island formation may lead to detrimental relaxation of the layer. Defects at the surface of the semiconductor substrate **200**, which may be due either to defects in the substrate which have propagated to the surface or to improper surface cleaning, may also cause roughening of epitaxial layer **220**. Once roughening occurs, strain relaxation occurs at the sidewalls of terraces and islands on the epitaxial surface. When these terraces and islands coalesce, they may deleteriously form high densities of threading dislocations at the coalescence boundaries.

Maintenance of step-flow growth during the epitaxial deposition aids the prevention of relaxation, and the proper conditions for step-flow growth depend on the substrate orientation of the semiconductor substrate **200**. When substrates are very closely oriented to on-axis (i.e., the surface normal of the substrate is very closely aligned to a major crystallographic axis), the density of steps across the surface of the substrate is low. Thus, incoming Al, Ga, or In atoms must diffusive relatively large distances to incorporate into the growing epitaxial layer at a step edge, i.e., maintain step-flow growth. Thus, step-flow growth may be maintained by (i) enhancing the long-distance diffusion of incoming atoms of the growth species and/or (ii) reducing the diffusion distance required to reach a step edge (i.e., increase the step density on the surface). Such long-distance diffusion may be enhanced by performing the epitaxial growth at higher temperatures (i.e., up to approximately 1100° C. or, in the case of In-free, high Al content (e.g., greater than approximately 50% Al content), by increasing the growth temperature to a range of greater than approximately 1100° C. to approximately 1300° C. In some embodiments, e.g., for Al concentrations greater than 50%, long-distance diffusion may also be enhanced by decreasing the ratio of the nitrogen species (i.e., the group V species) in the epitaxial reactor in comparison to the group III species. In an embodiment, a V-III ratio beneficial for enhancing long-distance diffusion of the growth species is less than approximately 1,000, and may even be less than approximately 10. The density of step edges on semiconductor substrate **200** may also be increased (thus reducing the required diffusion distances required to reach a step) by increasing the misorientation between the major crystallographic axis and the surface normal of the substrate. In an embodiment, the misorientation of semiconductor substrate **200** ranges between approximately 0.5° and approximately 2°, e.g., approximately 1°.

Kinetic barriers to strain relaxation may also be beneficially utilized to produce thick pseudomorphic epitaxial layers. Since any alloy of AlN, GaN, and InN (with nonzero content of either GaN or InN) will have a larger relaxed lattice parameter than an underlying AlN substrate, these epitaxial films will typically not relax by cracking. Relaxation may occur by the formation of misfit dislocations which run parallel to the interface between the AlN substrate and epitaxial alloy layer. These misfit dislocations may either result from the motion of existing threading dislocations which propagate into epitaxial layer **220** from semiconductor substrate **200**, or from new dislocation loops forming either from the surface or from some macroscopic defect on the surface of substrate **200**. Thus, the elimination of defect sources in semiconductor substrate **200** creates kinetic barriers to relaxation, facilitating the fabrication of thick pseudomorphic epitaxial layer **220**. In an embodiment, semiconductor substrate **200** has a threading dislocation density less than approximately 10^6 cm^{-2}. In other embodiments, semiconductor substrate **200** has a threading dislocation density less than approximately 10^4 cm^{-2} or even less than approximately 10^2 cm^{-2}. Semiconductor substrate **200** may also have a density of particulate surface defects less than approximately 100 cm^{-2}. Utilization of such optimized semiconductor substrates minimizes or eliminates glide of existing dislocations and dislocation nucleation at surface defects as relaxation mechanisms. The remaining relaxation mechanism—surface nucleation of dislocation loops—occurs only at strain energies sufficiently high to facilitate fabrication of thick pseudomorphic epitaxial layers. Therefore, the fabrication of thick strained epitaxial layer **220** having a thickness greater than its predicted critical thickness by at least approximately a factor of 5 is facilitated. Moreover, since In may have the additional effect of hindering dislocation motion and concomitant relaxation, a strained epitaxial layer **220** containing In may achieve a pseudomorphic thickness greater than its predicted critical thickness by at least approximately a factor of 10.

In addition, certain crystallographic orientations of semiconductor substrate **200** may be particularly favorable in the fabrication of thick epitaxial layers of highly strained alloys. In particular, Liu et al. point out, the main slip system of the

wurzite crystal structure of GaN and its alloys is <11.2>{00.2}. (See R. Liu, J. Mei, S. Srinivasan, H. Omiya, F. A. Ponce, D. Chems, Y. Narukawa and T. Mukai, "Misfit Dislocation Generation in InGaN Epilayers on Free-Standing GaN," *Jap. J. Appl. Physics* 45, L549 (2006), the entire disclosure of which is hereby incorporated by reference.) This slip system will not be active in a well-oriented c-face substrate (i.e., a substrate in which the surface normal is aligned with the c-axis of the crystal) since the lattice-mismatch strain will not result in any resolved stress to move dislocations along this plane. This phenomenon may limit the allowable miscut for c-face substrates to enable very large strains and/or thick pseudomorphic epitaxial layers thereon. However, as described above, step-flow growth is facilitated by a finite surface misorientation. Thus, in an embodiment, the misorientation of semiconductor substrate **200** is greater than 0° but is less than approximately 4°.

In one procedure, a large c-face AlN substrate with low dislocation density (roughly 5×10^3 cm^{-2}) was prepared as described in the '660 application. The miscut of this substrate was approximately 1°. The Al-polarity surface of the c-face AlN substrate—the (0001) face—was prepared as described in U.S. Pat. No. 7,037,838 ("the '838 patent"), the entire disclosure of which is hereby incorporated by reference. After introducing the substrate into an Aixtron model 200/4 RF-S organometallic vapor-phase epitaxy ("OMVPE") reactor, the substrate was heated to ~1100° C. under flowing hydrogen and ammonia gas mixture. Trimethylaluminum ("TMA") was then introduced and a 0.3-μm-thick AlN buffer layer was grown on the substrate at an approximate growth rate of 0.6 μm/hr. A graded layer $Al_xGa_{1-x}N$ was then grown by switching in trimethylgallium ("TMG") with ramping up TMG and ramping down the TMA gas flow to reach the target Al % over a 15 minute interval to grow approximately 0.1 μm of linearly graded alloy. After this transition layer, the TMA and TMG flows were kept constant and a final layer of ~63% Al concentration and approximately 0.6 μm thickness was grown with an approximate growth rate of 1.0 μm/hr. During growth, the chamber pressure was maintained at ~25 to 100 mbar. The V-III ratio was maintained between 500 and 2,000 during the growth sequence. The parallel strain (i.e., strain in the plane of the substrate) was measured to be slightly greater than 0.8% and represented pseudomorphic growth even though the layer exceeded the predicted critical thickness by more than an order of magnitude. The double-crystal ω rocking curve widths about the (00.2) and the (10.2) reflections (measured with a Philip X'Pert system) for the $Al_xGa_{1-x}N$ layer were 50 arcsec and 60 arcsec, respectively. The strain parallel to the interface was measured to be nearly 1% and the epitaxial layer was pseudomorphic to the underlying AlN substrate. Etch pit densities were measured using a molten KOH etch to determine the density of threading dislocations in the $Al_xGa_{1-x}N$ epitaxial layer. The measured densities were in the range of $0.8–3\times10^5$ cm^{-2}.

A similar procedure was used to grow a 0.6 μm-thick epitaxial layer of an $Al_xGa_{1-x}N$ alloy that had an Al concentration of 50%. In this case, the strain parallel to the interface remained ~1%, which represents approximately 80% of the fully pseudomorphic strain.

In another procedure, a large c-face AlN substrate with a dislocation density of approximately 5×10^3 cm^{-2} was prepared as described in the '660 application. The Al-polarity surface of the c-face AlN substrate (misaligned by approximately 1.5°) was prepared as described in the '838 patent. After introducing the substrate into a Veeco D180 OMVPE reactor, the substrate was heated to approximately 1100° C. under a flowing hydrogen and ammonia gas mixture. TMA was then introduced and a 0.4 μm-thick AlN buffer layer was grown on the substrate at an approximate growth rate of 0.4 μm/hr. A graded layer $Al_xGa_{1-x}N$ was then grown by switching in TMG with ramping up TMG while maintaining TMA gas flow to reach the target Al % over a 6-minute interval to grow approximately 0.05 μm of linearly graded alloy. After this transition layer, the TMA and TMG flows are kept constant and a final layer of ~58% Al concentration and approximately 0.5 μm thickness was grown with an approximate growth rate of 0.8 μm/hr. During growth, the chamber pressure was maintained at approximately 20 Torr. The V-III ratio was maintained between 900 and 3,200 during growth sequence. The parallel strain was measured to be slightly greater than 1.0% and represented pseudomorphic growth even though the layer exceeded the predicted critical thickness by more than an order of magnitude.

While imperfect surface preparation may increase the dislocation density, this can be remedied by improving the surface preparation. For low-defect AlN substrates, appropriate surface preparation techniques are described in the '838 patent and in U.S. Patent Application Publication No. 2006/0288929A1, the entire disclosure of which is hereby incorporated by reference.

As pseudomorphic epitaxial layer(s) **220** experience little or no lattice relaxation, the threading dislocation density therein may be approximately equal to the threading dislocation density of semiconductor substrate **200**. For example, substrates from AlN boules grown by the techniques described in the '660 application may have very low dislocation densities—under 10,000 cm^{-2}, typically about 1,000 cm^{-2}, and, in certain embodiments, under 500 cm^{-2} and even under 100 cm^{-2}—that are "inherited" by pseudomorphic epitaxial layers grown thereon. In other embodiments, the threading dislocation density of epitaxial layer **200** may be greater than that of semiconductor substrate **200** by no more than approximately a factor of 10. Such low threading dislocation densities enable fabrication of highly efficient ultraviolet light-emitting diodes ("UV LEDs") and laser diodes ("LDs"), as well as electronic devices, such as transistors for high-frequency (e.g., >2 GHz), high-power operation.

In an embodiment, strained epitaxial layer **220** is substantially free of local elastic strain relaxation caused by the formation of, e.g., macroscopic defects such as islands and pinholes (further described below). Moreover, the strain in epitaxial layer **220** may be approximately completely a result of lattice mismatch to substrate **200**. For example, epitaxial layer **220** will be approximately free of strain due to thermal expansion mismatch with substrate **200**.

For device applications, polarization effects in epitaxial layer **220** may affect device performance. For epitaxial layer **220** fabricated on top surface **210** which is non-polar (e.g., the a- or m-plane of a substrate **200** consisting of AlN), polarization effects in the layer are minimized. This makes a subsequently formed device inherently insensitive to polarization effects associated with the surface, and eliminates or minimizes dc-to-RF dispersion observed in conventional devices grown on polar surfaces, e.g., the c-plane. On the other hand, pseudomorphic structures grown on the c-plane along the [0001] direction may have strong polarization effects which influence the charge distribution within the device. Preferably, the polarization charge at the channel/barrier interface is carefully increased to counteract backside depletion effects associated with the AlN/GaN hetero-interface transitioning from the AlN buffer structure.

Device Applications

A key issue limiting the performance of deep-UV LEDs is high dislocation density in the active device region which

reduces the electrical efficiency, the internal quantum efficiency ("IQE"), and the lifetime of the devices. Briefly, as described in the Solid State Lighting Report (Dept. of Energy, 2007), the entire disclosure of which is hereby incorporated by reference, the electrical efficiency, η_V (defined as photon energy divided by the product of the applied voltage and electron charge, i.e., $h\lambda/eV$), represents the amount of electrical energy converted to photon energy. The applied forward voltage is determined by the diode characteristics, and should be as low as possible in order to get the maximum current (and hence maximize the number of electrons eligible to convert to photons) for a given input power. The IQE is the ratio of the photons created in the active region of the semiconductor chip to the number of electrons injected into the LED.

Referring to FIG. **3**A, a pseudomorphic UV light emitting diode ("PUVLED") structure **300** is formed. A semiconductor substrate **305**, which includes or consists essentially of one or more semiconductor materials, is provided. In an embodiment, semiconductor substrate **305** includes or consists essentially of a III-nitride semiconductor material, e.g., AlN. Semiconductor substrate **305** may be miscut such that the angle between its c-axis and its surface normal is between approximately 0.3° and approximately 4°. In a preferred embodiment, the misorientation of the surface of semiconductor substrate **305** is approximately 1°. The surface of semiconductor substrate **305** may have a group-III (e.g., Al-) polarity or N-polarity, and may be planarized, e.g., by chemical-mechanical polishing. In an embodiment, the surface of semiconductor substrate **305** is prepared as disclosed in the '838 patent. The RMS surface roughness of semiconductor substrate is preferably less than approximately 0.5 nm for a 10 μm×10 μm area. In some embodiments, atomic-level steps are detectable on the surface when probed with an atomic-force microscope. The threading dislocation density of semiconductor substrate **305** may be measured using, e.g., etch pit density measurements after a 5 minute KOH—NaOH eutectic etch at 450° C. Preferably the threading dislocation density is less than approximately 2×10^3 cm^{-2}. In some embodiments substrate **305** has an even lower threading dislocation density, as described above in reference to semiconductor substrate **200**. Semiconductor substrate **305** may be topped with a homoepitaxial layer (not shown) that includes or consists essentially of the same semiconductor material present in semiconductor substrate **300**, e.g., AlN.

In an embodiment, an optional graded buffer layer **310** is formed on semiconductor substrate **305**. Graded buffer layer **310** may include or consist essentially of one or more semiconductor materials, e.g., $Al_xGa_{1-x}N$. In a preferred embodiment, graded buffer layer **310** has a composition approximately equal to that of semiconductor substrate **305** at an interface therewith in order to promote two-dimensional growth and avoid deleterious islanding (such islanding may result in undesired elastic strain relief in graded buffer layer **310** and subsequently grown layers). The composition of graded buffer layer **310** at an interface with subsequently grown layers (described below) is generally chosen to be close to (e.g., approximately equal to) that of the desired active region of the device (e.g., the $Al_xGa_{1-x}N$ concentration that will result in the desired wavelength emission from the PUVLED). In an embodiment, graded buffer layer **310** includes $Al_xGa_{1-x}N$ graded from an Al concentration x of approximately 100% to an Al concentration x of approximately 60%.

A bottom contact layer **320** is subsequently formed above substrate **305** and optional graded layer **310**, and may include or consist essentially of $Al_xGa_{1-x}N$ doped with at least one impurity, e.g., Si. In an embodiment, the Al concentration x in bottom contact layer **320** is approximately equal to the final Al concentration x in graded layer **310** (i.e., approximately equal to that of the desired active region (described below) of the device). Bottom contact layer **320** may have a thickness sufficient to prevent current crowding after device fabrication (as described below) and/or to stop on during etching to fabricate contacts. For example, the thickness of bottom contact layer **320** may be less than approximately 200 nm. When utilizing a bottom contact layer **320** of such thickness, the final PUVLED may be fabricated with back-side contacts, as described below in reference to FIG. **4**B. In many embodiments, bottom contact layer **320** will have high electrical conductivity even with a small thickness due to the low defect density maintained when the layer is pseudomorphic.

A multiple-quantum well ("MQW") layer **330** is fabricated above bottom contact layer **320**. MQW layer **330** corresponds to the "active region" of PUVLED structure **300** and includes a plurality of quantum wells, each of which may include or consist essentially of AlGaN. In an embodiment, each period of MQW layer **330** includes an $Al_xGa_{1-x}N$ quantum well and an $Al_yGa_{1-y}N$ quantum well, where x is different from y. In a preferred embodiment, the difference between x and y is large enough to obtain good confinement of the electrons and holes in the active region, thus enabling high ratio of radiative recombination to non-radiative recombination. In an embodiment, the difference between x and y is approximately 0.05, e.g., x is approximately 0.35 and y is approximately 0.4. However, if the difference between x and y is too large, e.g., greater than approximately 0.3, deleterious islanding may occur during formation of MQW layer **330**. MQW layer **330** may include a plurality of such periods, and may have a total thickness less than approximately 50 nm. Above MQW layer **330** may be formed an optional thin electron-blocking (or hole-blocking if the n-type contact is put on top of the device) layer **340**, which includes or consists essentially of, e.g., $Al_xGa_{1-x}N$, which may be doped with one or more impurities such as Mg. Electron-blocking layer **340** has a thickness that may range between, e.g., approximately 10 nm and approximately 50 nm. A top contact layer **350** is formed above electron blocking layer **340**, and includes or consists essentially of one or more semiconductor materials, e.g., $Al_xGa_{1-x}N$, doped with at least one impurity such as Mg. Top contact layer **350** is doped either n-type or p-type, but with conductivity opposite that of bottom contact layer **310**. The thickness of top contact layer **350** is, e.g., between approximately 50 nm and approximately 100 nm. Top contact layer **350** is capped with a cap layer **360**, which includes or consists essentially of one or more semiconductor materials doped with the same conductivity as top contact layer **350**. In an embodiment, cap layer **360** includes GaN doped with Mg, and has a thickness between approximately 10 nm and approximately 200 nm, preferably approximately 50 nm. In some embodiments, high-quality ohmic contacts may be made directly to top contact layer **350** and cap layer **360** is omitted. In other embodiments, top contact layer **350** and/or electron-blocking layer **340** are omitted and the top contact is formed directly on cap layer **360** (in such embodiments, cap layer **360** may be considered to be a "top contact layer"). While it is preferred that layers **310**-**340** are all pseudomorphic, top contact layer **350** and/or cap layer **360** may relax without introducing deleterious defects into the active layers below which would adversely affect the performance of PUVLED structure **300** (as described below with reference to FIGS. **3**B and **3**C). As described below with reference to FIGS. **4**A and **4**B, etching and final contact formation completes the formation of PUVLED structure **300**. Each of layers **310**-**350** is pseudomorphic, and each layer individually may have a thickness greater

than its predicted critical thickness, as described above. Moreover, the collective layer structure including layers **310-350** may have a total thickness greater than the predicted critical thickness for the layers considered collectively (i.e., for a multiple-layer structure, the entire structure has a predicted critical thickness even when each individual layer would be less than a predicted critical thickness thereof considered in isolation).

As described above, in a preferred embodiment, layers **310-340** of PUVLED structure **300** are pseudomorphic, and cap layer **360** is intentionally relaxed. As shown in FIGS. **3**B and **3**C, layers **310-340** are formed as described above with reference to FIG. **3**A. Cap layer **360** is subsequently formed in a substantially strain-relaxed state via judicious selection of its composition and/or the deposition conditions. For example, the lattice mismatch between cap layer **360** and substrate **305** and/or MQW layer **330** may be greater than approximately 1%, greater than approximately 2%, or even greater than approximately 3%. In a preferred embodiment, cap layer **360** includes or consists essentially of undoped or doped GaN, substrate **305** includes or consists essentially of AlN, and MQW layer **330** includes or consists essentially of multiple $Al_{0.55}Ga_{0.45}N$ quantum wells interleaved with $Al_{0.7}Ga_{0.3}N$ barrier layers, and cap layer **360** is lattice mismatched by approximately 2.4%. Cap layer **360** may be substantially relaxed, i.e., may have a lattice parameter approximately equal to its theoretical unstrained lattice constant. A graded layer may be formed between layers **310-340** and cap layer **360**, and its composition at its interfaces with layers **340**, **360** may substantially match the compositions of those layers. The thickness of this graded layer, which is preferably pseudomorphically strained, may range between approximately 10 nm and approximately 50 nm, e.g., approximately 30 nm. In some embodiments, epitaxial growth may be temporarily stopped between growth of the graded layer and cap layer **360**.

In an exemplary embodiment, an electron-blocking layer **340** including or consisting essentially of $Al_{0.8}Ga_{0.2}N$ is formed over MQW layer **330**. Prior to formation of cap layer **360** including or consisting essentially of GaN, a graded layer is formed over electron-blocking layer **340**. The graded layer is graded in composition from $Al_{0.8}Ga_{0.2}N$ to GaN over a thickness of approximately 30 nm. The graded layer may be formed by, e.g., MOCVD, and in this embodiment is formed by ramping the flow of TMA and TMG (by ramping the flow of hydrogen through their respective bubblers) from the conditions utilized to form electron-blocking layer **340** to 0 standard cubic centimeters per minute (sccm) and 6.4 sccm, respectively, over a period of approximately 24 minutes, thus resulting in a monotonic grade from $Al_{0.8}Ga_{0.2}N$ to GaN (all of the other growth conditions are substantially fixed). The thickness of the graded layer in this exemplary embodiment is approximately 30 nm.

After growth of the graded layer, the TMG flow is cut off and epitaxial growth is stopped. Without wishing to be bound by a particular theory, the growth interruption may allow the surface of the epitaxial graded $Al_xGa_{1-x}N$ layer to equilibrate, thus enhancing island formation in cap layer **360** once growth is reinitiated. The growth interruption may last between approximately 15 seconds and approximately 5 minutes, e.g., approximately 1 minute. During the growth interruption, the ammonia flow is increased from approximately 2 l/min to approximately 81/min, the temperature is decreased by approximately 40° C. (e.g., from a growth temperature of approximately 1100° C. for electron-blocking layer **340** to approximately 1060° C.), and the chamber pressure is increased from approximately 20 Ton to approximately 100 Ton. The doping concentration may also be adjusted during the growth interruption. In an embodiment, supply of Mg dopant is increased by increasing hydrogen flow through the Mg-source bubbler from approximately 350 sccm to approximately 500 sccm. After the growth interruption, growth of a cap layer **360** including or consisting essentially of GaN is commenced, and cap layer **360** is grown to a thickness of approximately 200 nm at a rate of approximately 1.5 μm/hr. During growth of an exemplary cap layer **360** formed of GaN, the TMG flow (i.e., the hydrogen flow through the TMG source) is 64 sccm and the V/III ratio is approximately 1200. Cap layer **360** typically forms as a series of islands that coalesce upon further growth, as described below.

As depicted in FIG. **3**B, cap layer **360** may be initially formed as a group of islands (e.g., via a Stranski-Krastanov or Volmer-Weber growth mode) that are substantially relaxed. In some embodiments, an islanded cap layer **360** (e.g., a cap layer including or consisting essentially of uncoalesced islands) may be utilized as a contact layer to an underlying device. However, in preferred embodiments, further growth of cap layer **360** results in coalescence of islands into a unified cap layer **360** containing a plurality of defects **370**. The defects **370** may include misfit dislocations formed at the bottom interface of cap layer **360** that serve to relax cap layer **360** and also may serve to block propagation of other defects into underlying strained layer(s). However, the array of misfit dislocations may not be an array of screw dislocations characteristic of a twist boundary between wafer-bonded layers. Defects **370** may also include threading dislocations that propagate from the misfit dislocation network through the thickness of cap layer **360**. It should be emphasized the defects **370** are only formed in cap layer **360** (and possibly any layers formed thereover), but do not reach underlying layers such as MQW layer **330**. Since in most embodiments cap layer **360** merely serves as an electrical contact layer in a subsequently formed device (as detailed below), predominantly only majority carriers are supplied therefrom, a process substantially unaffected by the presence of defects **370**. In contrast, minority-carrier diffusion and radiative recombination occurs in active layers such as MQW layer **330**, a process quite sensitive to the presence of defects such as threading dislocations. In an embodiment, the defect density (e.g., the threading dislocation density) in cap layer **360** is greater than that in MQW layer **330** and/or substrate **305** by at least two orders of magnitude, at least three orders of magnitude, or even at least five orders of magnitude. In various embodiments, increased V/III ratio, decreased growth temperature, and/or increased chamber pressure (e.g., compared to growth conditions for underlying layers) facilitate the growth of cap layer **360** as a series of islands.

The intentional relaxation of cap layer **360** may enable the utilization of top contact layers more easily doped (and to higher levels) than layers more closely lattice matched to MQW **330** and/or substrate **305**. For example, p-type doping of AlN layers (and $Al_xGa_{1-x}N$ layers with large Al concentration x, e.g., x greater than approximately 50%) is often difficult, while GaN layers (and $Al_xGa_{1-x}N$ layers with low Al concentration x) may be p-type doped at high levels relatively easily. For example, a cap layer **360** including or consisting essentially of GaN may be p-type doped such that it has a hole concentration at room temperature ranging between approximately $1\times10^{17}/cm^3$ and approximately $1\times10^{20}/cm^3$, while a cap layer **360** including or consisting essentially of AlN may be p-type doped such that it has a hole concentration at room temperature of less than approximately $1\times10^{12}/cm^3$. The hole concentrations of such doped layers may be less than the

physical concentration of dopants, as dopants may not be electrically active in some layers.

Furthermore, the intentional relaxation of cap layer **360** enables formation of thicker contact layers, leading to decreased contact resistance in subsequently fabricated devices. Since cap layer **360** is relaxed, it may be grown to nearly arbitrary thicknesses while leaving the pseudomorphic strain state of underlying layers undisturbed. Also, since maintaining cap layer **360** in a pseudomorphic state increases the strain energy stored in the stack of layers **310-360**, the thicknesses of each of these layers may be constrained to prevent lattice relaxation and introduction of defects in the active device layers. Such a constraint may require use of thinner active layers (e.g., MQW layer **330**), thus decreasing the potential electrical performance of the device. Since in preferred embodiments cap layer **360** is intentionally relaxed, the strain energy is shared by fewer layers, relaxing thickness constraints for each of layers **310-340**.

In a preferred embodiment, PUVLED structure **300** (and/or strained epitaxial layer **220** described above) are formed substantially free (i.e., having less than approximately 1 mm^{-2}, or even approximately 0 mm^{-2}) of macroscopic defects such as pinholes, mounds, or "V pits." Such defects are often observed in the growth of, e.g., strained InGaN layers on GaN substrates with high dislocation densities. (See T. L. Song, J. Appl. Phys. 98, 084906 (2005), the entire content of which is hereby incorporated by reference). Macroscopic defects may cause local relaxation of the strain in the pseudomorphic layer(s), deleteriously affect devices fabricated from the epitaxial layers due to disruptions of the quantum well structures and/or shorting of the p- and n-type contacts, or increase the surface roughness of the layers. Macroscopic defect-free PUVLED structure **300** may advantageously be utilized in the fabrication of PUVLEDs sized greater than approximately 0.1 mm×approximately 0.1 mm. PUVLED structure **300** has an emission wavelength in the range of approximately 210 nm to approximately 320 nm, e.g., approximately 280 nm. As at least most of the layers in PUVLED structure **300** are pseudomorphic, the threading dislocation density in the layers is less than approximately 10^5 cm^{-2}, and may be approximately equal to the threading dislocation density in substrate **305**. In some embodiments, as detailed above, the threading dislocation of most layers may be approximately equal to that of the substrate and significantly higher in intentionally relaxed cap layers. In an embodiment, PUVLED structure **300** has a wall-plug efficiency (i.e., total optical power out divided by total electrical power in) greater than approximately 10% (or even greater than approximately 20% in some embodiments) and/or a lifetime greater than approximately 10,000 hours.

Laser diode (LD) structures may also benefit from a pseudomorphic structure. A preferred LD structure will be similar to that of PUVLED structure **300**, with the addition of layers which properly confine photons to create a resonant cavity. In an edge-emitter LD, the resonant cavity will be directed perpendicular to the growth direction and mirrors will be created by cleaving or etching the semiconductor layer structure. In this case, layer **320** below the MQW layer **330** and layers **340** and **350** above the MQW will need to be modified to act as effective cladding layers to ensure that the emitted photons effectively propagate perpendicular to layer growth direction without significant absorption. For example, one may increase the number of layers schematically labeled as **320**, **340** and **350** in FIGS. **3**A, **3**B, and/or **3**C. Alternatively, in a vertical cavity surface-emitting laser ("VCSEL"), layers **320**, **340**, and **350** may be replaced with multilayer structures that will act as mirrors (e.g., Bragg reflectors) to create a photon cavity that will direct photons along the growth direction of the semiconductor layers. In this way, a semiconductor LD fabricated with nitride semiconductors may have an emission wavelength shorter than approximately 300 nm, and, in some embodiments, shorter than approximately 280 nm.

Referring to FIGS. **4**A and **4**B, different contact schemes may be utilized in conjunction with PUVLED structure **300**. PUVLED **400** is formed by etching, e.g., plasma etching, through the layer sequence in PUVLED structure **300** and stopping on or in bottom contact layer **310**. Contacts **410**, **420** are formed on bottom contact layer **310** and on cap layer **360**, respectively. Contacts **410**, **420** are formed of a conductive material, e.g., a metal such as Ni/Au alloy (typically used for p-type contacts) or a Ti/Al/Ti/Au stack (typically used for n-type contacts), and may be formed by, e.g., sputtering or evaporation. Contacts **410**, **420** may include or consist essentially of the same or different conductive materials (such that optimal contact is made to the oppositely doped bottom contact layer **310** and cap layer **360**). Contact **420** may also include an ultraviolet ("UV") reflector. The UV reflector is designed to improve the extraction efficiency of photons created in the active region of the device by redirecting photons which are emitted toward contact **420** (where they cannot escape from the semiconductor layer structure) and redirecting them toward a desired emission surface, e.g., the bottom surface of PUVLEDs **400**, **450**.

In PUVLED **450**, contact **420** is also formed above cap layer **360**. However, contact **410** (which may be a plurality of separate contacts), is formed on the backside of the PUVLED active layer structure. In this case, substrate **305** is optionally thinned to approximately 150 μm by, e.g., mechanical grinding or polishing. In other embodiments, the substrate **305** is thinned to approximately 20 μm or even completely removed. A mask layer (not shown), formed of, e.g., Ni, is formed on the backside of substrate **305** and patterned by standard photolithography. The exposed regions of substrate **305** are etched by, e.g., plasma or wet etching, and the etch is stopped on or in bottom contact layer **310**. Etch stopping on bottom contact layer **310** is facilitated by detection of Ga in the plasma etcher as substrate **305** will be pure AlN in many embodiments. Contact **410** is then formed on the exposed portions of bottom contact layer **310**. Contact **410** may be interdigitated to maximize the light output from PUVLED **450**. Importantly, the tapered structures created on the backside of substrate **305** will help gather photons from a much larger emission angle from the MQW structure in layer **340** and direct them out the emission surface near the tips of the taped features shown on the etched backside of the substrate **305** shown in FIG. **4**B. This will substantially improve the photon extraction efficiency of the PUVLED since, without the tapered structures, only a small fraction of the photons directed toward a flat emission surface (such as that shown in FIG. **4**A) will fall with the critical acceptance cone for emission due to the large index of refraction for these semiconductor materials. For AlN, the acceptance cone is only approximately 25°, which means that approximately 90% of the photons directed toward a flat emission surface (assuming isotropic emission of radiation into the hemisphere directed toward the flat surface) will undergo total internal reflection and be unable to escape from the device and, thus, not be realized as useful emission.

In some embodiments, the photon extraction of PUVLED **400** depicted in FIG. **4**A may also be enhanced by patterning the backside of substrate **305**, as shown in FIG. **4**C. Rather than utilizing a deposited mask for patterning, the backside of substrate **305** may be patterned by exposure to a wet chemical

etchant. In some embodiments, substrate **305** is thinned before being patterned. The thinning steps may be omitted in some cases, depending on the absorption coefficient of the substrate **305** and its initial thickness. Photon extraction from PUVLED **400** may be inhibited because photons that reach the outer wall of the substrate **305** have a finite probability of being reflected back inside and then being absorbed. Reducing the thickness of substrate **305** helps to reduce the chances of absorption, but does not reduce the chances of photon reflection at the backside surface. Thus, preferred embodiments of the invention feature patterning the back surface of substrate **305** so that most photons that reach it do so at an angle that is within the corresponding escape cone. In the case of an AlN/air interface, and for a wavelength of 280 nm, the escape cone angle is approximately 25°. In such an embodiment, photons that reach the wall with a trajectory angle smaller than approximately 25°, depending on their wavelengths, will most likely exit the device without being reflected back at the surface. As described herein, a pattern of substantially conical features ("cones") with an apex angle of approximately 26° are formed on the back surface of substrate **305**, thus improving photon extraction.

If, for example, substrate **305** has a total thickness variation higher than about 20 μm, then the back surface may be ground, for example, with a 600 to 1800 grit wheel. The removal rate of this step may be purposefully maintained at a low level (approximately 0.3-0.4 μm/s) in order to avoid damaging the substrate **305** or the device structure **400**. After the optional grinding step, the back surface may be polished with a polishing slurry, e.g., a solution of equal parts of distilled water and a commercial colloidal suspension of silica in a buffered solution of KOH and water. The removal rate of this step may vary between approximately 10 μm/min and approximately 15 μm/min. Substrate 305 may be thinned down to a thickness of approximately 200 μm to approximately 250 μm, although the scope of the invention is not limited by this range. The thinning step is preferably followed by wafer cleaning in, e.g., one or more organic solvents. In one embodiment of the invention, the cleaning step includes immersion of substrate **305** in boiling acetone for approximately 10 minutes, followed by immersion in boiling methanol for approximately 10 minutes.

Once substrate **305** is cleaned, the backside thereof is patterned by etching in a suitable solution (e.g., a basic solution such as KOH in deionized (DI) water). In another embodiment of the invention, the etching agent is a solution of NaOH in DI water. The molarity of the basic solution may vary between approximately 1M and approximately 20M, and the etching time may vary between approximately 1 minute and approximately 60 minutes. The temperature of the etching solution may vary between approximately room temperature up to approximately 100° C. Similar results may be obtained when using a higher molarity solution for shorter periods of time and vice versa. In one embodiment of the invention, substrate **305** is etched in a 4M solution of KOH and DI water for 8 minutes while maintaining the solution at approximately 20° C. According to another aspect of this invention, the patterned "cones" begin developing on the back surface of substrate **305** that was not polished with a polishing slurry when etched in a molten 20M KOH bath at 100° C. for approximately one hour.

Table 1 shows the percentage increase in the output power delivered by PUVLED **400** after the back surface of substrate **305** was etched at room temperature with solutions of different concentrations of KOH.

Time (min)	0.1 M	1 M	4 M
1	12%	20%	22%
2		31%	24%
4		29%	18%
10	20%		
30	23%	35%	31%

In another embodiment, the output power of PUVLED **400** fabricated on an AlN substrate **305** increased by up to 78% after the N-surface of the substrate was etched in a 4M solution of KOH and DI water for approximately 8 minutes while maintaining the solution at approximately 20° C.

The etched surface of substrate **305** may also improve the directionality of the light that is emitted by PUVLED **400**. In particular, it is often desirable to have the emitted light focused in a forward direction rather than in the typical, more broadly distributed Lambertian output through a smooth semiconductor surface. The photons in the escape cone emitted through a smooth semiconductor will be refracted and distributed relatively uniformly throughout the half sphere corresponding to the area above the surface of the semiconductor. The number of photons emitted at large angles (from the surface normal) is slightly lower due to the higher probability of reflection at the interface, and drops to approximately 50% of the peak intensity at an angle of approximately 84° from the surface normal in many embodiments featuring unpatterned substrates **305**. For the etched surface however, the light is much more focused towards the surface normal, with the intensity falling to approximately 50% of the peak intensity at an angle of only approximately 30° from the surface normal in many embodiments, thus enabling much higher power densities.

EXAMPLE

A device structure including an $Al_{0.7}Ga_{0.3}N$:Si layer, a five-period MQW layer consisting of n—$Al_{0.7}Ga_{0.3}N$ barriers and $Al_{0.55}Ga_{0.45}N$ wells, a $Al_{0.8}Ga_{0.2}N$ electron blocking layer (EBL), and a p—GaN contact layer was grown on a c-plane AlN substrate using conventional MOCVD. UVLEDs were fabricated using standard LED processing techniques. A circular mesa with a 360 μm diameter was defined by inductively coupled plasma (ICP) etching. A Ti/Al/Ti/Au layer was used for the n-contact and a Ni/Au layer was used for the p-contact. Following device fabrication, the substrate was thinned to a thickness of approximately 200 μm, and the backside was roughened for improved light extraction (as detailed above). Light output was measured on-wafer through the partially absorbing AlN substrate using a calibrated spectrometer and fiber optic probe.

Cross-sectional transmission electron microscopy confirmed that the dislocation density in the n$Al_{0.7}Ga_{0.3}N$ layer was quite low with no dislocations in the field of view. The low dislocation density continues through the MQW and EBL. However, the lattice mismatch between the pseudomorphic $Al_xGa_{1-x}N$ layers and the p—GaN contact layer is high (approximately 2.4%), and the contact layer at least initially forms in a Stranski-Krastanov or Volmer-Weber growth mode. Thus, the cap layer initially forms as a series of islands which only coalesce once the film thickness is increased to around 0.2 μm, resulting in a high density of threading dislocations through the layer and misfit dislocations, which relieve strain, at its bottom interface. The threading dislocations do not propagate into the active region and thus enable

the achievement of high internal and external quantum efficiencies from the devices having low-dislocation-density pseudomorphic active layers.

Pulsed operation of a PUVLED emitting at 248 nm gave a peak external quantum efficiency (EQE) of 1.44% with an output power of 1.44 mW and a peak power of 16.3 mW with an EQE of 1.09%. When operated in continuous-wave mode, a 243 nm device reached a peak EQE of 0.73% and an output power of 1 mW at 25 mA, even with some self-heating. The same device was able to achieve 14.6 mW and an EQE of 0.72% at 400 mA when operated at low duty cycles in pulsed mode. Other devices across several substrates, different epitaxy runs, and process lots exhibited similar good performance with averages of 1.1 mW from 240 to 250 nm and 2.5 mW from 250 to 260 nm with devices over 5 mW in both ranges. These results are a direct consequence of the low dislocation density in the active region due to the pseudomorphic growth and represent significant improvements in the performance of short-wavelength LEDs.

The terms and expressions employed herein are used as terms of description and not of limitation, and there is no intention, in the use of such terms and expressions, of excluding any equivalents of the features shown and described or portions thereof, but it is recognized that various modifications are possible within the scope of the invention claimed.

What is claimed is:

1. A semiconductor device comprising:

an aluminum nitride single-crystal substrate;

at least one pseudomorphic strained layer disposed thereover, the strained layer comprising at least one of AlN, GaN, InN, or an alloy thereof; and

disposed over the at least one strained layer, a semiconductor layer that is lattice-mismatched to the substrate and substantially relaxed.

2. The semiconductor device of claim **1**, wherein the relaxed semiconductor layer comprises a plurality of defects, the defects not propagating into the at least one strained layer.

3. The semiconductor device of claim **1**, further comprising a metal contact layer disposed over the relaxed semiconductor layer.

4. The semiconductor device of claim **1**, wherein the relaxed semiconductor layer comprises p-type-doped gallium nitride.

5. The semiconductor device of claim **1**, wherein the relaxed semiconductor layer is p-type doped to a hole concentration at room temperature ranging between approximately $1\times10^{17}/cm^3$ and approximately $1\times10^{20}/cm^3$.

6. The semiconductor device of claim **1**, further comprising, disposed on a bottom surface of the substrate, a pattern comprising a plurality of cones.

7. The semiconductor device of claim **6**, wherein each of the plurality of cones has an apex angle of approximately 26°.

8. The semiconductor device of claim **1**, wherein a defect density of the relaxed semiconductor layer is at least two orders of magnitude larger than a defect density of the substrate.

9. A method of forming a semiconductor device, the method comprising:

forming, over a single-crystal substrate, at least one pseudomorphic strained layer comprising at least one of AlN, GaN, InN, or an alloy thereof; and

forming, over the at least one strained layer, a semiconductor layer that is lattice-mismatched to the substrate and substantially relaxed without (i) relaxing the at least one strained layer, and (ii) propagation of defects from the semiconductor layer into the at least one strained layer.

10. The method of claim **9**, further comprising forming a metal contact layer over the relaxed semiconductor layer.

11. The method of claim **9**, wherein the substrate comprises aluminum nitride and the relaxed semiconductor layer comprises gallium nitride.

12. The method of claim **9**, wherein forming the relaxed semiconductor layer comprises forming at least a portion of the relaxed semiconductor layer as a series of islands.

13. The method of claim **9**, wherein the at least one strained layer and the relaxed semiconductor layer are both formed by epitaxial deposition.

14. The method of claim **9**, further comprising forming a pattern of cones on a back surface of the substrate.

15. The method of claim **14**, wherein the pattern is formed by etching.

16. The method of claim **9**, further comprising removing at least a portion of the substrate.

17. The semiconductor device of claim **1**, wherein the relaxed semiconductor layer consists essentially of doped or undoped GaN.

18. The method of claim **9**, wherein the relaxed semiconductor layer consists essentially of doped or undoped GaN.

19. The semiconductor device of claim **1**, further comprising an array of misfit dislocations at an interface between the relaxed semiconductor layer and a layer disposed beneath and in direct contact with the relaxed semiconductor layer.

20. The method of claim **9**, wherein forming the relaxed semiconductor layer comprises forming an array of misfit dislocations at an interface between the relaxed semiconductor layer and a layer disposed beneath and in direct contact with the relaxed semiconductor layer.

* * * * *

EXHIBIT 9

US 20140231745A1

(19) **United States**

(12) **Patent Application Publication**

Northrup et al.

(10) **Pub. No.: US 2014/0231745 A1**

(43) **Pub. Date: Aug. 21, 2014**

(54) **P-SIDE LAYERS FOR SHORT WAVELENGTH LIGHT EMITTERS**

(75) Inventors: **John E. Northrup**, Palo Alto, CA (US); **Bowen Cheng**, Atherton, CA (US); **Christopher L. Chua**, San Jose, CA (US); **Thomas Wunderer**, Palo Alto, CA (US); **Noble M. Johnson**, Menlo Park, CA (US); **Zhihong Yang**, San Jose, CA (US)

(73) Assignee: **PALO ALTO RESEARCH CENTER INCORPORATED**, Palo Alto, CA (US)

(21) Appl. No.: **13/619,598**

(22) Filed: **Sep. 14, 2012**

Publication Classification

(51) **Int. Cl.**

H01L 33/06 (2006.01)
H01L 33/00 (2006.01)
H01L 33/32 (2006.01)

(52) **U.S. Cl.**

CPC ***H01L 33/06*** (2013.01); ***H01L 33/32*** (2013.01); ***H01L 33/0075*** (2013.01)

USPC **257/13**; 438/47

(57) **ABSTRACT**

A light emitting device includes a p-side heterostructure having a short period superlattice (SPSL) formed of alternating layers of $Al_{xhigh}Ga_{1-xhigh}N$ doped with a p-type dopant and $Al_{xlow}Ga_{1-xlow}N$ doped with the p-type dopant, where $x_{low} \leq x_{high} \leq 0.9$. Each layer of the SPSL has a thickness of less than or equal to about six bi-layers of AlGaN.

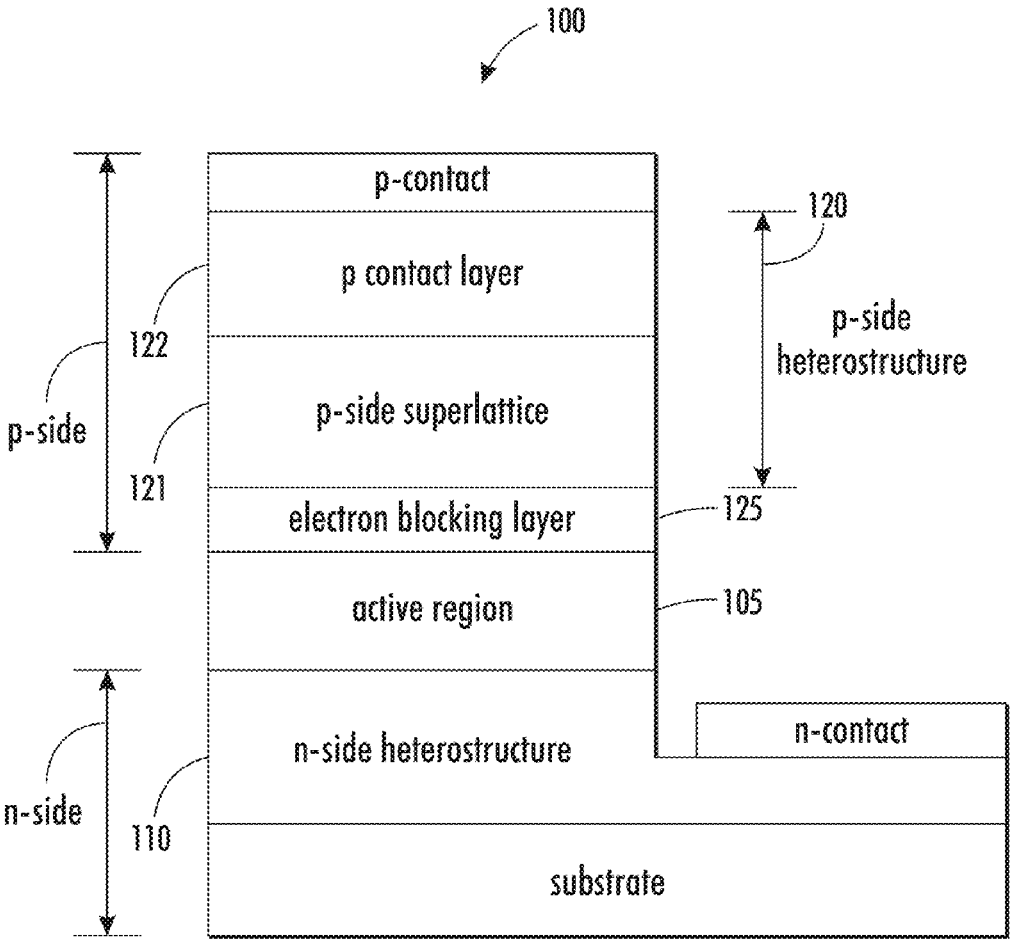

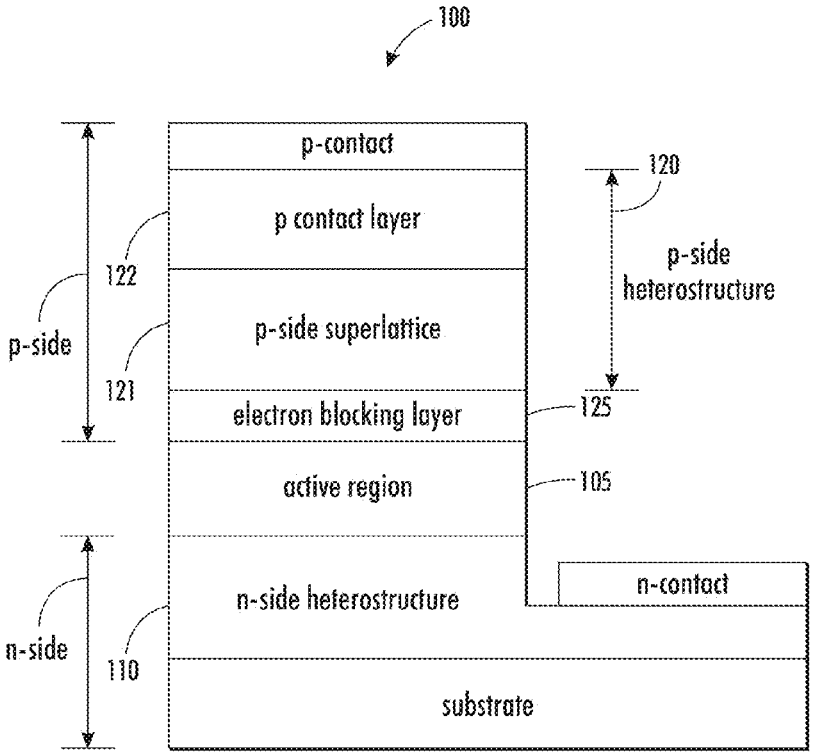
100
p-contact
p contact layer
p-side superlattice
electron blocking layer
active region
n-side heterostructure
substrate
n-contact
122
121
110
125
105
120
p-side
heterostructure
p-side
n-side

FIG. 1

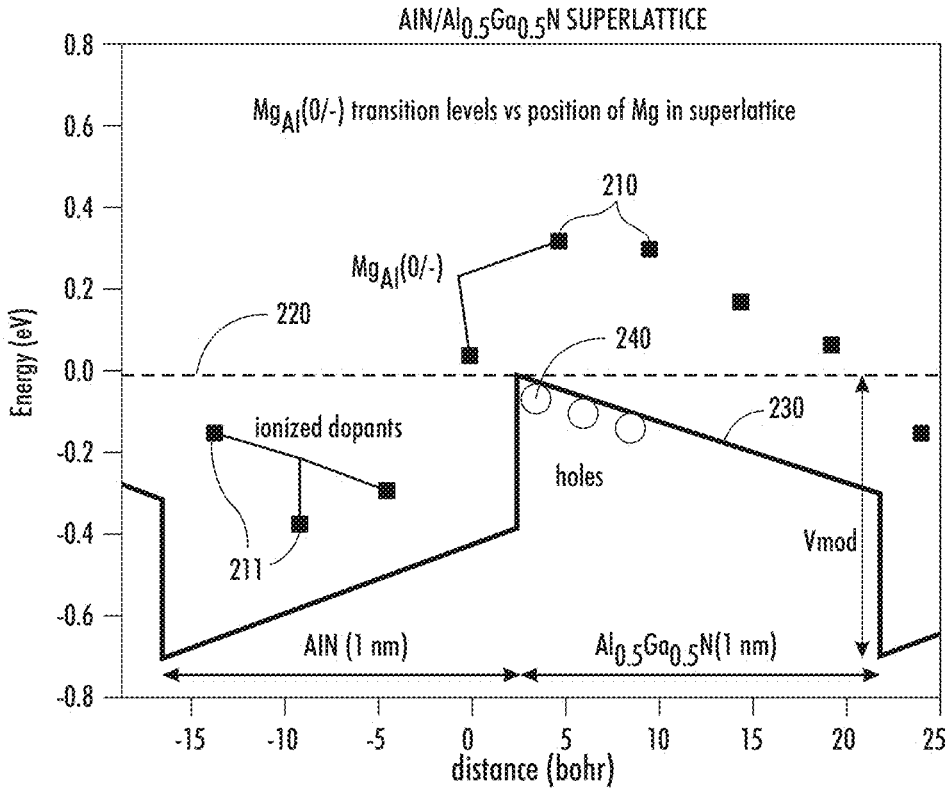
AlN/Al0.5Ga0.5N SUPERLATTICE
MgAl(0/-) transition levels vs position of Mg in superlattice
210
MgAl(0/-)
220
240
230
ionized dopants
holes
Vmod
211
AlN (1 nm)
Al0.5Ga0.5N(1 nm)
Energy (eV)
distance (bohr)
0.8
0.6
0.4
0.2
0.0
-0.2
-0.4
-0.6
-0.8
-15
-10
-5
0
5
10
15
20
25

FIG. 2

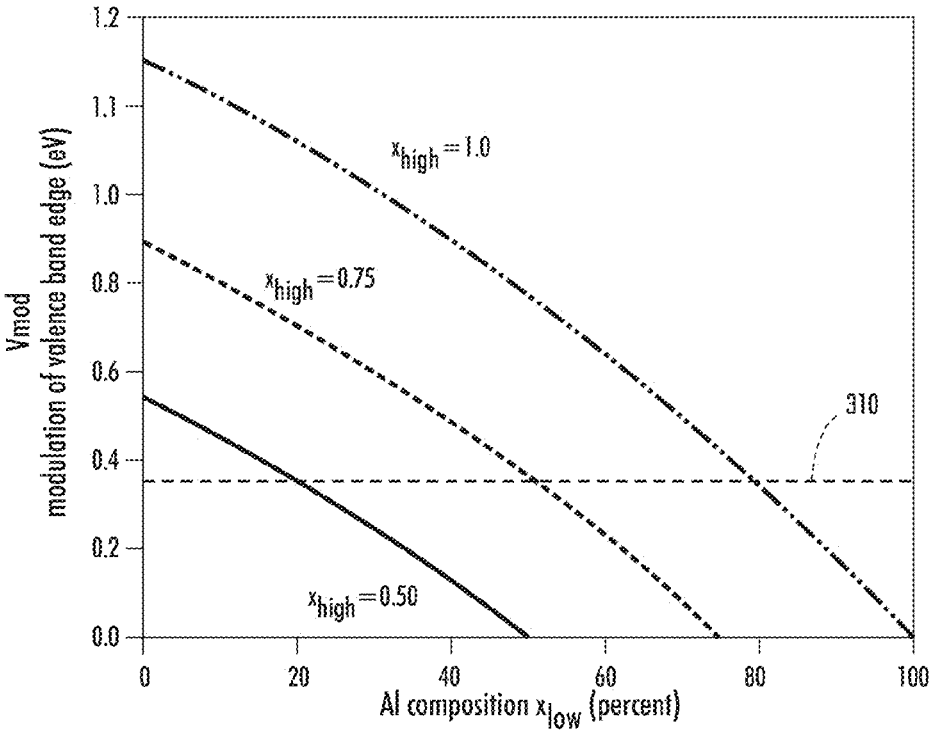
1.2
1.1
1.0
0.8
0.6
0.4
0.2
0.0
Vmod
modulation of valence band edge (eV)
$x_{high}=1.0$
$x_{high}=0.75$
$x_{high}=0.50$
310
0
20
40
60
80
100
Al composition x_{low} (percent)

FIG. 3

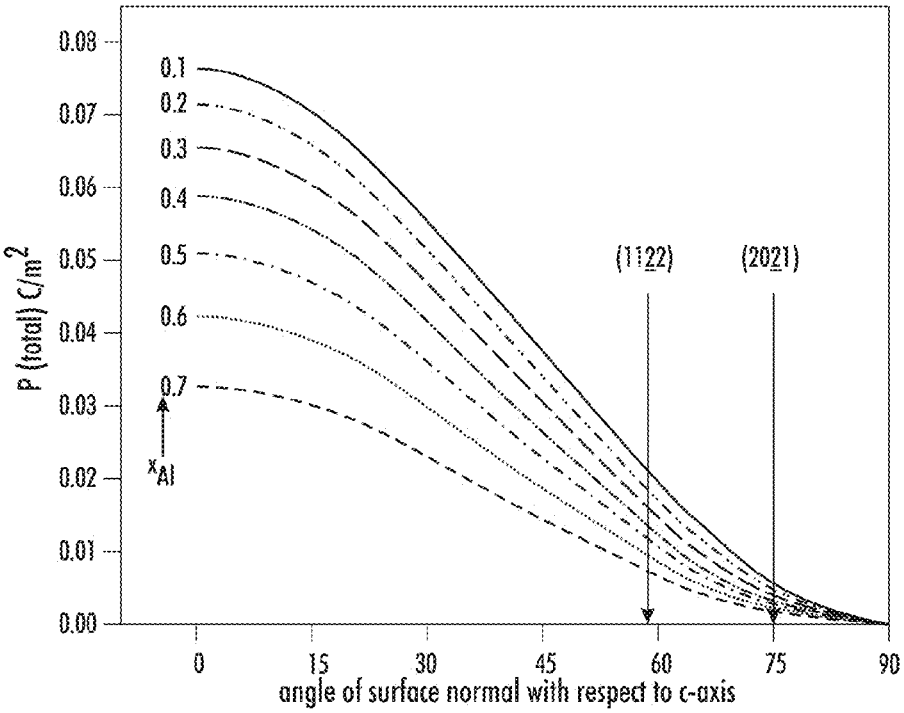
0.08
0.07
0.06
0.05
0.04
0.03
0.02
0.01
0.00
P (total) C/m2
0.1
0.2
0.3
0.4
0.5
0.6
0.7
xAl
(1122)
(2021)
0
15
30
45
60
75
90
angle of surface normal with respect to c-axis

FIG. 4

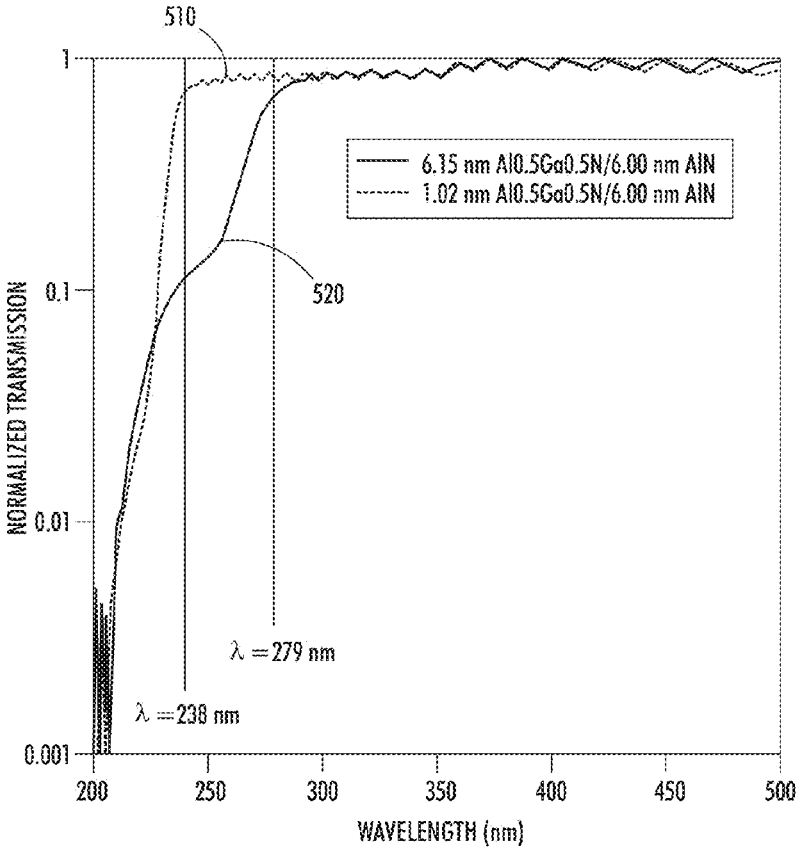
510
1
0.1
0.01
0.001
NORMALIZED TRANSMISSION
6.15 nm Al0.5Ga0.5N/6.00 nm AlN
1.02 nm Al0.5Ga0.5N/6.00 nm AlN
520
λ =279 nm
λ =238 nm
200
250
300
350
400
450
500
WAVELENGTH (nm)

FIG. 5

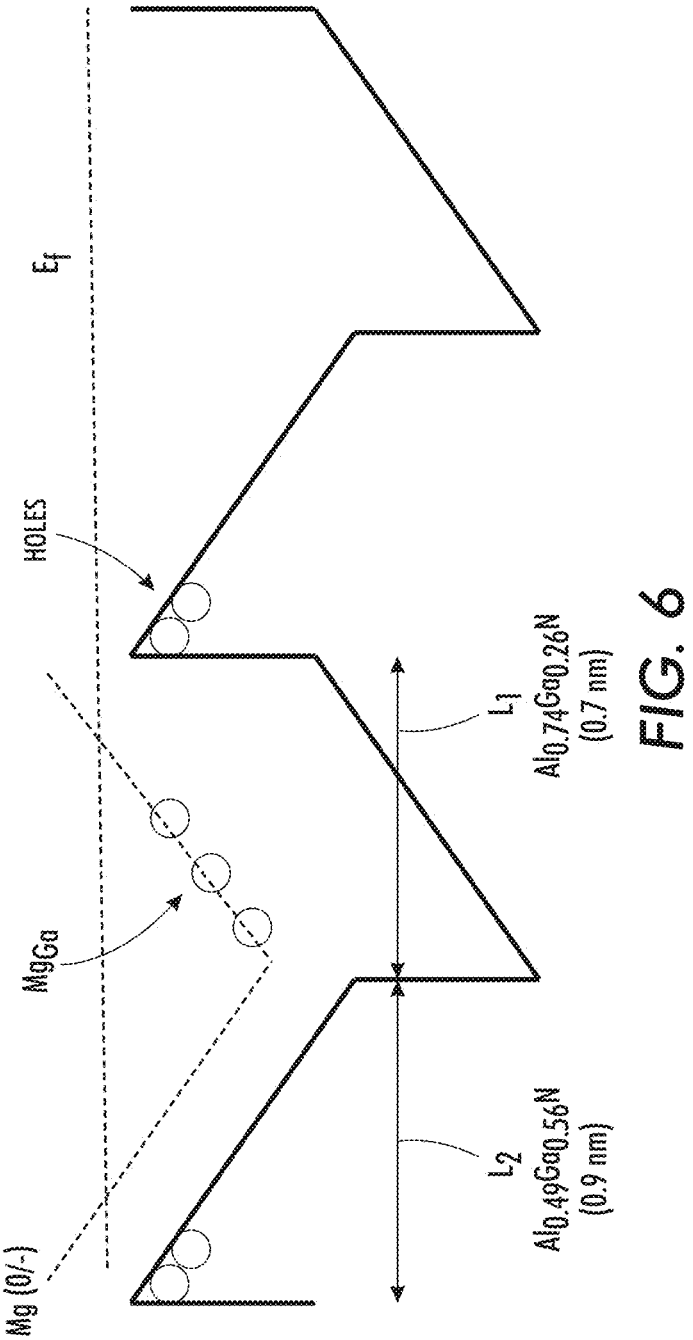

FIG. 6

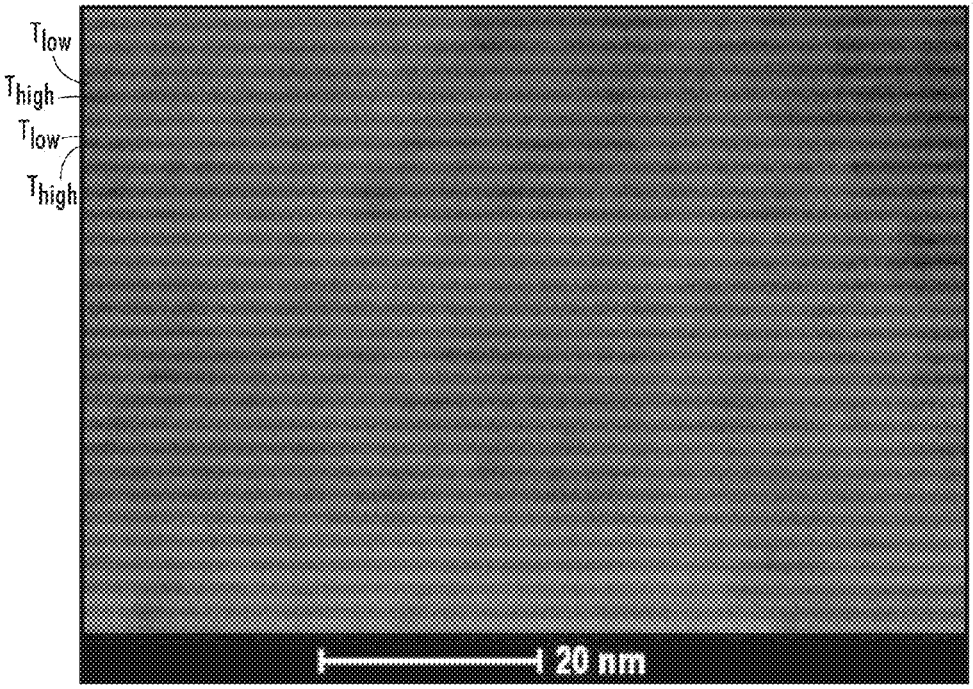

FIG. 7

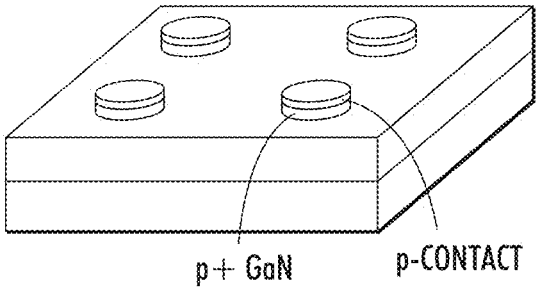
p+ GaN
p-CONTACT

FIG. 8

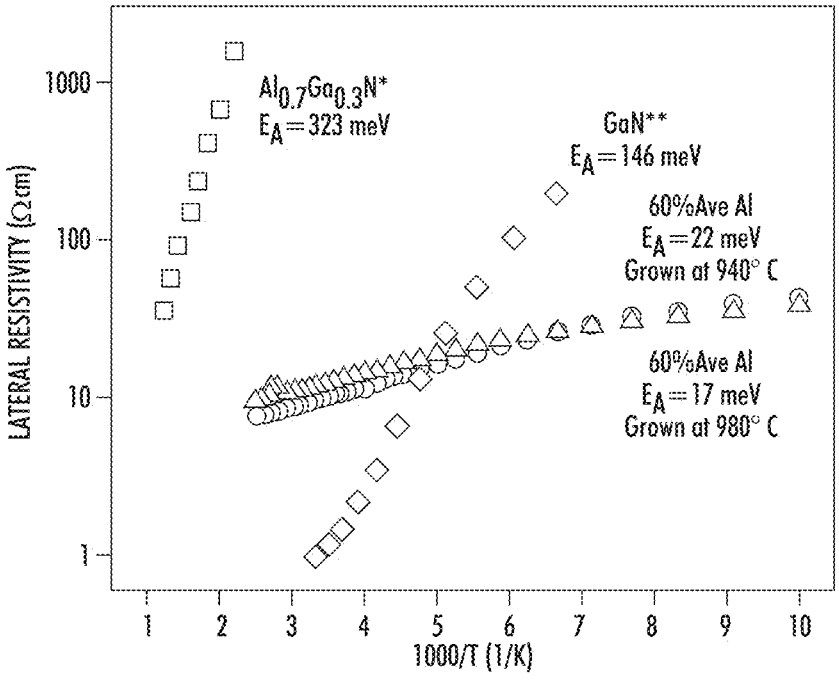
LATERAL RESISTIVITY (Ω cm)
1000
100
10
1
1
2
3
4
5
6
7
8
9
10
1000/T (1/K)
Al0.7Ga0.3N*
EA = 323 meV
GaN**
EA = 146 meV
60%Ave Al
EA = 22 meV
Grown at 940° C
60%Ave Al
EA = 17 meV
Grown at 980° C

FIG. 9

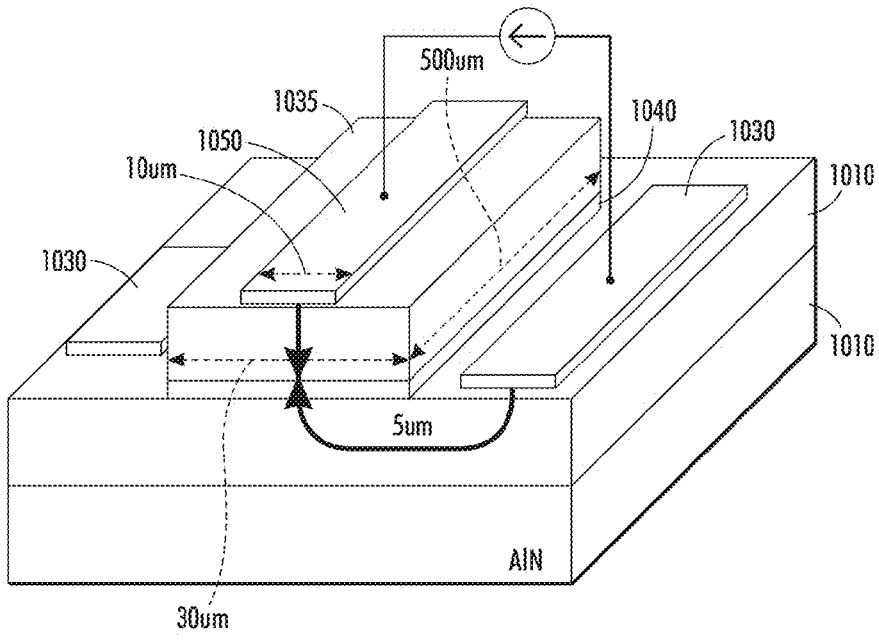

FIG. 10

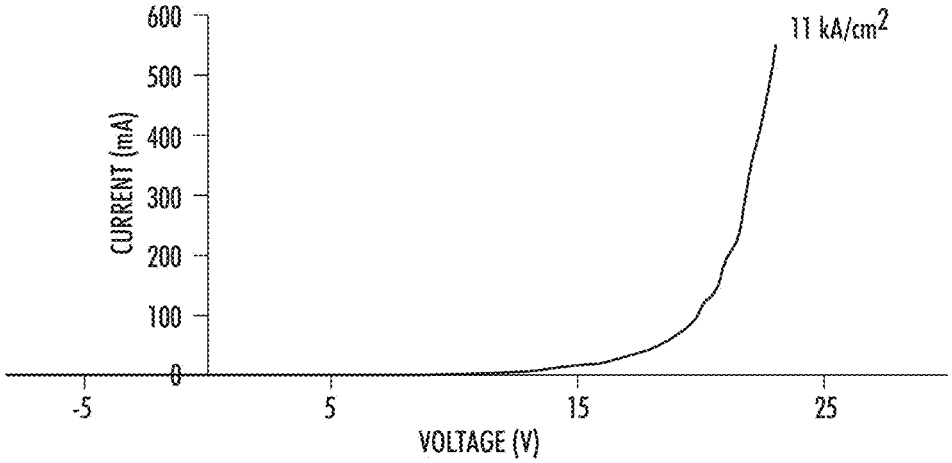
11 kA/cm2
CURRENT (mA)
600
500
400
300
200
100
0
-5
5
15
25
VOLTAGE (V)

FIG. 11

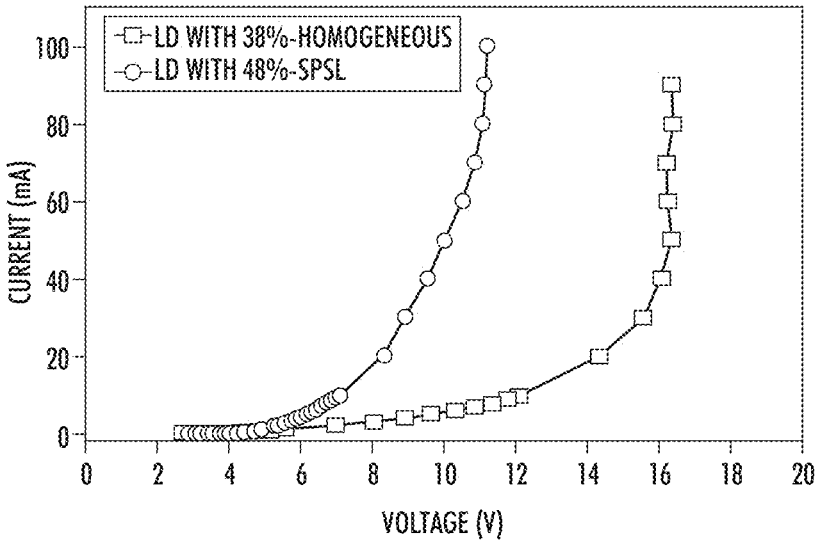
LD WITH 38%-HOMOGENEOUS
LD WITH 48%-SPSL
CURRENT (mA)
100
80
60
40
20
0
0
2
4
6
8
10
12
14
16
18
20
VOLTAGE (V)

FIG. 12

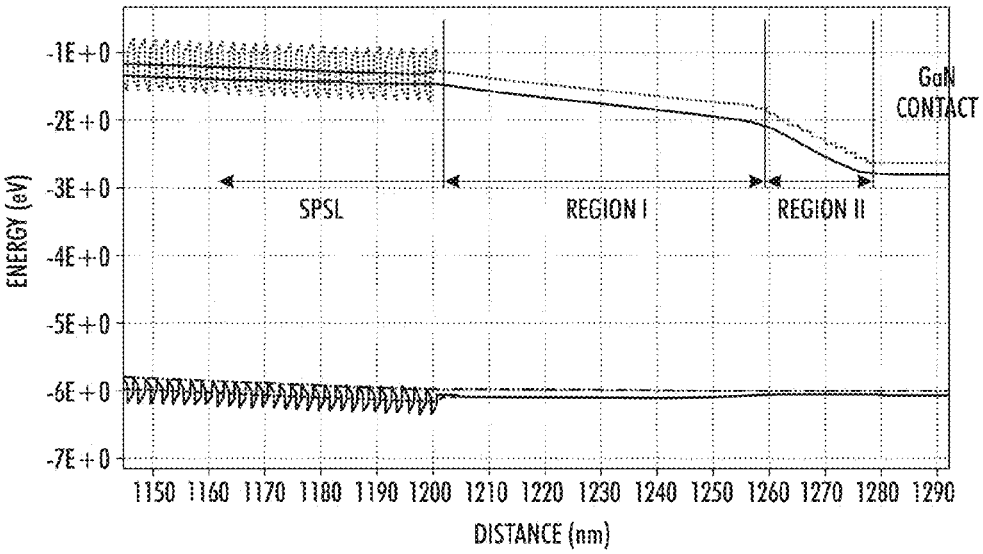
-1E+0
-2E+0
-3E+0
-4E+0
-5E+0
-6E+0
-7E+0
ENERGY (eV)
SPSL
REGION I
REGION II
GaN CONTACT
1150 1160 1170 1180 1190 1200 1210 1220 1230 1240 1250 1260 1270 1280 1290
DISTANCE (nm)

FIG. 13

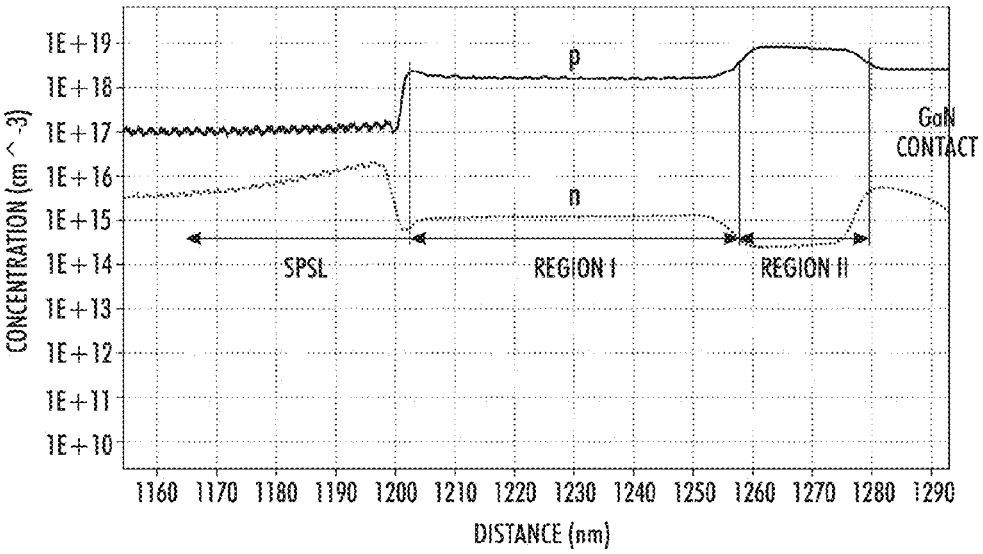
1E+19
1E+18
1E+17
1E+16
1E+15
1E+14
1E+13
1E+12
1E+11
1E+10
CONCENTRATION (cm ^ -3)
p
n
SPSL
REGION I
REGION II
GaN CONTACT
1160 1170 1180 1190 1200 1210 1220 1230 1240 1250 1260 1270 1280 1290
DISTANCE (nm)

FIG. 14

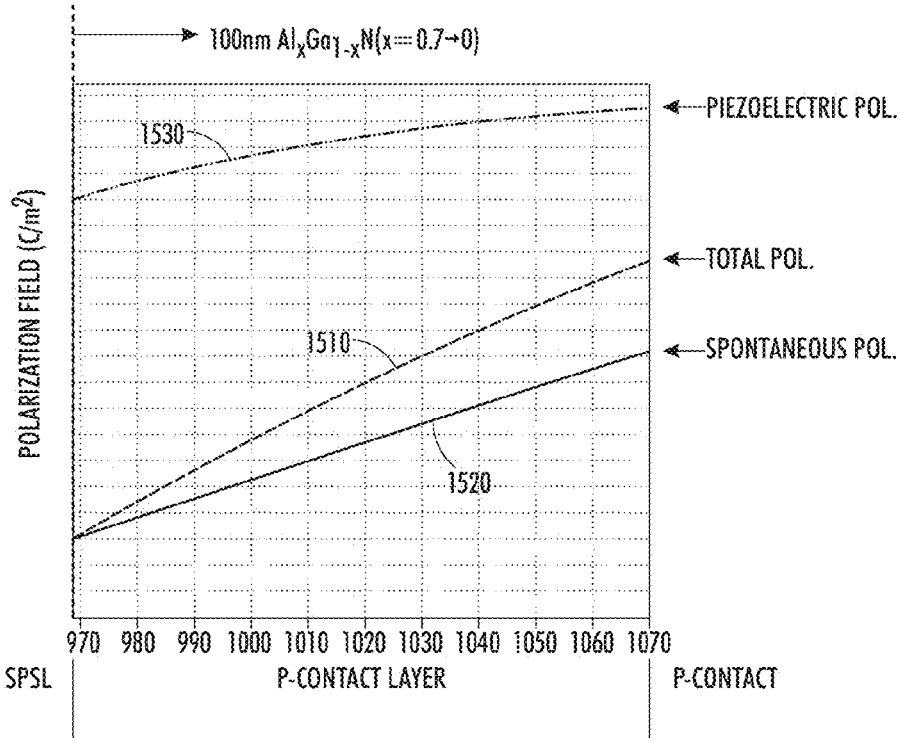
100nm $Al_xGa_{1-x}N(x=0.7\rightarrow0)$
PIEZOELECTRIC POL.
TOTAL POL.
SPONTANEOUS POL.
1530
1510
1520
POLARIZATION FIELD (C/m^2)
970 980 990 1000 1010 1020 1030 1040 1050 1060 1070
SPSL
P-CONTACT LAYER
P-CONTACT

FIG. 15

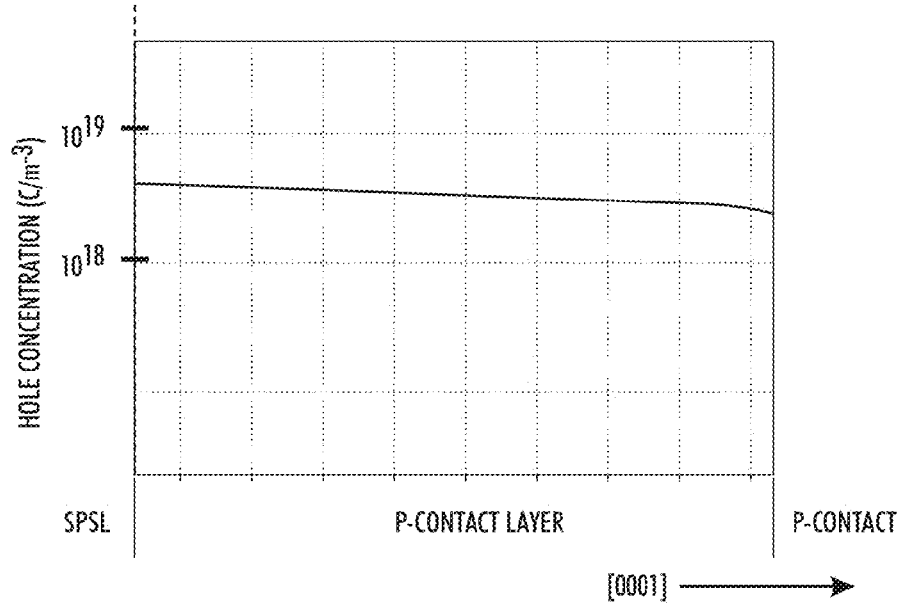
HOLE CONCENTRATION (C/m^3)
10^{19}
10^{18}
SPSL
P-CONTACT LAYER
P-CONTACT
[0001]

FIG. 16

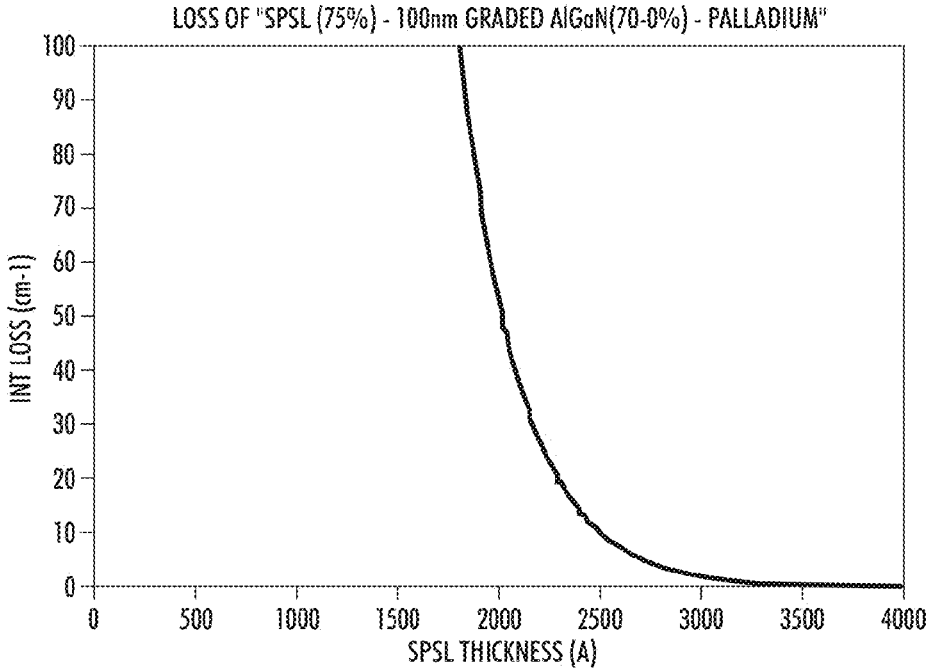
LOSS OF "SPSL (75%) - 100nm GRADED AlGaN(70-0%) - PALLADIUM"
INT LOSS (cm-1)
100
90
80
70
60
50
40
30
20
10
0
0
500
1000
1500
2000
2500
3000
3500
4000
SPSL THICKNESS (A)

FIG. 17

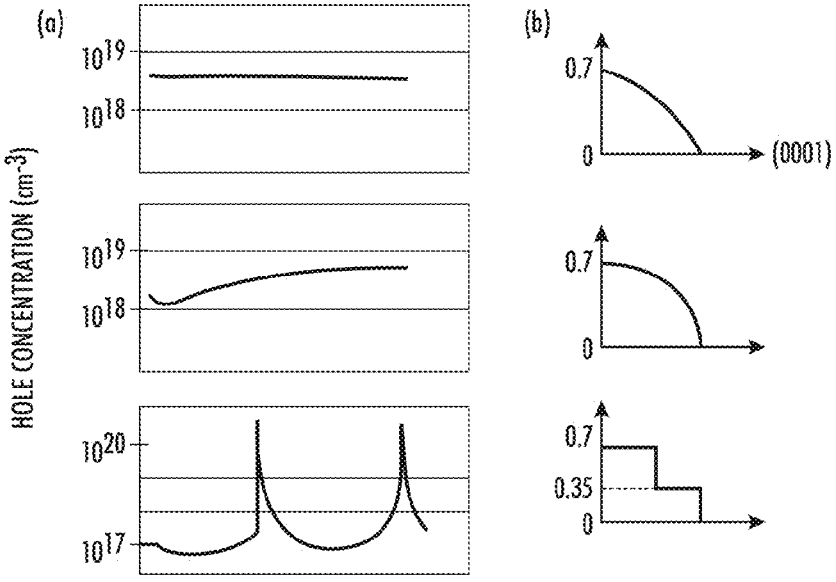
(a)
(b)
HOLE CONCENTRATION (cm-3)
10^19
10^18
10^19
10^18
10^20
10^17
0.7
0
(0001)
0.7
0
0.7
0.35
0

FIG. 18

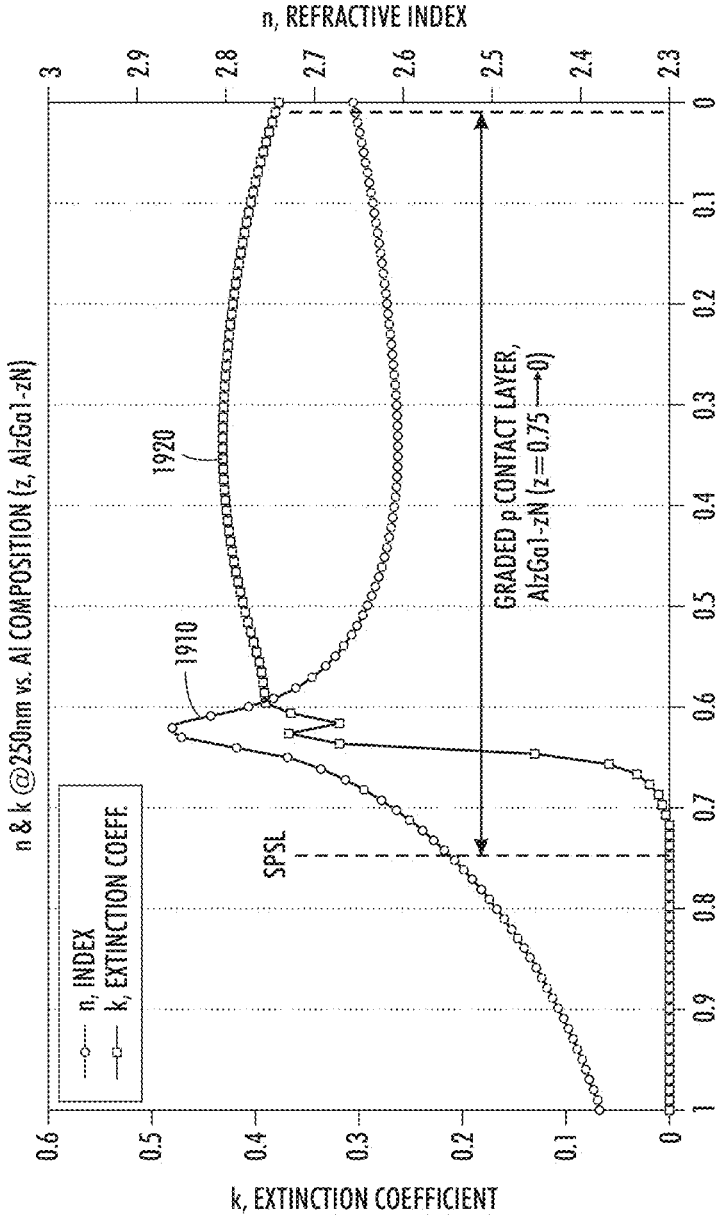
n, REFRACTIVE INDEX
n & k @250nm vs. Al COMPOSITION (z, AlzGa1-zN)
k, EXTINCTION COEFFICIENT
z, AlzGa1-zN (%)
n, INDEX
k, EXTINCTION COEFF.
1920
1910
SPSL
GRADED p CONTACT LAYER, AlzGa1-zN (z=0.75→0)

FIG. 19

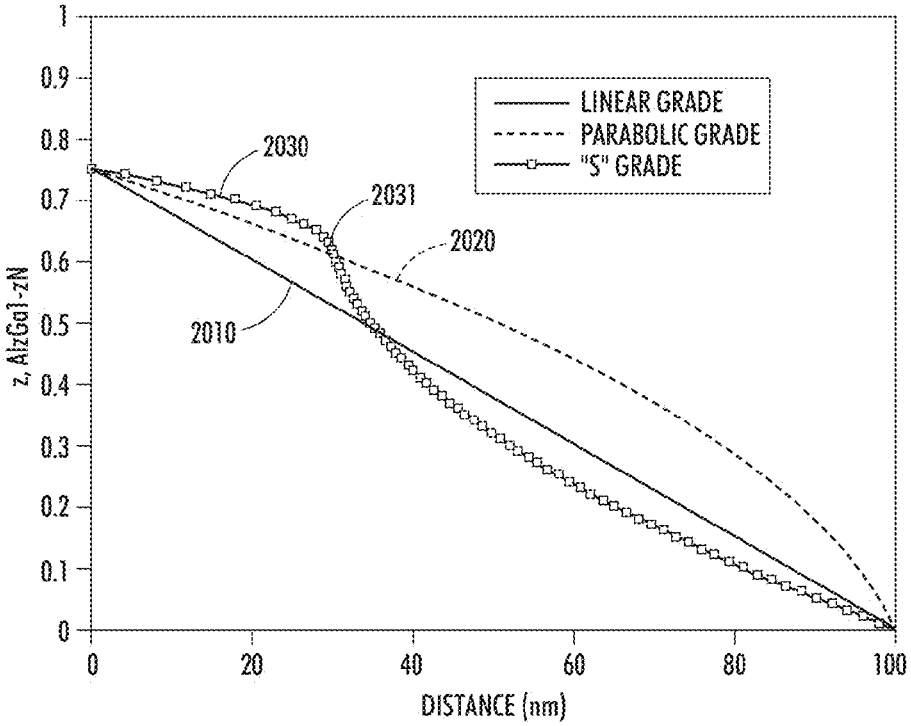

FIG. 20

	z@d=0nm	z@d=50nm	z@d=100nm
LINEAR	0.75	0.375	0
PARABOLIC	0.75	0.5	0

	z@d=0nm	z@d=15nm	z@d=30nm	z@d=65nm	z@d=100nm
S	0.75	0.71	0.62	0.2	0

WAIST

FIG. 21

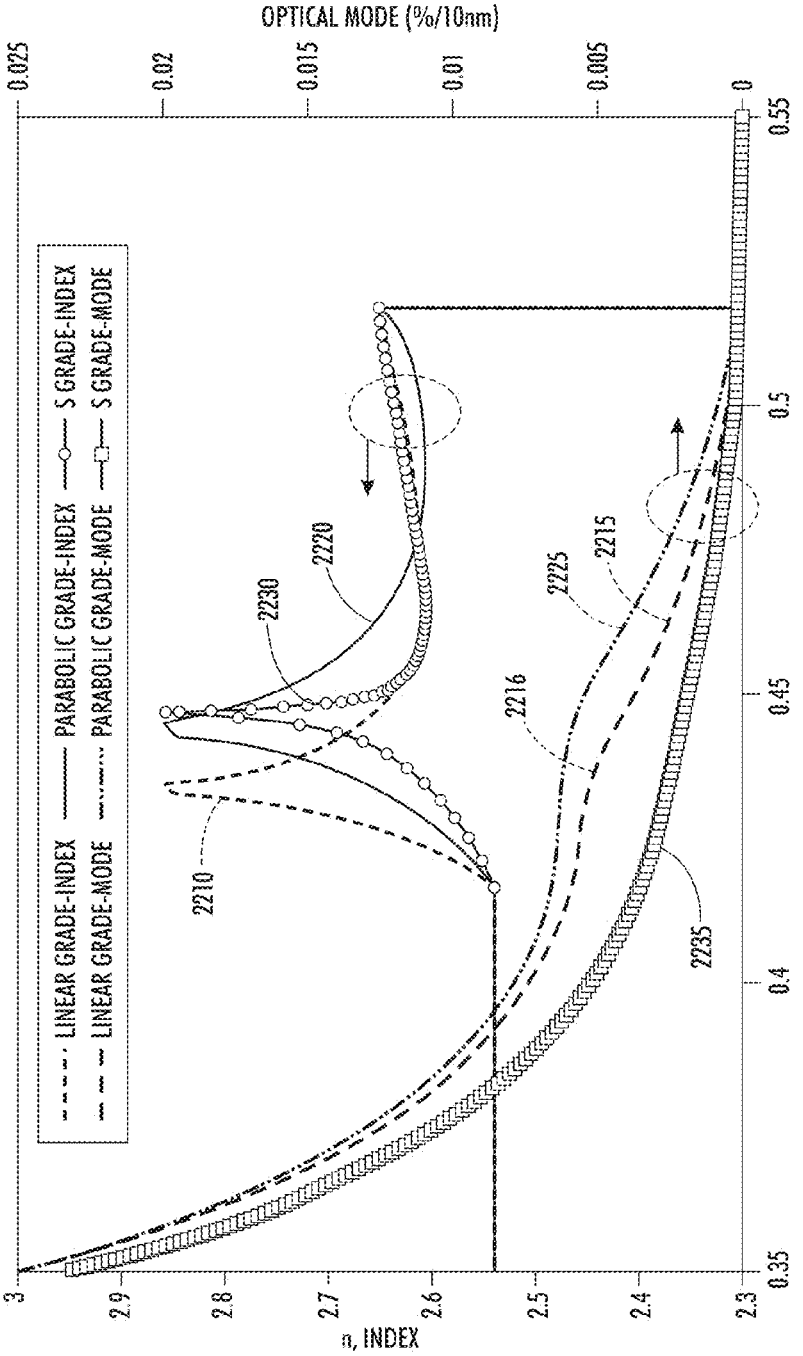
OPTICAL MODE (%/10nm)
0.025
0.02
0.015
0.01
0.005
0
LINEAR GRADE-INDEX
PARABOLIC GRADE-INDEX
S GRADE-INDEX
LINEAR GRADE-MODE
PARABOLIC GRADE-MODE
S GRADE-MODE
2210
2220
2230
2215
2225
2216
2235
0.55
0.5
0.45
0.4
0.35
DISTANCE (um)
3
2.9
2.8
2.7
2.6
2.5
2.4
2.3
n, INDEX

FIG. 22

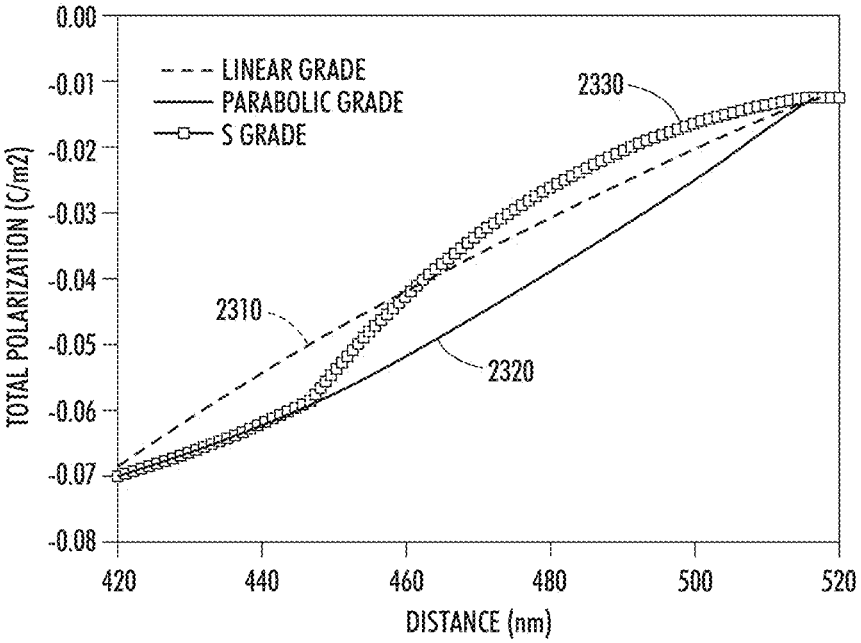
0.00
-0.01
-0.02
-0.03
-0.04
-0.05
-0.06
-0.07
-0.08
TOTAL POLARIZATION (C/m2)
LINEAR GRADE
PARABOLIC GRADE
S GRADE
2330
2310
2320
420
440
460
480
500
520
DISTANCE (nm)

FIG. 23

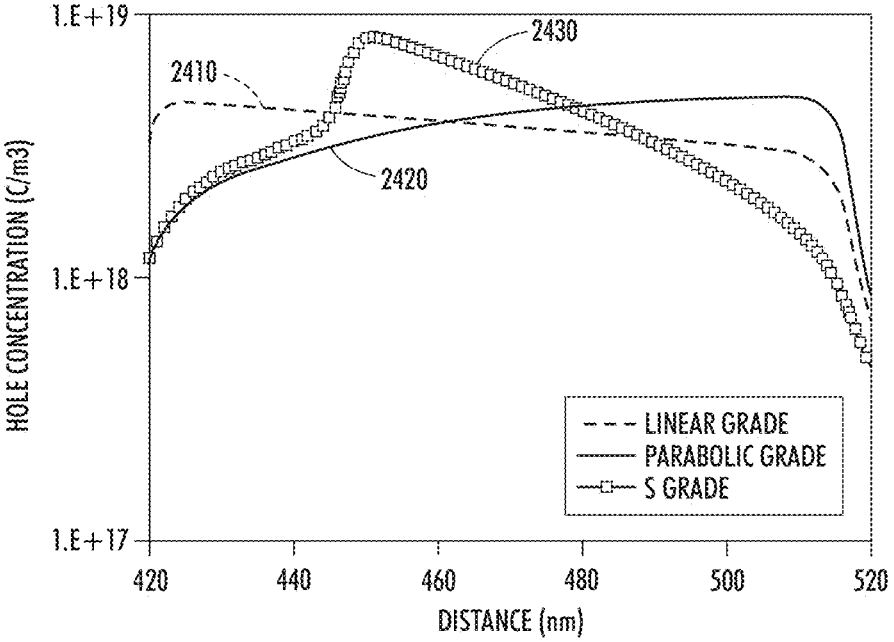
1.E+19
1.E+18
1.E+17
HOLE CONCENTRATION (C/m3)
2430
2410
2420
LINEAR GRADE
PARABOLIC GRADE
S GRADE
420
440
460
480
500
520
DISTANCE (nm)

FIG. 24

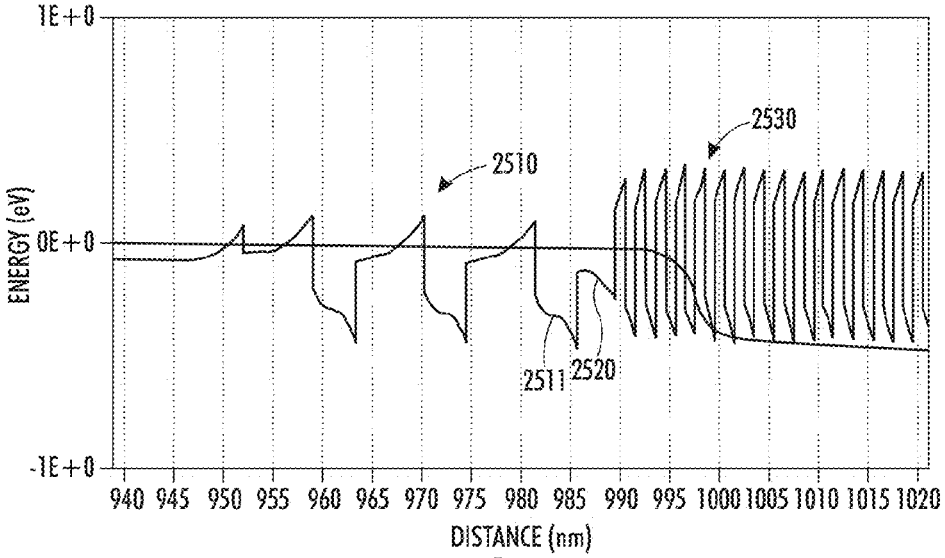
1E+0
0E+0
-1E+0
ENERGY (eV)
2510
2530
2511
2520
940 945 950 955 960 965 970 975 980 985 990 995 1000 1005 1010 1015 1020
DISTANCE (nm)

FIG. 25

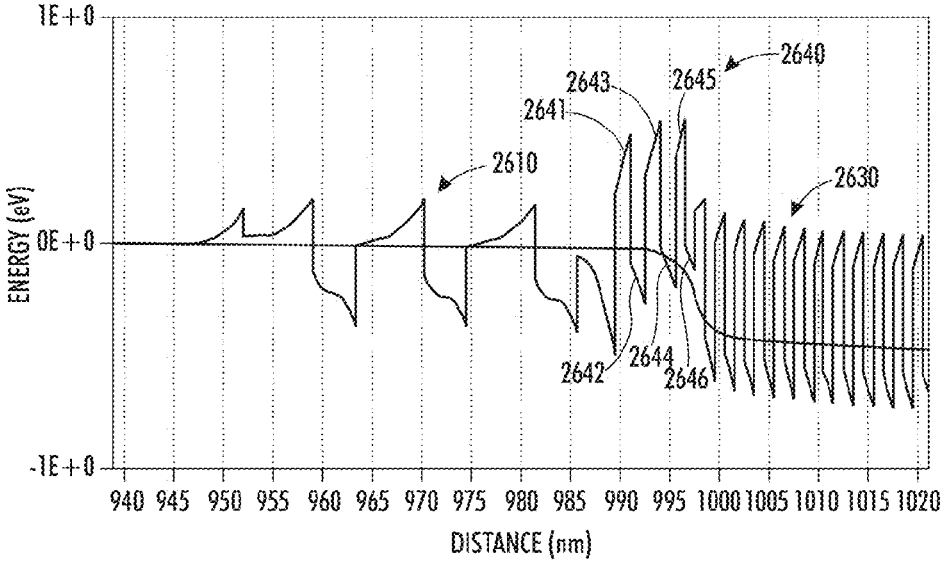
1E+0
0E+0
-1E+0
ENERGY (eV)
2610
2643
2641
2645
2640
2630
2642
2644
2646
940 945 950 955 960 965 970 975 980 985 990 995 1000 1005 1010 1015 1020
DISTANCE (nm)

FIG. 26

P-SIDE LAYERS FOR SHORT WAVELENGTH LIGHT EMITTERS

STATEMENT REGARDING FEDERALLY SPONSORED RESEARCH AND DEVELOPMENT

[0001] This invention was made with U.S. Government support through the Defense Advanced Research Projects Agency (DARPA) under Army Research Laboratory (ARL) Cooperative Agreement #W911NF-10-02-0102. The Government has certain rights in this invention.

SUMMARY

[0002] Various embodiments described herein involve light emitting devices comprising a p-side heterostructure that includes a short period superlattice (SPSL) having alternating layers of $Al_{xhigh}Ga_{1-xhigh}N$ doped with a p-type dopant and $Al_{xlow}Ga_{1-xlow}N$ doped with the p-type dopant, where $x_{low} \leq x_{high} \leq 0.9$. Each layer of the SPSL has a thickness of less than or equal to about six bi-layers of AlGaN. These light emitting devices include an n-side heterostructure and an active region configured to emit light disposed between the SPSL and the n-side heterostructure.

[0003] Some embodiments describe a light emitting device comprising a p-side heterostructure that includes a short period superlattice (SPSL) having alternating layers of $Al_{xhigh}Ga_{1-xhigh}N$ doped with a p-type dopant and $Al_{xlow}Ga_{1-xlow}N$ doped with the p-type dopant, where $x_{low} \leq x_{high} \leq 0.9$. The device includes an n-side heterostructure and an active region configured to emit light disposed between the SPSL and the n-side heterostructure. The alternating layers cause modulation in a valence band potential in the SPSL and the modulation is approximately equal to an acceptor level energy of the p-type dopant.

[0004] Some embodiments involve a light emitting device that includes a p-side heterostructure, an n-side heterostructure, and an active region configured to emit light that is disposed between the p-side heterostructure and the n-side heterostructure. The light emitting device also includes a metallic p-contact and a p-contact layer disposed between the p-side heterostructure and the p-contact. The p-contact layer comprises $Al_zGa_{1-z}N$ and having a thickness, D, where z has an S-shaped Al composition profile that varies over a substantial portion of the thickness of the p-contact layer. In some cases, the p-side heterostructure comprises a short period superlattice (SPSL) including alternating layers of $Al_{xhigh}Ga_{1-xhigh}N$ doped with a p-type dopant and $Al_{xlow}Ga_{1-xlow}N$ doped with a p-type dopant, where $x_{low} \leq x_{high} \leq 0.9$.

[0005] Some embodiments involve a light emitting device that includes a p-side heterostructure comprising a short period superlattice (SPSL), an n-side heterostructure; and an active region configured to emit light disposed between the SPSL and the n-side heterostructure. The SPSL comprises a first portion and a second portion, the first portion proximate the active region and comprising a first number of alternating layers of $Al_{x1high}Ga_{1-x1high}N$ and $Al_{x1low}Ga_{1-x1low}N$. The second portion comprises a second number of alternating layers of $Al_{x2high}Ga_{1-x2high}N$ and $Al_{x2low}Ga_{1-x2low}N$. A thickness of each layer of the SPSL has a thickness of less than or equal to about six bi-layers of AlGaN.

[0006] Methods of fabricating a light emitting device include growing an n-side heterostructure on a substrate, growing an active region on the n-side heterostructure, and growing a short period superlattice (SPSL) proximate to the active region. Growing the SPSL includes growing alternating layers of $Al_{xhigh}Ga_{1-xhigh}N$ doped with a p-type dopant and $Al_{xlow}Ga_{1-xlow}N$ doped with the p-type dopant, where $x_{low} \leq x_{high} \leq 0.9$ and each layer of the SPSL having a thickness of less than or equal to about six bi-layers of AlGaN.

[0007] The above summary is not intended to describe each embodiment or every implementation. A more complete understanding will become apparent and appreciated by referring to the following detailed description and claims in conjunction with the accompanying drawings.

BRIEF DESCRIPTION OF THE DRAWINGS

[0008] FIG. **1** depicts a cross sectional view of a light emitting device that may incorporate various optional layers that rely on polarization enhanced doping achieved by a varying Al composition in accordance with various embodiments;

[0009] FIG. **2** shows calculated transition levels for Mg atoms in a short period superlattice (SPSL) that exhibits polarization enhanced doping;

[0010] FIG. **3** is a family of graphs that show the total modulation of the valence band edge (V_{mod}) plotted as a function of x_{low} for a fixed x_{high};

[0011] FIG. **4** shows the total polarization of compressively strained AlGaN on relaxed AlN with respect to the angle between the surface normal and the c-axis;

[0012] FIG. **5** shows the optical transmission spectra of SPSLs having layers of several thicknesses;

[0013] FIG. **6** shows the calculated band structure of an Mg doped $Al_{0.74}Ga_{0.26}N/Al_{0.49}Ga_{0.51}N$ SPSL, where T_{high} is 0.7 nm and T_{low} is 0.9 nm;

[0014] FIG. **7** is an electron microscope image of a cross section of an AlGaN/AlGaN SPSL having alternating T_{high} and T_{low} layers of about 1 nm each;

[0015] FIG. **8** is a diagram that illustrates the test geometry used for testing the electrical resistivity of the SPSLs as a function of temperature;

[0016] FIG. **9** shows SPSL resistivities as a function of temperature for two different test SPSL heterostructures;

[0017] FIG. **10** is a schematic diagram of test structures used to test the current-voltage (IV) characteristics of light emitting devices that include the polarization enhanced SPSLs as discussed herein;

[0018] FIG. **11** shows the DC current-voltage (IV) characteristics of devices utilizing the polarization enhanced SPSL;

[0019] FIG. **12** compares the IV characteristic of a device utilizing a 48% average Al composition polarization enhanced SPSL with the IV characteristic of a device utilizing a conventional homogeneous AlGaN p-cladding layer having an Al composition of 38%;

[0020] FIG. **13** shows a simulation of the band structure for a device containing both a polarization enhanced SPSL and a piece-wise linearly graded $Al_zGa_{1-z}N$ p-contact layer;

[0021] FIG. **14** shows the carrier concentration in each of the two graded regions of the p-contact layer;

[0022] FIG. **15** shows polarization fields in Coulombs per meter squared (C/m2) for a linearly graded AlzGa1-zN p-contact layer with respect to distance;

[0023] FIG. **16** shows the hole concentration in the linearly graded $Al_zGa_{1-z}N$ p-contact layer with respect to distance;

[0024] FIG. **17** shows the intensity loss with respect to thickness of an SPSL having with x_{high}=1.0 and x_{low}=0.5 used in conjunction with a graded AlGaN p-contact layer having an Al composition that grades from 0.7 at the SPSL to 0 at the palladium (Pd) p-contact;

[0025] FIG. **18** illustrates three examples of hole concentrations calculated for several non-linear graded profiles;

[0026] FIG. **19** is a graph of the refractive index, n, and extinction coefficient, k, with respect to Al composition for wavelength λ=250 nm in an $Al_zGa_{1-z}N$ layer;

[0027] FIG. **20** illustrates linear, parabolic, and S-shaped Al composition profiles;

[0028] FIG. **21** provides tables of values of z at various distances within the p-contact layer for each of the Al composition profiles of FIG. **20**;

[0029] FIG. **22** provides the refractive index and transverse optical mode plots for the Al composition profiles of FIG. **20**;

[0030] FIG. **23** provides the total polarization for the Al composition profiles of FIG. **20**;

[0031] FIG. **24** provides the hole concentration for the Al composition profiles of FIG. **20**;

[0032] FIG. **25** is an energy diagram that shows the conduction band energy in the region of the quantum wells, in the region of the last barrier of the active region and in the region of the polarization enhanced SPSL; and

[0033] FIG. **26** is an energy diagram of an SPSL that is modified near the active region to form a section of the SPSL that provides the functionality of an electron blocking layer (EBL) for the active region.

[0034] Like reference numbers refer to like components; and

[0035] Drawings are not necessarily to scale unless otherwise indicated.

DESCRIPTION

[0036] Light emitting diodes and laser diodes that produce ultraviolet (UV) light have been used in a wide variety of applications including water purification, disinfection, security, UV curing, phototherapy, and medical diagnostics. For example, UV light can be produced by larger bandgap semiconductor materials, such as III-nitride materials including AlN, AlGaN, InGaN, InAlGaN, and others. However, doping these materials to achieve high hole concentration is difficult because the activation energy of dopants in these larger bandgap materials is relatively high. Approaches described in this disclosure relate to polarization enhanced doping that increases the hole concentration in one or more layers of light emitting devices

[0037] Polarization enhanced doping operates to increase the concentration of mobile carriers due to polarization fields that are present in the semiconductor layers. Polarization enhanced doping arises due to the electronegativities of atoms that create a dipole when two (or more) atoms having different electronegativities are chemically bonded in a compound. The dipole of the compound can result in polarization macroscopically across the layers in a crystal. The amount of polarization across the layers is influenced by the crystalline structure as well as the strain present in the crystalline lattice. III-nitride semiconductors grow crystals having wurtzite configuration, wherein the atomic crystal arrangement is such that a spontaneous polarization charge is present even under no applied strain.

[0038] The polarization of the crystal layers creates fixed charges at the interface between two layers of material with different polarization. Because the polarization charges are fixed, they do not themselves contribute to electrical transport in the crystal, however, the polarization charges can induce the creation of mobile carriers. The polarization charges are present when the polarization field within the crystal changes with distance. For example, a changing polarization field occurs across an interface of polar crystals. When fixed charges are present at the interface, the fixed charges are neutralized by mobile charges in the material. The amount of mobile charge that the polarization charges induce at the interface of two nitride layers is dependent on the composition and structure of the crystal. In the case of AlGaN, for example, the aluminum composition of the AlGaN at the junction determines the amount of polarization and thus the number of mobile charges induced at the interface. Note that polarization enhanced doping may be applied to carriers of either type. In nitride based light emitting devices, polarization enhanced doping is particularly relevant to enhancing hole concentration due to the difficulty of doping the nitride layers to achieve high p-type donor concentrations and simultaneously providing high conductivity layers.

[0039] FIG. **1** depicts a cross sectional view of a light emitting device **100** that may incorporate various optional layers that rely on polarization enhanced doping achieved by a varying Al composition. In the example shown in FIG. **1**, the light emitting device **100** includes an active region **105** disposed between a p-side heterostructure **120** and an n-side heterostructure **110**. For example, the p-side heterostructure **120** may comprises a p-side short period superlattice (SPSL) **121** comprising alternating layers of $Al_{xhigh}Ga_{1-xhigh}N/Al_{x-low}Ga_{1-xlow}N$, where x_{high} can range from about 1 to about 0.5 and x_{low} can range from about 0.75 to about 0, for example. P-contact layer **122** is disposed between the SPSL **121** and the p-contact, which may be a metal such as palladium (Pd). The p-contact layer **122** may comprise $Al_zGa_{1-z}N$ and may be graded according to an Al composition profile that decreases as a function of distance in a direction from the SPSL **121** towards the p-contact.

[0040] The layers of the n-side heterostructure **110**, active region **105**, and p-side heterostructure **120** can be epitaxially grown on a substrate comprising a hexagonal symmetry material, such as a group III-nitride material. Suitable materials for the substrate may comprise one or more of GaN, AlN, SiC, sapphire, Si, GaAs, ZnO, a group III-N alloy, and a template comprising a group III-N material.

[0041] In many cases, AlN provides a particularly suitable substrate for the AlGaN layers of the light emitting device because these AlGaN device layers have high Al content. Epitaxially growing high Al composition layers on AlN provides low mismatch between the substrate lattice and the lattice of the epitaxially grown layers. For example, the light emitting device may include a bulk AlN substrate, wherein the n-side heterostructure, active region, and p-side heterostructure are grown on the bulk AlN substrate. As an alternative to the bulk AlN substrate, an AlN template epitaxially grown on a substrate of sapphire or other material may be used.

[0042] The layers of the light emitting device **100** may be grown on a polar or semi-polar surface or facet of the substrate. In some embodiments, the substrate may comprise sapphire, a group-III nitride, SiC, or ZnO, wherein the n-side heterostructure, active region and p-side heterostructure are epitaxially grown on an (0001) or (0001) surface of the substrate. In some embodiments, the substrate may comprise a group-III nitride, SiC, or ZnO, wherein the n-side heterostructure, active region and p-side heterostructure are epitaxially grown on a semi-polar facet of the substrate.

[0043] The active region **105** may include one or more quantum wells that are separated by barriers and/or multiple

quantum well structures that are separated by spacers. Electrons from the n-side of the device and holes from the p side of the device diffuse to the active region **105** where they can recombine to generate light. The quantum wells, barriers, and/or spacers may be formed using any nitride based material system, such as InGaN, AlGaN, InAlN, InAlGaN, or other nitrides, or polar oxides such as the BeMgZnO system. In some cases, an electron blocking layer (EBL) **125** is disposed between the last quantum well structure of the active **105** region and the p side heterostructure **120** to help contain electrons within the active region **105**. Because light emission depends on recombination of holes and electrons in the active region **105**, it is beneficial to retain electrons in the active region to increase the likelihood of recombination.

[0044] It can be difficult to achieve sufficiently high p-type conductivity together with sufficiently high optical transparency in the semiconducting material in the p-side heterostructure **120** situated between the metal p-contact and the active region **105** in a short wavelength (λ~250 nm) laser in the nitride system. For example, AlGaN used in the p-side layers **120** must be sufficiently conductive and at the same time sufficiently transparent at the lasing wavelength. Magnesium can be used as a p-type dopant for AlGaN, and because the energy of the Mg acceptor level in AlGaN increases with Al composition, it becomes more difficult to achieve high hole concentration and conductivity as the Al composition increases. Transparency, however, is more readily achieved in AlGaN when Al composition is large, and this places a competing constraint on Al composition in the p-side layers. Another constraint is the need to establish a good electrical contact between the nitride material and the metal electrode of the p-contact. This requirement is more readily satisfied by forming the contact between a metal and GaN (approximately zero Al composition).

[0045] Embodiments discussed herein involve designs for p-layer structures that simultaneously achieve sufficient p-type conductivity, sufficient optical transparency and enable the establishment of a low resistivity electrical contact between the p-type material and the metal electrode. The approaches discussed herein can involve an acceptor-doped $Al_{xhigh}Ga_{1-xhigh}N/Al_{xlow}Ga_{1-xlow}N$ SPSL **121** that can optionally be used in conjunction with a acceptor-doped graded AlGaN p-contact layer **122** that connects the SPSL **121** to a metal p-contact. A suitable acceptor for AlGaN comprises magnesium (Mg). Other possible p-type dopants for AlGaN include Be and C. The graded p-contact layer may comprise $Al_zGa_{1-z}N$ where z is graded according to a profile, which may be constant, linear, parabolic, and/or S-shaped, for example. Sufficiently low optical absorption losses, sufficiently high p-type conductivity, and a good electrical contact can be achieved with these approaches.

[0046] In some embodiments, the Al composition in the SPSL **121** alternates between a relatively high value (x_{high}~0.9) and a relatively low value (x_{low}~0.5). The thickness of the $Al_{xhigh}Ga_{1-xhigh}N$ layers is denoted herein as T_{high} and the thickness of the $Al_{xlow}Ga_{1-xlow}N$ is denoted T_{low}. T_{high} and T_{low} can be in a range of about 0.7 nm to about 1.5 nm, for example, or less than about 6 bi-layers. The term "bi-layer" designates a pair of layers comprising one layer of group III atoms and one layer of N atoms. The layer of group III atoms comprises a mixture of Al and Ga atoms. Each bi-layer of AlGaN has a thickness of about 0.25 nm. The overall thickness of the SPSL **121** is subject to several constraints. According to one constraint, for an SPSL used as a cladding layer, it is desirable for the SPSL to be relatively thick to contain the optical mode. As a competing constraint, it is desirable for the SPSL to be relatively thin to decrease the electrical resistivity and increase the vertical current flow through the SPSL. As a competing constraint, it is desirable for the SPSL to be relatively thin to decrease the electrical resistivity and therefore allow high current flow through the SPSL with relatively less heating. To achieve these competing constraints, the total thickness of the SPSL may be greater than about 200 nm and less than about 450 nm, for example. The average Al composition in the SPSL **121** can be calculated $x_{ave}=(x_{high}T_{high}+x_{low}T_{low})/(T_{high}+T_{low})$. The average Al composition must be sufficiently high to prevent significant absorption of the light generated in the device. For example, for λ equal to about 290 nm, an average Al composition can be in a range of greater than about 45% and less than about 80%. For λ greater than about 330 nm, an average Al composition can be in a range of greater than about 30% and less than about 80%.

[0047] If the SPSL is used as a cladding layer in a laser diode, it can be helpful to push the optical mode away from the p-side of the device, which can be achieved using a relatively high average Al composition, e.g., greater than about 60% for λ=290 nm. The use of higher Al composition in the p-cladding of the laser diode may appear to be counterintuitive because resistivity of the p-cladding layer increases with Al composition. However, as a competing constraint, the high Al composition can operate to push the optical mode to the n-side of the device and thus reduce optical loss.

[0048] FIG. **2** illustrates polarization enhanced doping in an SPSL. For devices comprising an AlGaN SPSL grown on c-plane substrates, the c-axis of the AlGaN is perpendicular to the plane of the layers. In such a SPSL there will be a large discontinuity in the polarization at each interface. The magnitude of the discontinuity depends on the strain in the layers, and on the change in the composition at the interface. This discontinuity in the polarization gives rise to an electric field in each layer, which, together with the valence band offset between $Al_{xhigh}Ga_{1-xhigh}N$ layers, e.g., AlN in FIG. **2** and the $Al_{xlow}Ga_{1-xlow}N$ layers, e.g., $Al_{0.5}Ga_{0.5}N$ in FIG. **2**, gives rise to a modulation of the potential within the crystal. The modulation of the potential leads to the ionization of p-type dopants and the formation of holes. P-type dopants (such as Mg atoms) that are located in layers with high Al composition are likely to become ionized by capturing an electron. The electron is removed from the layers with lower Al composition, and this creates a hole. The holes tend to accumulate at an interface between the layers as indicated schematically in FIG. **2**.

[0049] FIG. **2** shows calculated transition levels **210**, **211** for Mg atoms. The dashed line represents the calculated Fermi energy **220** and the solid line represents the valence band maximum **220** of the SPSL. When the transition level **211** for a given Mg atom is below the Fermi energy **220**, that Mg atom will likely be ionized and in a negatively charged state. Mg atoms located in the Al-rich part of the SPSL have transition levels **211** that are below the valence band maximum **230** of the SPSL structure. These Mg atoms will likely become negatively charged and this gives rise to holes **240**. The Mg atoms located in regions having less Al have transition levels **210** that are above the Fermi energy **220**. These Mg atoms are likely to remain in the neutral charge state.

[0050] The SPSL gives rise to a modulation in the valence band edge. The modulation of the valence band edge in a short period SPSL, defined as V_{mod}, is approximately equal to the

sum of the valence band offset (VBO) between the two materials in the SPSL and the change in potential in the SPSL arising from the polarization charges at the interfaces. For the AlGaN system we can estimate the valence band offset (VBO) as follows. The VBO between $Al_{xhigh}Ga_{1-xhigh}N$ and $Al_{xlow}Ga_{1-xlow}N$ is approximately equal to:

$$VBO=0.3\ \{E_{gap}(Al_{xhigh}Ga_{1-xhigh}N)-E_{gap}(Al_{xlow}Ga_{1-xlow}N)\}.$$

where E_{gap} is the energy gap between the valance band and the conduction band. Approximately 30% of the difference in the band gaps contributes to an offset in the valence bands and the remaining 70% contributes to an offset in the conduction bands. Combining this with $E_{gap}(Al_{xhigh}Ga_{1-xhigh}N)$=xhigh E_{gap}(AlN)+(1-xhigh)E_{gap}(GaN)−b xhigh(1-xhigh), we may obtain an estimate for VBO as a function of the xhigh and xlow for the two materials. We employ E_{gap}(AlN)=6.2 eV, E_{gap}(GaN)=3.4 eV, and b=0.7 eV to obtain VBO.

[0051] The electric fields E_{xhigh} and E_{xlow} in the superlattice composed of alternating layers of $Al_{xhigh}Ga_{1-xhigh}N$ and $Al_{xlow}Ga_{1-xlow}N$ with thicknesses T_{high} and T_{low} may be written as

$$E_{xhigh}=T_{low}(P_{xlow}-P_{xhigh})/(T_{high}\epsilon_{xlow}+T_{low}\epsilon_{xhigh}),$$

$$E_{xlow}=T_{high}(P_{xhigh}-P_{xlow})/(T_{high}\epsilon_{xlow}+T_{low}\epsilon_{xhigh})$$

In these expressions P_{xlow} and P_{xhigh} are the polarizations in the $Al_{xlow}Ga_{1-xlow}N$ and the $Al_{xhigh}Ga_{1-xhigh}N$ and ϵ_{xhigh} and ϵ_{xlow} are the dielectric constants of the two materials. The change in potential across the SPSL segment of thickness T_{high} is T_{high} E_{xhigh} and the change in potential across the superlattice segment of thickness T_{low} is T_{low} E_{xlow}. Note that T_{high} E_{xhigh}=−T_{low} E_{xlow}. The total modulation of the valence band edge (V_{mod}) is the sum of the contributions arising from the band offset and the polarization fields. V_{mod} is plotted in FIG. **3** as a function of x_{low} for a fixed x_{high}. For the simulation of FIG. **3**, T_{high} and T_{low} are each equal to one nanometer.

[0052] In many cases, the SPSL has a total modulation in the valence band potential that is comparable (e.g., about equal) to the energy of the acceptor level of the p-type dopant. For the AlGaN system the most common acceptor is Mg and the energy of the acceptor level in $Al_{0.5}Ga_{0.5}N$ is approximately 0.35 eV above the valence band maximum, as shown by the dashed line **310** in FIG. **3**. When the modulation of the valence band produced by the SPSL is sufficiently large, the number of ionized acceptors is significantly enhanced in comparison to a homogeneous layer. This requirement places a constraint on the Al compositions in the SPSL. Specifically the difference between x_{high} and x_{low} should be greater than about 0.25 in order to achieve a significant benefit from the polarization enhanced approach. This is seen in the FIG. **3**, where the total modulation in the potential as a function of x_{low} is shown for x_{high} set equal to 0.5, 0.75, or 1.0. If we choose x_{high} to be 0.75 then we choose x_{low} to be less than about 0.5. Performing the same estimation for T_{high}=T_{low}=0.75 nm leads to a similar conclusion. Thus, a possible embodiment of an effective $Al_{xhigh}Ga_{1-xhigh}N/Al_{xlow}Ga_{1-xlow}N$ SPSL approach is one where T_{high} and T_{low} are each less than or equal to one nanometer, and $x_{high}-x_{low}$ is greater than about 0.25.

[0053] The device illustrated in FIG. **1** can be grown in a polar orientation on the group-III face (0001) of the III-N material, e.g., the Al face of an AlN substrate. It is also possible to exploit polarization enhanced doping in devices grown on a semi-polar facet of the substrate. For semi-polar orientations, however, the change in polarization at the interfaces is reduced, and so the electric fields in the layers are reduced in comparison to c-plane interfaces. Thus, the enhancement of hole concentration is expected to be reduced in devices grown in semi-polar orientations as compared with devices grown in polar orientations.

[0054] FIG. **4** shows the total polarization of compressively strained AlGaN on relaxed AlN with respect the angle between the surface normal and the c-axis. The total polarization is dependent on both the spontaneous polarization of the material and the piezoelectric polarization which arises from compressive strain in the AlGaN layer and unstrained The total polarization ΔP_{total} of c-plane compressively strained GaN on bulk AlN is approximately 0.08 C/m^2. For a c-axis oriented interface between $Al_{0.5}Ga_{0.5}N$ and AlN the discontinuity in the polarization is approximately 0.05 C/m^2. The polarization discontinuity would be reduced if a semi-polar surface orientation such as $(11\bar{2}2)$ is employed.

[0055] As previously discussed in connection with FIG. **2**, a possible SPSL design that exploits polarization enhanced doping includes alternating 1 nm layers of $Al_{0.5}Ga_{0.5}N$ and AlN. One nanometer of material corresponds to about 4 (0001) layers of AlN. For a superlattice having these specifications, the total potential modulation, indicated by arrow **230** in FIG. **2**, is about 0.7 eV. Based on the calculations discussed in connection with FIG. **2**, a substantial fraction of Mg atoms present in the superlattice will be ionized.

[0056] An SPSL comprising 1 nm layers of $AlN/Al_{0.5}Ga_{0.5}N$ illustrates one configuration, note that other layer thicknesses and compositions can also be useful. For example, to increase the modulation, a larger contrast in Al composition may be useful. For example, a lattice that includes alternating layers of $Al_{0.25}Ga_{0.75}N$ and AlN (75% contrast) would provide additional contrast when compared to the $Al_{0.5}Ga_{0.5}N$/AlN embodiment. The amount of contrast may be constrained by a maximum Al composition and a minimum Al composition. For example, it becomes more difficult to incorporate the p-type dopant into a layer that has a very high Al content, e.g., above 0.9. Furthermore, lower Al compositions, e.g., less than about 0.25 absorb more of the light generated by the device. Optimal Al compositions for the superlattice structures take into account all the constraints including difficulty of doping high Al composition AlGaN, absorption of light at lower Al compositions, and sufficient contrast to achieve modulation for polarization enhanced doping. In some implementations, optimal Al compositions for the layers of the polarization enhanced SPSL may alternate from x_{high} less than about 0.9 to x_{low} greater than about 0.44.

[0057] The thicknesses of the AlGaN layers in the polarization enhanced SPSL must be sufficiently small so that vertical transport of holes perpendicular to the layers is possible. The band gap of bulk $Al_xGa_{1-x}N$ for x less than about 0.5 is too low to prevent absorption of light at wavelengths less than or equal to 250 nm. However, quantum confinement in the SPSL increases the energy gap of the SPSL so that absorption of light in an SPSL having alternating layers $AlN/Al_{0.5}Ga_{0.5}N$/or $Al_{xhigh}Ga_{1-xhigh}N/Al_{xlow}Ga_{1-xlow}N$ with average Al composition of greater than about 0.60, e.g., $Al_{0.74}Ga_{0.26}N/Al_{0.44}Ga_{0.56}N$, would be acceptably low. This type of SPSL is therefore appropriate for a laser emitting at around 250 nm.

[0058] FIG. **5** is a graph that shows the optical transmission spectra of a p-side SPSL hole transport layer comprising 1.02 nm layers of $Al_{0.5}Ga_{0.5}N$ alternating with 1.45 nm layers of

AlN (shown in graph **510**) and a similar superlattice with thicker AlGaN/AlN layers (6.15 nm layers of $Al_{0.5}Ga_{0.5}N$ alternating with 6 nm layers of AlN) (shown in graph **520**). The sample with thicker AlGaN layers shows a transmission dip at around λ=279 nm, corresponding to the band edge absorption of the AlGaN component of the superlattice. When the superlattice layers are made thinner according to the design discussed in connection with FIG. **2**, the absorption edge moved to λ=238 nm, indicating that the hole transport layer has the desired property of low absorption at the design wavelength of λ=250 nm. Comparison of these spectra **510**, **520** illustrates the enhanced optical transmission for the SPSL having thinner layers.

[0059] The thicknesses, T_{high}, and T_{low}, of individual layers of an $Al_{xhigh}/Ga_{1-xhigh}N/Al_{xlow}Ga_{1-xlow}/N$ within the SPSL may be only a few (e.g., **6**) atomic bi-layers thick, as previously discussed. The high polarization fields within the SPSL promotes ionization of dopants, leading to improved hole generation and to lower electrical conductivity. FIG. **6** shows the calculated band structure of an Mg doped $Al_{0.74}Ga_{0.26}N/Al_{0.49}Ga_{0.51}N$ SPSL, where T_{high} is 0.7 nm and T_{low} is 0.9 nm. The energy levels of the Mg donors below the Fermi level, E_f, within the L1 region imply that Mg atoms within the L1 region of the SPSL can be ionized by the polarization fields. The resulting holes are then free to migrate to the lower energy wells within the adjacent L2 regions. Since the SPSL layers are very thin, vertical hole transport can be supported by tunneling. FIG. **7** is a cross section transmission electron micrograph (TEM) showing the SPSL structures that maintain sharp interfaces between the thin layers having thicknesses T_{high} and T_{low} of less about 1 nm.

[0060] The AlGaN/AlGaN SPSL shown in FIG. **7** was grown using metal organic chemical vapor deposition (MOCVD). Processes disclosed herein include heterostructure crystal growth conditions that enable sharp interfaces to be formed between such ultra-thin layers. It can be challenging to grow these SPSLs that vary the Al composition across thin layers with sharp interfaces because if appropriate growth conditions are not maintained, the very thin layers can merge into one alloy. For example, in some cases, growing the SPSL layers at temperatures of about 930 to 980° C. and pressure of about 200 torr allows for optimal crystal quality and incorporation of Mg dopants.

[0061] Growing the layers at a fairly slow growth rate can be used to achieve crystal quality and Mg incorporation. In one example, layers are grown at a rate of 0.01 to 0.04 nm per sec, corresponding to a metal organic Trimethylgallium (TMG) flow rate of 0.5 sccm and to an ammonia flow rate of 4 liters per minute. The high ammonia flow rate relative to TMG leads to a high V-III partial pressure, which can provide high crystal quality.

[0062] In general, the layers can be grown under relatively low ambient pressures of between about 80 torr up to about 700 torr and at a relatively low temperature between about 750° C. and about 1300° C. The selected growth temperature needs to achieve acceptable crystal quality, acceptor donor incorporation, and relatively sharp features between the layers of the SPSL.

[0063] Polarization-assisted hole-doped SPSL designs disclosed herein can support high levels of vertical current injection. The average Al composition in the superlattice depends on the wavelength of the emitted light. Total thickness as well as individual layer thickness of the SPSL in the device are chosen to reduce electrical resistance and allow hole transport by tunneling. We successfully injected pulsed currents with peak current densities of up to 21 kA/cm^2 through the devices. The devices also displayed reasonable voltages and handled DC current densities of as high as 11 kA/cm^2. These SPSL designs were incorporated into different laser diode heterostructures that were processed into two types of testable laser structures. The test geometry schematically shown in FIG. **8** was used for testing the electrical resistivity of the SPSLs as a function of temperature. Test structures schematically shown in FIG. **10** were used to test the current-voltage (IV) characteristics of the SPSLs.

[0064] Turning now to tests of electrical resisitivity as a function of temperature, FIG. **8** shows the test geometry used for temperature testing of the SPSLs. Test devices were fabricated by forming Pd p-contacts on the p-contact layer (p+ GaN layer) and etching away the p+GaN layer material at regions between the contacts. The pattern of the p-contacts is processed into Van Der Pauw pattern for resistivity measurement.

[0065] FIG. **9** shows SPSL resistivities as a function of temperature for two different test SPSL heterostructures. Both designs have x_{high}=74%, T_{high}=0.7 nm and x_{low}=49%, T_{low}=0.9 nm-thick which is the layer combination indicated in FIG. **6**. The corresponding average aluminum composition is 60% for both SPSLs is, and they both behave optically like 60% AlGaN. One structure was grown at a temperature of 940° C., while the other structure was grown at 980° C. FIG. **9** shows that the lateral electrical resistivities of these test SPSLs have nearly a-thermal behaviors, wherein the lateral resistivity changes by less than about 50 Ω-cm over a temperature range of 400 K to 100 K. The sample grown at 940° C. and the sample grown at 980° C. show similar behaviors. This weak temperature dependence suggests that the doping ionization mechanism is indeed a-thermal, which would be expected in the polarization-induced hole activation process previously described.

[0066] For comparison, FIG. **9** also plots the resistivity behavior of p-doped GaN and homogeneous p-doped $Al_{0.7}Ga_{0.3}N$. Both the p-GaN and the homogeneous p-AlGaN exhibit sharp increases in electrical resistivities with reduced temperatures as is characteristic of thermal hole activation. The thermal activation energy of the SPSL samples are 22 meV and 17 meV for the 940° C. and the 980° C. samples, respectively. In comparison, the activation energies are 323 meV for the homogeneous p-AlGaN and 146 meV for the p-GaN. Additionally, the AlGaN polarization enhanced SPSL designs described herein produce low resistivity of about 20 Ω-cm at temperatures less than about 175 K and/or about 10 Ω-cm at room temperature.

[0067] FIG. **10** shows a three dimensional schematic view of the test structure used for IV testing of the SPSL structures. The test structure **1000** is a light emitting device that includes an AlN substrate **1010** with n-side heterostructure **1020**, active region **1040**, and p-side heterostructure **1035** (that includes the polarization enhanced SPSL) grown in that order on the AlN substrate **1010**. A metallic n-contact **1030** makes electrical contact to the n-side heterostructure and a metallic p-contact **1050** makes electrical contact with the p-side heterostructure. FIG. **11** shows the DC current-voltage (IV) characteristics of devices utilizing the polarization enhanced SPSL. The results indicate successful vertical current injection through the device as the very thin layers of the polarization enhanced SPSL can achieve DC current densities of about J=11 kA/cm^2. FIG. **12** compares the IV characteristic

of a device utilizing a 48% average Al composition polarization enhanced SPSL with the IV characteristic of a device utilizing a conventional homogeneous AlGaN p-cladding having an Al composition of 38%.

[0068] Referring back to FIG. **1**, a graded p-contact layer **122** may be used alone or in conjunction with the polarization enhanced SPSLs described above. The graded p-contact layer has higher Al composition at the interface between the p-heterostructure and the p-contact layer and a lower Al composition at the interface between the p-contact layer and the p-contact. In some cases, the Al composition decreases linearly or piece-wise linearly across the p-contact layer, although other profiles are also useful, as discussed herein.

[0069] A simulation of the band structure for a device containing both a polarization enhanced SPSL and a graded $Al_zGa_{1-z}N$ p-contact layer is shown in FIG. **13**. In this device, the Al composition is graded from the average composition of the superlattice ($z=x_{ave}=0.59$) at the polarization enhanced SPSL down to z=0 at the p-contact. In this particular device, the grading is piecewise linear in two regions as shown in FIG. **13**. The grading takes place in two steps: from z=0.59 to z=0.41 over a distance of 63 nm (Region I) and from z=0.41 to z=0 over a distance of 20 nm (Region II). As seen in FIG. **14**, the hole concentration in each of the two graded regions of the p-contact layer is enhanced relative to the hole concentration in the SPSL. This approach allows for the optical absorption in Region I to be very low because the energy band gap of the $Al_zGa_{1-z}N$ in Region I is greater than the energy of the light emitted from the active region. Region I does not therefore contribute to the optical loss. By inclusion of a sufficiently thick Region I, it is possible to reduce the overlap of the optical mode with the absorbing GaN contact and thereby reduce optical loss. By employing a graded Region I the thickness of the SPSL can be reduced.

[0070] Grading the Al composition in the p-contact region produces a three-dimensional hole gas that extends over a region of thickness D, where D can be the thickness of the p-contact (if the grading is done across the entire layer, or other thickness across which the grading occurs. For example, the Al composition of $Al_zGa_{1-z}N$ in the p-contact layer may be graded linearly from z=0 at the interface between the p-contact layer and the p-contact to $z=\Delta zAl$ at the interface between the p-contact and the SPSL. In a linear approximation, the hole concentration h in such a region is given approximately by:

$$h=\Delta P\text{total}\Delta z\text{Al}/D \quad [1]$$

[0071] In this expression ΔPtotal is the change in the total polarization at an interface between AlN and GaN, ΔzAl represents the change in the Al composition across the thickness of the p-contact layer, D. For compressively strained GaN on bulk AlN ΔPtotal=0.08 C/m^2. The hole density h in the graded layer will be approximately 3×10^{18} cm^{-3} for d=100 nm and ΔzAl=0.7. This hole concentration is sufficient to achieve acceptable conductivity in this region. Higher concentrations can be obtained by employing a smaller value of D.

[0072] FIG. **15** shows polarization fields in Coulombs per meter squared (C/m^2) for a linearly graded $Al_zGa_{1-z}N$ p-contact layer with respect to distance. FIG. **16** shows the hole concentration in the $Al_zGa_{1-z}N$ p-contact layer with respect to distance for the linearly graded design. For the designs shown in FIGS. **15** and **16**, the thickness of the p-contact layer, D, is 100 nm and z changes from 0.7 to 0. The total polarization **1510** is dependent on the spontaneous polarization **1520** and piezoelectric polarization **1530**, which arises from strain in the layer.

[0073] As indicated in FIG. **16**, the hole concentration is substantially uniform across the 100 nm layer. The polarization field of the graded layer creates a nearly uniform hole gas and therefore enhances conductivity in the vertical direction (the [0001] direction) through the device.

[0074] The thickness and the effective index of refraction of the SPSL should be sufficient to prevent the lasing mode from overlapping with absorbing regions, such as the graded layer and metal contacting electrode. FIG. **17** shows the intensity loss with respect to SPSL thickness of a AlGaN/AlN superlattice with $x_{high}=1.0$ and $x_{low}=0.5$ used in conjunction with a graded AlGaN p-contact layer having an Al composition that grades from 0.7 at the SPSL to 0 at the palladium (Pd) p-contact. Based on the optical modeling shown in FIG. **17**, total thickness of such an SPSL should be greater than about 250 nm (2500 Å) to reduce the combined absorption loss in the graded p-contact layer and the Pd metal contact to below 10 cm^{-1}. This absorption loss should be sufficient to obtain lasing.

[0075] It may be beneficial to vary the Al composition non-linearly. FIG. **18** illustrates three examples of hole concentrations calculated for several non-linear graded Al composition profiles. Graphs depicting three exemplary non-linear profiles are provided at the right side of FIG. **18**. At the left side of FIG. **18**, hole concentrations produced by the non-linear configurations are shown. FIG. **18** depicts three example profiles and corresponding hole concentrations denoted as top, middle, and bottom examples. In each example, the Al composition decreases from 0.7 to zero over a 100 nm distance.

[0076] An appropriate grading profile sustains a high hole concentration, (10^{18}-10^{19} cm^{-3}) across substantially all of the p-contact layer. The slightly non-linear profile shown in the top example of FIG. **18** provides a substantially uniform and high concentration across the profile distance. In the middle and bottom examples, the Al composition profile changes over a substantial majority of the profile distance. The profile shown in the middle example is more non-linear when compared to the top profile, and has slightly higher hole concentration at side of the layer that would be proximate the p-contact when compared to the top example. A "step profile," as shown in the bottom example of FIG. **18**, leads to an accumulation of holes at the interfaces and reduced hole concentrations in regions between the interfaces. The regions of lower hole concentration are more resistive (~10^{17} cm^{-3}) and therefore in many cases the top and middle profiles would be more desirable.

[0077] Linear graded, parabolic graded, and graded "S" profiles may be considered for the p-contact layer. In these configurations, the Al composition in the p-contact layer is higher at or near the interface between the p-side heterostructure and the p-contact layer and when compared to the Al composition at or near the interface between the p-contact layer and the p-contact. The graded profiles in the p-contact layer include an Al composition changes over a substantial majority of the distance between the p-side heterostructure and the p-contact. Both "parabolic" and "S" designs utilize built-in piezoelectric and spontaneous polarization and can induce over 1×10^{18}/cm^3 hole concentration across the layers in simulation. The S design can effectively suppress the absorption loss from the contact and the layer itself to 14

cm^{-1}, which is about one third of linear (40 cm^{-1}) and/or parabolic (44 cm^{-1}) designs. An appropriate design rule for an S-graded layer includes that the Al composition of AlGaN that gives the highest refractive index at the lasing wavelength should occur at the waist of S. The "waist" of the S profile, d_w, is an inflection point where the curve corresponding to Al composition vs. distance has a change in curvature from positive to negative.

[0078] Absorption losses increase with decreasing Al composition. Designs that sweep z in an $Al_zGa_{1-z}N$ composition of the graded p-contact layer from a Δz value (at the SPSL) to a lower value e.g., zero, (at the p-contact) may result in light from the active region propagating along or through a lossy region of the p-contact layer. For a laser diode, it is optimal to keep absorption losses below a minimal value, and this places restrictions on the Al composition in the graded p-contact region. It is possible to reduce the absorption losses in the graded p-contact layer by the choice of Al composition profile in this region. In some cases discussed herein, nonlinear graded layer designs can be used to suppress the absorption loss and induce a three dimensional hole gas simultaneously for laser diode applications.

[0079] FIG. **19** is a graph that plots the refractive index **1910**, n, and extinction coefficient **1920**, k, with respect to Al composition for wavelength, λ=250 nm in a graded $Al_zGa_{1-z}N$ p-contact layer. The peak in the refractive index and the sharp increase in the extinction coefficient occur at the value of z where the energy band gap of $Al_zGa_{1-z}N$ is nearly equal to the energy of light having wavelength of 250 nm. This wavelength corresponds to an energy of about 4.96 eV and a value of z of about 0.62. We refer to this value of z as $z_{gap}(\lambda)$. The band gap of $Al_zGa_{1-z}N$ is approximately equal to E_{gap} (eV)=6.2 z+3.4 (1-z)−0.7 z(1-z). $z_{gap}(\lambda)$ is equal approximately to the solution of the equation 1240/λ=6.2 z+3.4 (1-z)−0.7 z(1-z) with λ expressed in nm. For values of z less than 0.62 the absorption of light in $Al_zGa_{1-z}N$ increases. The extinction coefficient, k, relates to the absorption of light in the layer. In this simulation, the refractive index of $Al_zGa_{1-z}N$, where z decreases from 1 to 0 is simulated and plotted for λ=250 nm in FIG. **19**. The average composition of the SPSL requires z to be higher than 0.62 in order to provide optical mode confinement (low refractive index) and high transparency (low k). To avoid the discontinuity at the interface between the SPSL and the graded p-contact layer, the grading starts from Al composition of the SPSL, e.g., z=0.75, and then continuously decreases to z=zero (GaN) across a thickness. GaN at the metal contact allows for the establishment of an ohmic contact.

[0080] From simulations of the amplitude of the optical mode we find that high values of the refractive index n near the refractive index peak region can cause the mode to extend more into the lossy region. By reducing the width of the peak in n as a function of distance (as shown in FIG. **22**) the loss can be reduced. By reducing the thickness of $Al_zGa_{1-z}N$ regions for which z is near $z_{gap}(\lambda)$ the loss can be reduced. Reduction in the thickness of $Al_zGa_{1-z}N$ regions for which z is near $z_{gap}(\lambda)$ can be achieved by careful choice of the Al grading profile. A "pinning waveguide" is formed in the graded layer when sweeping z across the average Al composition of 0.62. This local energy trap attracts the optical mode and therefore enhances the overlaps with absorbing portion (higher k). In other words, the mode tends to be "attracted" to regions where the material exhibits a relatively higher index of refraction. If the mode extends more into regions with higher loss, then the total loss will be greater.

[0081] To study the loss resulting from different Al grading profiles three designs were compared. The first example involves a linear graded p-contact layer that starts with an Al composition of z=0.75 at d=0 at the interface between the SPSL and the p-contact layer and decreases to z=0 at d=D at the interface between the p-contact layer and the p-contact, as shown in trace **2010** of FIG. **20**. The second example, shown by trace **2020**, involves a parabolic Al composition profile that varies z parabolically with distance, d, from d=0 to d=D according to the equation $d=-133.3z^2-33.3z+100$, where 0.75>z>0, as shown in trace **2020**. A third example, shown in trace **2030**, involves an S-graded design (similar to a flipped S-shape) comprising two parabolic segments, which are connected at the inflection point of the curve. In this example, the first parabolic segment is characterized by $d=-1602.5z^2-1964.7z-572$, where 0.75>z>0.62. The second parabolic segment is characterized by $d=147.8z^2-204.6z+100$ where 0.62>z>0. In general, where d is distance in the p-contact layer, d=0 at an interface between the p-side heterostructure and the p-contact layer, d=D at an interface between the p-contact layer and the p-contact, and d_W is a point between d=0 and d=D. An S-shaped profile in the p-contact layer includes a first portion in which z is concave downward between the d=0 and $d=d_W$ and a second portion in which z is concave upward from $d=d_W$ to d=D. In some cases, d_W is greater than about 30% of the total thickness of the p-contact layer. The total thickness of the p-contact layer, D, may be about 100 nm, for example. In various implementations of the S-shaped profile, z can decrease from about 0.7 proximate to the p-side heterostructure, e.g., at d=0, to about 0 proximate to the p-contact, e.g., at d=D.

[0082] The tables shown in FIG. **21** provide values of z at various values of d for each of the profiles. The inflection point, d_w, **2031** (also denoted the "waist") of the S-curve of FIG. **20** occurs at d_w=30 nm and z=0.62. The inflection point **2031** occurs at a point where the Al composition is approximately equal to $z=z_{gap}$(250 nm) in this example.

[0083] The refractive index and transverse optical mode of the three example designs were simulated, and are shown in FIG. **22**. Traces **2210**, **2220**, **2230** show the refractive index of the linear, parabolic, and S profiles, respectively, with respect to distance. Traces **2215**, **2225**, **2235** show the optical mode for the linear, parabolic, and S profiles, respectively, with respect to distance. In the linearly graded design the relatively broad peak in the index induces a hump **2216** in the optical mode plot **2215**. The hump **2216** in the optical mode **2215** of the linear profile may increase the optical loss since it causes an increased extension of the optical mode into lossy material where z<0.62. The loss incurred in the linear design is 40 cm^{-1}. The optical mode trace **2225** for the parabolic graded profile pushes the point for which the peak index occurs to a larger distance from the interface between the p-contact layer and the SPSL. However, the width of the index peak is increased by the parabolic design, and as a result, the optical loss incurred in the parabolic design (44 cm^{-1}) is greater than in the linear graded design. In the S-shaped design, the peak is narrowed, as shown in trace **2230**. The distance from interface to the index peak is extended in the S design and this helps to suppress the loss. The absorption loss in the S-shaped

design is reduced to about 14 cm^{-1}. This absorption loss is about one third of 40 cm^{-1} and 44 cm^{-1} of linear and parabolic designs, respectively.

[0084] Piezoelectric plus spontaneous polarization fields of the three designs were simulated. FIG. **23** provides graphs **2310**, **2320**, **2330** of the total polarization for the linear, parabolic and S profiles, respectively. The corresponding hole concentrations induced by polarization at zero voltage for the linear **2420**, parabolic **2420**, and S-shaped profiles **2430**, respectively, are plotted in FIG. **24**. All three designs enable the hole concentration to exceed $1\times10^{18}/cm^3$ across the p-contact layer.

[0085] Review of the three designs indicates that in some cases, the S profile shows superior properties when compared with the properties of the parabolic and linear designs. The S-shaped profile simultaneously suppresses optical loss and maintains high hole concentration across the p-contact layer. It may be noted that the Al composition at the inflection point of the S-profile design is very close to the Al composition of the device quantum wells.

[0086] An appropriately designed graded p-contact layer in a light emitting device can enable the use of an SPSL having a reduced thickness when compared with a light emitting device employing a p-contact layer having a substantially constant Al composition. For example, in a piece-wise linearly graded p-contact layer, where d is distance in the p-contact layer, z decreases linearly with slope g_1 in a first region (see, e.g., Region I of FIG. **13**) extending from d=0 at an interface between the p-side heterostructure) and the p-contact layer to $d=d_{mid}$, and z decreases linearly with slope g_2 in a second region (see, e.g., Region II of FIG. **13**) extending from $d=d_{mid}$ to d=D at an interface between the p-contact layer and the p-contact. In some implementations, a magnitude of g_2 is greater than a magnitude of g_1. For this piecewise linear configuration, a thickness of the SPSL may be less than about 260 nm for d_{mid} greater than about 60 nm.

[0087] As another example, for an S-shaped Al composition profile, where d is distance in the p-contact layer, d=0 at an interface between the p-side heterostructure and the p-contact layer, d=D at an interface between the p-contact layer and the p-contact, and d_W is a point between d=0 and d=D. The p-contact layer includes a first portion in which z is concave downward between the d=0 and $d=d_W$ and a second portion in which z is concave upward from $d=d_W$ to d=D. For a p-contact layer having an S-shaped Al composition, the thickness of the SPSL may be less than about 260 nm for d_W greater than about 60 nm.

[0088] In some embodiments, as illustrated in the energy diagram of FIG. **25**, the SPSL layers may extend to the active region. FIG. **25** is an energy diagram that shows the conduction band energy in the region of the quantum wells **2512**, in the region of the last barrier **2520** of the active region and in the region of the polarization enhanced SPSL **2530**. The polarization enhanced SPSL **2530** is immediately adjacent to the last barrier **2520** which in turn is immediately adjacent the last quantum well **2511** of the active region. In this example, the SPSL has the composition $x_{high}=0.74$, $x_{low}=0.44$, $T_{high}=1$ nm and $T_{low}=1$ nm throughout the SPSL.

[0089] In some cases, the dimensions and/or composition of the SPSL may be modified near the active region forming a section of the SPSL that provides the functionality of an electron blocking layer (EBL) for the active region. An example of this approach is illustrated by the conduction band energy diagram of FIG. **26**. In this example, several of the SPSL layers, e.g., about six SPSL layers near the active region **2610**, form a multilayer electron blocking section (MEBS) **2640**. The SPSL layers of the MEBS **2640** have modified thickness and/or composition (T_{high}, T_{low}, x_{high}, x_{low}) when compared to the standard layers of the SPSL **2630**. In the example shown in FIG. **26**, x_{high} and x_{low} of the standard SPSL layers are 0.74 and 0.44, respectively; T_{high} and T_{low} of the standard SPSL layers are both 1.0 nm and 1.0 nm. In the example shown in FIG. **26**, layer **2641** has $x_{high}=0.87$ and $T_{high}=1.5$ nm; layer **2642** has $x_{low}=0.62$ and $T_{low}=1.5$ nm; layer **2643** has $x_{high}=0.87$ and $T_{high}=1.5$ nm; layer **2644** has $x_{low}=0.62$ and $T_{low}=1.5$ nm; layer **2645** has $x_{high}=0.87$ and $T_{high}=1.0$ nm; and layer **2646** has $x_{low}=0.62$ and $T_{low}=1.0$ nm. Other values of x_{high}, x_{low}, T_{high}, T_{low} are possible so long as the Al compositions and/or layer thicknesses of the MEBS layers are selected to provide significant retention of electrons in the active region.

[0090] Systems, devices or methods disclosed herein may include one or more of the features, structures, methods, or combinations thereof described herein. For example, a device or method may be implemented to include one or more of the features and/or processes described herein. It is intended that such device or method need not include all of the features and/or processes described herein, but may be implemented to include selected features and/or processes that provide useful structures and/or functionality.

[0091] In the following detailed description, numeric values and ranges are provided for various aspects of the implementations described. These values and ranges are to be treated as examples only, and are not intended to limit the scope of the claims. For example, embodiments described in this disclosure can be practiced throughout the disclosed numerical ranges. In addition, a number of materials are identified as suitable for various implementations. These materials are to be treated as exemplary, and are not intended to limit the scope of the claims.

[0092] The foregoing description of various embodiments has been presented for the purposes of illustration and description and not limitation. The embodiments disclosed are not intended to be exhaustive or to limit the possible implementations to the embodiments disclosed. Many modifications and variations are possible in view of the above teaching.

1. A light emitting device, comprising:

a p-side heterostructure comprising a short period superlattice (SPSL) including alternating layers of $Al_{x\text{-}high}Ga_{1-xhigh}N$ doped with a p-type dopant and $Al_{x\text{-}low}Ga_{1-xlow}N$ doped with the p-type dopant, where $x_{low}\leq x_{high}\leq 0.9$ and each layer of the SPSL has a thickness of less than or equal to about six bi-layers of AlGaN;

an n-side heterostructure; and

an active region configured to emit light disposed between the SPSL and the n-side hetero structure.

2. The device of claim **1**, wherein each $Al_{xhigh}Ga_{1-xhigh}N$ layer has a thickness, T_{high}, and each $Al_{xlow}Ga_{1-xlow}N$ layer has a thickness T_{low}, wherein T_{high} and T_{low} are in a range of about 0.7 nm to about 1.3 nm.

3. The device of claim **1**, wherein the SPSL has a total thickness of greater that about 200 nm and less than about 450 nm.

4. The device of claim **1**, wherein $x_{high}-x_{low}$ is greater than or equal to about 0.25.

5. The device of claim **1**, wherein an average Al composition in the SPSL is about 0.60.

6. The device of claim **1**, wherein x_{low} is about 0.44 and x_{high} is about 0.75.

7. The device of claim **1**, wherein resistivity of the SPSL changes by less than about 50 Ω-cm over a temperature range of about 400 K to about 100 K.

8. The device of claim **1**, wherein resistivity of the SPSL is less than about 10 Ω-cm at room temperature.

9. The device of claim **1**, wherein the n-side heterostructure, active region, and p-side heterostructure are grown on at least one of a substrate comprising one or more of GaN, AlN, SiC, sapphire, Si, GaAs, ZnO, a group III-N alloy, and a template comprising a group III-N material.

10. The device of claim **1**, wherein the n-side heterostructure, active region, and p-side heterostructure are epitaxially grown on a bulk AlN substrate.

11. The device of claim **1**, further comprising a substrate of sapphire, a group-III nitride, SiC, or ZnO, wherein the n-side heterostructure, active region, and p-side heterostructure are epitaxially grown on an (0001) or (000$\bar{1}$) surface of the substrate.

12. The device of claim **1**, further comprising a substrate of a group-III nitride, SiC, or ZnO, wherein the n-side heterostructure, active region and p-side heterostructure are epitaxially grown on a semi-polar facet of the substrate.

13. A light emitting device, comprising:

a p-side heterostructure comprising a short period superlattice (SPSL) comprising alternating layers of $Al_{x\text{-}high}Ga_{1\text{-}high}N$ doped with a p-type dopant and $Al_{xlow}Ga_{1\text{-}xlow}N$ doped with the p-type dopant, where $x_{low} \leq x_{high} < 0.9$;

an n-side heterostructure; and

an active region configured to emit light disposed between the SPSL and the n-side heterostructure, wherein the alternating layers cause modulation in a valence band potential in the SPSL and the modulation is approximately equal to an acceptor level energy of the p-type dopant.

14. The device of claim **13**, wherein the p-type dopant is Mg and the modulation is greater than about 0.35 eV.

15. A light emitting device, comprising:

a p-side heterostructure;

an n-side heterostructure;

an active region configured to emit light disposed between the p-side heterostructure and the n-side heterostructure;

a metallic p-contact; and

a p-contact layer disposed between the p-side heterostructure and the p-contact, the p-contact layer comprising $Al_zGa_{1\text{-}z}N$ and having a thickness, D, where z has an S-shaped Al composition profile that varies over a substantial portion of the thickness of the p-contact layer.

16. The device of claim **15**, wherein:

d is distance in the p-contact layer, wherein d=0 at an interface between the p-side heterostructure and the p-contact layer, and d=D at an interface between the p-contact layer and the p-contact, and d_W is a point between d=0 and d=D; and

the S-shaped profile comprises:

a first portion in which z is concave downward between the d=0 and d=d_W; and

a second portion in which z is concave upward from d=d_W to d=D.

17. The device of claim **16**, wherein d_W is greater than about 30% of the thickness of the p-contact layer.

18. The device of claim **17**, wherein D is about 100 nm.

19. The device of claim **15**, wherein z decreases from about 0.7 proximate to the p-side heterostructure to about 0 proximate to the p-contact.

20. A light emitting device, comprising:

a p-side heterostructure comprising a short period superlattice (SPSL) comprising alternating layers of $Al_{x\text{-}high}Ga_{1\text{-}xhigh}N$ doped with a p-type dopant and $Al_{x\text{-}low}Ga_{1\text{-}xlow}N$ doped with the p-type dopant, where $x_{low} \leq x_{high} \leq 0.9$;

an n-side heterostructure;

an active region configured to emit light disposed between the SPSL and the n-side heterostructure;

a metallic p-contact; and

a p-contact layer disposed between the p-side heterostructure and the p-contact, the p-contact layer comprising $Al_zGa_{1\text{-}z}N$ and having a thickness, D, where z varies over a substantial portion of the thickness of the p-contact layer.

21. The device of claim **20**, wherein $x_{low} \leq x_{high} \leq 0.9$ and a thickness of each of the alternating layers is less than or equal to about six AlGaN bi-layers.

22. The device of claim **20**, wherein:

z decreases linearly with slope g_1 in a first region extending from d=0 at an interface between the p-side heterostructure and the p-contact layer to d=d_{mid}; and

z decreases linearly with slope g_2 in a second region extending from d=d_{mid} to d=D at an interface between the p-contact layer and the p-contact, wherein a magnitude of g_2 is greater than a magnitude of g_1.

23. The device of claim **22**, wherein a thickness of the SPSL is less than about 260 nm and d_{mid} is greater than about 60 nm.

24. The device of claim **20**, wherein:

d is distance in the p-contact layer;

d=0 at an interface between the p-side heterostructure and the p-contact layer;

d=D at an interface between the p-contact layer and the p-contact;

d_W is a point between d=0 and d=D; and

the p-contact layer includes:

a first portion in which z is concave downward between d=0 and d=d_W; and

a second portion in which z is concave upward from d=d_W to d=D.

25. The device of claim **24**, wherein the thickness of the SPSL is less than about 260 nm and d_W is greater than about 60 nm.

26. A light emitting device, comprising:

a p-side heterostructure comprising a short period superlattice (SPSL);

an n-side heterostructure; and

an active region configured to emit light disposed between the SPSL and the n-side heterostructure, wherein the SPSL comprises a first portion and a second portion, the first portion proximate the active region and comprising a first number of alternating layers of $Al_{x1high}Ga_{1\text{-}x1high}N$ doped with a p-type dopant and $Al_{x1low}Ga_{1\text{-}x1low}N$ doped with the p-type dopant, the second portion comprising a second number of alternating layers of $Al_{x2high}Ga_{1\text{-}x2high}N$ doped with a p-type dopant and $Al_{x2low}Ga_{1\text{-}x2low}N$ doped with a p-type dopant, and

wherein a thickness of each layer of the SPSL has a thickness of less than or equal to about six bi-layers of AlGaN.

27. The device of claim **26**, wherein $x_{2low} \leq x_{2high} \leq 0.9$.

28. The device of claim **26**, wherein an Al composition and thickness of the $Al_{x1high}Ga_{1-x1high}N$ and $Al_{x1low}Ga_{1-x1low}N$ layers are configured to provide significant retention of electrons in the active region.

29. The device of claim **26**, wherein at least some layers of the first portion have a thickness greater than a thickness of the layers of the second portion.

30. The device of claim **26**, wherein the first number is about 6.

31. A method of fabricating a light emitting device, comprising:

growing an n-side heterostructure on a substrate;

growing an active region on the n-side heterostructure;

growing a short period superlattice (SPSL) proximate to the active region, comprising:

growing alternating layers of $Al_{xhigh}Ga_{1-xhigh}N$ doped with a p-type dopant and $Al_{xlow}Ga_{1-xlow}N$ doped with the p-type dopant, where $x_{low} \leq x_{high} \leq 0.9$ and each layer of the SPSL having a thickness of less than or equal to about six bi-layers of AlGaN.

32. The method of claim **31**, wherein growing the alternating layers comprises growing the alternating layers using metalorganic chemical vapor deposition (MOCVD) at an ambient pressure of in a range of about 80 to about 700 torr.

33. The method of claim **31**, wherein growing the alternating layers comprises growing the alternating layers at a temperature between about 750° C. and 1300° C.

34. The method of claim **31**, wherein growing the alternating layers comprises growing the alternating layers at a growth rate between about 0.01 nm per second to 0.04 nm per second.

* * * * *